DIATOM BASED PALEOCLIMATE RECONSTRUCTION FROM THE INDIAN SECTOR OF SOUTHERN OCEAN

A THESIS SUBMITTED IN PARTIAL FULFILMENT FOR THE DEGREE OF

DOCTOR OF PHILOSOPHY

IN THE SCHOOL OF EARTH, OCEAN AND ATMOSPHERIC SCIENCES,

GOA UNIVERSITY

By

POOJA P. GHADI
School of Earth, Ocean and Atmospheric Sciences
Goa University
Taleigao Plateau, Goa, India-403206

DECEMBER 2023

THIS THESIS IS DEDICATED TO MY PARENTS

DECLARATION

As required by the Goa University Ordinance OA-19, I state that the thesis entitled "**DIATOM BASED PALEOCLIMATE RECONSTRUCTION FROM THE INDIAN SECTOR OF SOUTHERN OCEAN**" is my original research work and has not been submitted previously. The present study carried out is first of its kind from the study area mentioned. The literature related to the problem investigated has been cited.

Place: Taleigao Plateau **POOJA P. GHADI**

Date:

CERTIFICATE

This is to certify that the work of the thesis titled "**DIATOM BASED PALEOCLIMATE RECONSTRUCTION FROM THE INDIAN SECTOR OF SOUTHERN OCEAN**" submitted by **Ms. Pooja P. Ghadi** was carried out under my supervision.

Dr. Rahul Mohan (Scientist F**)**
Research Guide
National Centre for Polar and Ocean Research
Vasco-da-Gama, Goa

Acknowledgement

I express my sincere gratitude to my guide, ***Dr. Rahul Mohan*** *for his mentorship and the confidence on me which allowed me to work in generous freedom. His immense knowledge, valuable guidance and support has helped me to complete the research work on time. I am really fortunate to have him as my Ph.D. supervisor.*

I express my gratitude to ***Dr. Abhilash Nair*** *who supported me throughout the completion of the work. His thought provoking questions and suggestions has always helped me to be closer to my destination.*

I fall short of words to thank ***Dr. C. Rivonker****, School of Earth, Ocean and Atmospheric Sciences and* ***Dr. S. Naik****, National Institute of Oceanography for their suggestions and advice during the Doctoral Research Committee meetings. Their inspirational words, scientific ideas and constructive critisism has helped me in completion of my research.*

My sincere thanks to ***Dr. Xavier Crosta****, University of Bordeuax, France for training and guiding and all the help with dataset.*

I am thankful to the Director, National centre for Polar and Ocean Research (NCPOR) ***Dr. Thamban Meloth,*** *former Director* ***Dr. M. Ravichandran****, the Vice-Chancellor Goa University* ***Dr. H. Menon****, and Dean of Faculty of School of Earth, Ocean and Atmospheric Sciences,* ***Dr. C. Rivonker*** *Goa University for providing facilities and help in administrative matters.*

I am indebted to Micropaleontology and Geology Laboratory, NCPOR- Goa for providing me the conducive environment during my Ph.D. days. The fellow lab mates were always a source of inspiration towards the work, scientific and non-scientific discussions.

A special thanks to my friends and colleagues ***Dr. Cheryl, Nibedita, Pallavi, Dr. Mahesh, Dr. Shramik, Dr. Saalim, Dr. Ravi, Dr. Padmasini, Dr. Noor, HariKrishanan, Valancy, Ankita, Sahina, Shweta, Akshaya, Mruna and Omkar.***

My deepest gratitude to ***Sarvajit Karapurkar*** *for all his support, constant motivation and believing me unconditionally thus helping me in all the ups and downs.*

I would like to thank my parents for being so supportive of my chosen career path and throughout my life's journey.

I am grateful to my teacher at Goa University ***Dr. AAA Viegas*** *for constantly motivating me to reach the finish line. My special thanks to my collegues* ***Dr. Nicole, Dr. Niyati , and Mr. Mahesh*** *for always checking on me during the writing phase.*

My M.Sc. students of batch 2020-22 and 2021-23 are also thanked for being supportive.

My head bows before the God almighty, the cherisher and sustainer of the world, who gave me boundless blessings, rendered through various hands, which helped me in completing this work successfully.

This research was financially supported by CSIR-India (CSIR grant no. 1121620548; Ref No: 18/12/2016(ii) EU-V) and all the laboratory work was carried out at NCPOR.

TABLE OF CONTENT

Sr. No.	Title	Page No.
	Contents	i - iii
	Figures and Tables	iv
	Abbreviations	vii
	Abstract	ix
Chapter 1	**Introduction**	**1 - 13**
1.1.	Modern Climate change and relevance of paleoclimate to climate change	1
1.2	Why Polar Regions	1
1.3	The Southern Ocean (SO)	3
1.4	Sea Ice	6
1.5	Diatoms	8
1.6	Objectives	12
Chapter 2	**Material and methodology**	**14 - 22**
2.1	Southern ocean	13
2.2	Study area : Indian Sector of SO	14
2.3	Sediment sampling	15
2.3.1	SK 200/33	15
2.3.2	MD 12 3401 cq	15

2.4	Chronology	16
2.5	Sample preparation	16
2.6	Taxonomic notes	17
2.7	Diatom counts	17
2.8	Transfer function for sea surface temperature (SST) and sea ice estimation	19
2.9	Diatom size measurements	20
2.10	Biogenic silica analysis	22
Chapter 3	**Annotated index of key diatom species**	23 - 44
3.1	The diatom	22
3.2	The Sea ice diatom group	23
3.3	The POOZ diatom group	29
3.4	The Water Stratification diatom group	37
3.5	The SAZ group	39
Chapter 4	**Antarctic sea-ice and paleoproductivity variation over the last 156000 years in the Indian Sector of Southern Ocean**	**45 - 65**
4.1	Introduction	43
4.2	Chronology	44
4.2.3	Diatom sample preparation	48
4.2.4	Sea surface temperature and sea ice estimation	48

4.2.5	Biogenic silica analysis	48
4.2.6	Additional data	48
4.3	Results	49
4.3.1	Down core variation in diatom assemblages	49
4.3.2	Down core variations in summer SST and WSI	51
4.4	Discussion	51
4.4.1	Latitudinal shifts in Antarctic winter sea-ice extent and hydrological fronts in the Indian sector	51
4.4.2	Zonal comparison of winter sea ice in the Southern Ocean	55
4.4.3	Latitudinal changes in SW Indian sector paleoproductivity	59
4.5	Conclusion	62
4.11	Additional data plots	63
Chapter 5	**Glacial-Interglacial flux and size variability of *Fragilariopsis Kerguelensis and Thalassiosira Lentiginosa* from the Indian Sector of the Southern Ocean**	**66 - 82**
5.1	Introduction	65
5.2	Material and methods	67
5.2.1	Study area and sediment core details	67
5.2.2	Sediment core chronology	68

5.2.3	Diatom extraction and size measurements	70
5.2.4	Additional data	70
5.3	Results	70
5.4	Discussion	71
5.4.1	Terminations	72
5.4.2	Glacials	75
5.4.3	Interglacials	78
5.5	Conclusions	79
5.6	Additional data plots	80
Chapter 6	**Paleo sea surface temperature and sea ice variability from the Kerguelen Island region, Southern Ocean**	**83 - 94**
6.1	Introduction	81
6.2	Material and methodology	82
6.2.1	Study area and core details	82
6.2.2	Chronology	84
6.2.3	Diatom sample preparation and counting	86
6.2.4	Sea surface temperature and sea ice estimation	86
6.3	Results	86
6.4	Discussion	88
6.5	Conclusion	91

	Summary	**95 - 97**
	References	**97 - 121**

FIGURES AND TABLES

Chapter 1 Introduction

Fig. 1.1 Southern Ocean Map

Fig. 1.2 Agulhas leakage and position of STF

Fig. 1.3 Southern Hemisphere sea ice concentration

Fig. 1.4 Scanning Electron Image of diatoms

Chapter 2 Material and methodology

Fig. 2.1 Sectors of Southern Ocean

Fig. 2.2 Sediment core location map of SK 200/33 and MD 12 3401 cq

Table 2.1 Sediment core details

Table 2.2 Diatom groups

Fig. 2.3 Scanning electron microscope images of diatoms used for morphometric analysis.

Chapter 3 Annotated index of key diatom species

Fig. 3.1 SEM and LM image of *Actinocyclus actinochilus*

Fig. 3.2 SEM and LM image of *Fragilariopsis curta*

Fig. 3.3 SEM and LM image of *Fragilariopsis cylindrus*

Fig. 3.4 SEM and LM image of *Fragilariopsis ritscheri*

Fig. 3.5 SEM and LM image of *Fragilariopsis obliquecostata*

Fig. 3.6 SEM and LM image of *Fragilariopsis sublinearis*

Fig. 3.7 SEM and LM image of *Fragilariopsis kerguelensis*

Fig. 3.8 SEM and LM image of *Fragilariopsis rhombica*

Fig. 3.9 SEM and LM image of *Fragilariopsis* separanda

Fig. 3.10 SEM and LM image of *Thalassiosira gracilis*

Fig. 3.11 SEM and LM image of *Thalassiosira lentiginosa*

Fig. 3.12 SEM and LM image of *Thalassiosira oliverana*

Fig. 3.13 SEM and LM image of *Thalassiothrix antarctica*

Fig. 3.14 SEM and LM image of *Trichotoxon reinboldi*

Fig. 3.15 SEM and LM image of *Chaetoceros resting spores*

Fig. 3.16 SEM and LM image of *Thalassiosira antarctica*

Fig. 3.17 SEM and LM image of *Azpetia tabularis*

Fig. 3.18 SEM and LM image of *Hemidiscus cuneiformis*

Fig. 3.19 SEM and LM image of *Thalassiosira oestrupii*

Chapter 4 Antarctic sea-ice and paleoproductivity variation over the last 156000 years in the Indian Sector of Southern Ocean

Fig. 4.1 Study area map of SK 200/33

Table 4.1 SK 200/33 core chronology

Fig. 4.2 Age model for sediment core SK 200/33

Fig. 4.3 Relative abundances of diatom groups along with SST and WSIC for SK 200/33

Fig. 4.4 Latitudinal comparison plot of SK 200/33 records

Fig. 4.5 Zonal comparison plot of SK 200/33 records

Fig. 4.6 Schematic representation of sea-ice extent and hydrological fronts during glacial and interglacial stages

Fig. 4.7 Latitudinal comparison of changes in paleoproductivity

Fig. 4.8 Schematic representation of sea-ice variability and its impact on biological productivity

Fig. 4.9 Correlation between winter sea-ice and SST

Fig. 4.10 Box and whisker plot for biogenic silica variation

Chapter 5 **Glacial-Interglacial flux and size variability of *Fragilariopsis kerguelensis and Thalassiosira lentiginosa* from the Indian Sector of the Southern Ocean**

Fig. 5.1 Study area map of SK 200/33 along with the core sites used as a supporting dataset

Fig. 5.2 Age model for sediment core SK 200/33

Table 5.1 SK 200/33 core chronology

Fig. 5.3 Valve size variation of diatoms records from SK 200/33

Fig. 5.4 Box and whisker plot for size variation of diatoms from SK 200/33

Fig. 5.5 Glacial-interglacial variation of valve size of diatoms and comparison with winter sea ice

Fig. 5.6 Comparison between SST and *F. kerguelensis* valve area

Fig. 5.7 Comparison between SST and *T. lentiginosa* valve area

Fig. 5.8 Age tuning of SK 200/33

Fig. 5.9 Pearson's correlation graph of diatom

Chapter 6 Paleo sea surface temperature and sea ice variability from the Kerguelen Island region, Southern Ocean

Fig. 6.1 Study area map of MD 12 3401 cq along with the core sites used as a supporting dataset

Table 6.1 MD 12 3401 cq core chronology

Fig. 6.2 Age model for sediment core MD 12 3401 cq

Fig. 6.3 Downcore relative and absolute abundance

Fig. 6.4 Comparison of the SST from Indian Sector of SO with of the cores from the latitudinal transect

ABBREVATIONS USED IN THESIS

Abbreviation	Description
IPCC	Intergovernmental Panel on Climate Change
SO	Southern Ocean
ACC	Antarctic Circumpolar Current
Sv	Sverdrup
ppmv	parts per million by volume
STF	Subtropical front
SAF	Sub-Antarctic front
APF	Antarctic polar front
SASW	Subantarctic Surface Water
AAIW	Antarctic Intermediate Waters
CDW	Circumpolar Deep Water
AABW	Antarctic Bottom Water
MIS	Marine Isotope Stage
SST	Sea Surface Temperature
WSI	Winter Sea Ice
LGM	Last Glacial Maxima

SH	Southern Hemisphere
SIE	Sea Ice Extent
SIZ	Sea ice zone
POOZ	Permanently Open Ocean Zone
PFZ	Polar Frontal Zone
SAZ	The Sub-Antarctic Zone
HCl	Hydrochloric acid
H_2O_2	Hydrogen peroxide
DAA	Diatom absolute abundance
MAT	Modern analog technique
WSIC	Winter sea ice concentration
WSID	Winter sea ice duration
NIS	Nuclear Inelastic Scattered
LM	Light Microscope
SEM	Scanning Electron Microscope
SWW	Southern Hemisphere Westerlies Winds
SW	South-western
SACCF	Southern ACC Front

AMS	Accelerator Mass Spectrometry
EPICA	European Project for Ice Coring in Antarctica
EDC	EPICA Dome C
Na_2CO_3	Sodium carbonate
VA	Valve Area
AA	Absolute Abundance
AL	Apical Length
TL	Trans-Apical Length

ABSTRACT

The present study aims to understand the Antarctic sea ice history and past productivity over a glacial interglacial time scale. New significant study relevant to sea ice extent (SIE) and sea surface temperature (SST) from the Indian Southern Ocean (SO) sector, which had been largely unstudied in the SO during past interglacial periods has been carried out. The focus is on a quantitative and process-oriented understanding of past SO changes to improve the understanding of future climate and environment. The introductory chapter describes the significance of this study. It focuses on climate change and relevance of paleoclimate, use of proxies for better understanding of the climate change. Further information is also provided on how diatoms, the unicellular algae, are used as a proxy. Chapter 2 discusses the material and methodology used for the successful completion of this study. It gives details about the two sediment cores used, SK 200/33 and MD12 3401 cq and their chronology. The chapter further discusses about diatom extraction method, preparation of permanent slides and their identification. Chapter 3 is exclusively on annotations of the diatoms groups namely sea ice group, water stratification group, permanent open ocean zone group and sub Antarctic zone group. The chapter is facilitated by light microscopy and Scanning Electron microscopy images. The results achieved are discussed in Chapter 4, 5 and 6.

In Chapter 4, with the help of the diatom assemblages preserved in the sediment core SK 200/33 SST and winter sea ice (WSI) records have been established over a glacial interglacial time scale. It is observed that during each glacial period, the data shows SST of 1-2 ˚C and WSID of 2 months/year. When this data is combined with previously published regional SST and WSI data from other sectors, it suggests that during each glacial period, all hydrological features migrated northward by a few degrees of latitude, allowing the Southern Antarctic Circumpolar Current (SACCF) to be placed at ~ 55 degrees south, the WSI edge near 49 degrees south, and the mean APF at 46 degrees south. Chapter 5 emphasis on the morphometric analysis of the two diatom species *Fragilariopsis kerguelensis* and *Thalassiosira lentiginosa*. They recorded overall low mean valve area (VA) downcore. This is ascribed to low SST, high sea-ice cover limiting the ability of these species to make use of the low macro-nutrients stock. Chapter 6 provides a high resolution study from Kerguelen Region MD 12 3401 cq sediment core. Down-core SST logs at the core site show an overall temperature range of 5°C to 12°C. The overall abundance of diatoms varies between 60 and 80 x 10^6 valves/g sediment. Strong warming is noted during glacial periods. Comparative study of the core with that of the cores from

surrounding region indicates the control of surface currents i.e. Agulhas current and its retroflection over the estimated SSTs.

CHAPTER - 1

INTRODUCTION

1.1. Modern Climate change and relevance of paleoclimate to climate change

Since the preindustrial times the average atmospheric concentration of carbon dioxide (CO_2) has risen steadily from 280 ppmv (parts per million by volume) to 400 ppmv over the last 200 years. (Karl and Trenberth 2003, Hertzberg and Schreuder 2016). The continued CO_2 levels rise is a threat to the earth's habitability. Increase in atmospheric CO_2 precede and cause parallel increase in Earth's temperature (IPCC 2007). It is important to fully understand the dynamics of the climate but due to short span of the instrumental record, our information about the earths past climate is limited. This problem is overcome by the use of proxy records to understand the detailed and longer climate history. The proxies are the natural libraries which are climate dependent and hence the reliable source of past-climatic information. The paleoclimate data provides a base for reconstructing past climate and also to understand the reasons associated with the changing climate. This better understanding of the past climate in turn, will help to forecast any future climatic deviation (Bradley, R. S. (1999). The sediments, either of marine or lacustrine origin, speleotherms, ice cores, etc. forms the repositories of this past climatic environments. Although interpreting this information from proxies is not easy as they are embedded with extraneous noise which are incorporated from the nonclimatic signals. Hence, these records are extracted by careful interpretation and calibration. Paleoclimate signals are rich source of information about our earths past and Polar Regions are the best storehouse of this records.

1.2. Why Polar Regions

Polar Regions can be defined in different ways based on geography and terrain. However, geometrically, Arctic and the North Pole and the Antarctic and the South Pole are considered as the Polar Regions. They serve to be the flagship area in climate change because the impacts projected to occur by 2050 are already seen in the Polar Regions. This has resulted into the marked and unprecedented changes (IPCC 2022). Polar Regions plays an important role in regulating the global climate system. The climatic changes are causing a cascading risks to all the polar ecosystem especially to the phytoplankton community. The primary productivity is low in the Central Arctic Ocean due to light and nutrient limitations (Randelhoff and Guthrie, 2016; Ardyna and Arrigo, 2020). But the interior shelf regions do show increased productivity owing to changes in sea ice content (Ardyna and Arrigo, 2020; Lannuzel et al., 2020). Also no consistent change in the primary production at the circumpolar scale is seen even though the area is affected by large scale environmental changes like availability of light, nutrients and

deepening of summer mixed layers (Panassa et al., 2018; Sallée et al., 2021, IPCC 2022). Different sectors from Southern ocean (SO) shows different trend. The increase in primary productivity is seen in the Pacific sector whereas a decreasing trend is noticed in Atlantic sector and in Ross Sea (Kahru et al., 2017; Henley et al., 2020; Pinkerton et al., 2021). The primary productivity of the oceans are highly sensitive to changes in physical forcing, nutrient supply and sea ice dynamics (Moore and Abbott, 2000; Arrigo et al., 2008, Vernet et al., 2008; Wang and Moore, 2012). The biota also gets impacted due to ocean acidification. The calcifying organisms are most affected in southern ocean due to ocean acidification. However siliceous organisms especially diatom species appear relatively resilient to the decreasing level of pH (IPCC 2022).

Comparing the two different Polar Regions of the earth, it is seen that the most of the parts of the Northern Hemisphere is affected by seasonal snowfall. It is very sensitive to climate change because it reacts quickly to changes in temperature. On contrary to that, Antarctica is covered with a large ice sheet. It has remained relatively unchanged on a scale of decades and centuries. It is therefor, the areas around Antarctica, especially the oceans and the coastal areas of the continent are the most sensitive for climate change and changes on a shorter time scale. The atmosphere and oceans play a key role in poleward flux of heat, wherein ocean significantly contributes to the 40% of it. Oceans also owe a major potential for feedbacks between ocean circulation, sea ice, and the ocean carbon cycle (Charrassin et al., 2008). Very important ocean is Southern Ocean which contributes significantly in Southern Hemisphere.

1.3. The Southern Ocean (SO)

The Southern Ocean is the vast oceanic region surrounding Antarctica which is a region of extremes (Fig. 1.1). It plays a crucial role in the global climate system (Wüst, 1935; Deacon, 1937,). The SO is a global ocean connector which acts as a cross-roads of the global ocean circulation (Rintoul et al., 2001; Lumpkin and Speer, 2007; Iudicone et al., 2008, Carter et al., 2022). The Antarctic Treaty Limits 60°S as a political northern limit of the SO. However, as per the various literatures the ocean well north of 60°S i.e. ~ 40°S is considered as SO for all scientific studies.

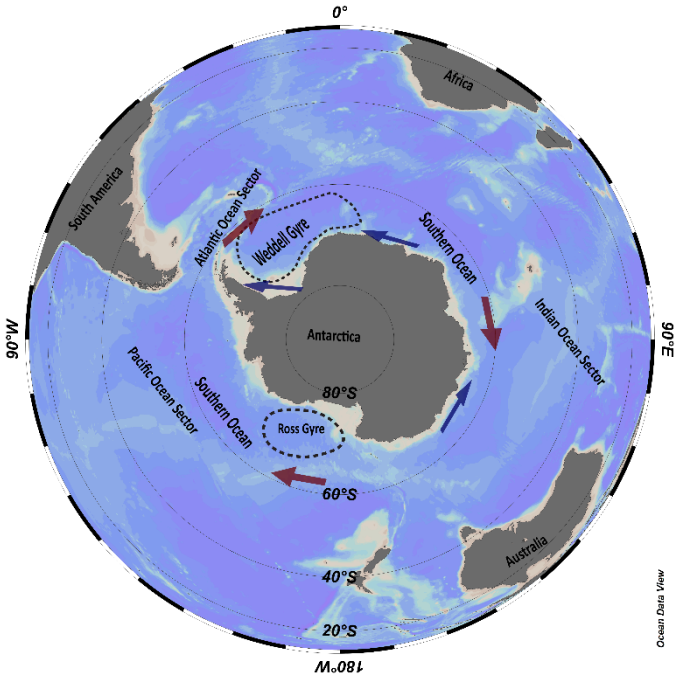

Fig 1.1: Southern Ocean Map showing oceanographic features such as Antarctic Circumpolar Current (red arrow), Antarctic coastal current (blue arrow), Ross Gyre, Weddell Gyre and sectors of Southern Ocean.

It occupies the 20% of the world ocean. The SO holds the distinctive characteristics which are the results of prolonged evolutionary processes. Various studies like Kennett 1977; Knox 1980; Kennett 1983 and Anderson 1998 has provided a detailed synthesis of the information of the SOs evolution and palaeoceanography. The summary of the major events during evolution of SO is as follows: Until Middle to Late Mesozoic time period, the Antarctica was at its high latitude position (Kenneett 1977) and it is during 60–80 million years before present (myr BP), New Zealand started drifting from Australia and Antarctica. Nearly 50-55 myr BP Australia began its journey towards north thus forming an ocean (Kenneett 1977). But the major current i.e. the circum-Antarctic current was not developed between Antarctica and Australia since the South Tasman Rise was still part of Victoria Land (Knox 2006).

It was during the Late Eocene to Early Oligocene, significant changes began to occur wherein the modern climatic regime came into existence. Due to dramatic decline in the austral temperatures, the coastal surface water freezed, which might have caused sea level glaciation, and thus resulting in the formation of Antarctic Bottom Water. This gave rise to advancement of the thermohaline circulation system. The South Tasman Rise eventually got separated from

the Victoria Land, during 25-28 BP, to allow enough Passage for the formation of the Antarctic Circumpolar Current (ACC).

One of the most prominent feature of SO is ACC which is driven by Westerly winds (Gille, 1994). It is the longest current with an estimated pathway of 24,000 km (Whitworth, 1983) transporting more than 130×10^6 m^3 s^{-1} (Sv) of surface, deep and intermediate waters between the Atlantic, Indian, and Pacific oceans (Rintoul et al., 2001). The uninterrupted nature of the ACC results in the focusing of large vertical exchanges between layers spanning the global ocean pycnocline (Garabato et al. 2016).

Within the flow of ACC, enhanced meridional gradient or physical fronts are encountered throughout the SO. From north to south the physical fronts are positioned as Subtropical front (STF), Sub-Antarctic front (SAF) and Antarctic polar front (APF) (Whiteworth and Nowlin, 1987). Understanding the structure and location of the major fronts of the SO is of considerable importance as it provide clues to the still poorly understood dynamics of the current. The location of fronts, especially, STF, is considered of great importance. Studies have suggested that the inter-ocean (Indian-Atlantic ocean) exchange patterns (Agulhas leakage) are attributed to the latitudinal shift of STF, wherein southward migration of the STF increases Agulhas leakage (Caley et al. 2011). Agulhas current flows on the east coast of Africa. It carries warm and saline water (Lutjeharms and Valentine, 1984). This current continues south until it meets the STF. At the STF Agulhas current is blocked and it retroflects eastward (back to Indian Ocean). But the small gap between STF and the tip of Africa allows the leakage of some warm-saline water from Indian Ocean into Atlantic Ocean (Fig. 1.2) (Beal et al. 2011).

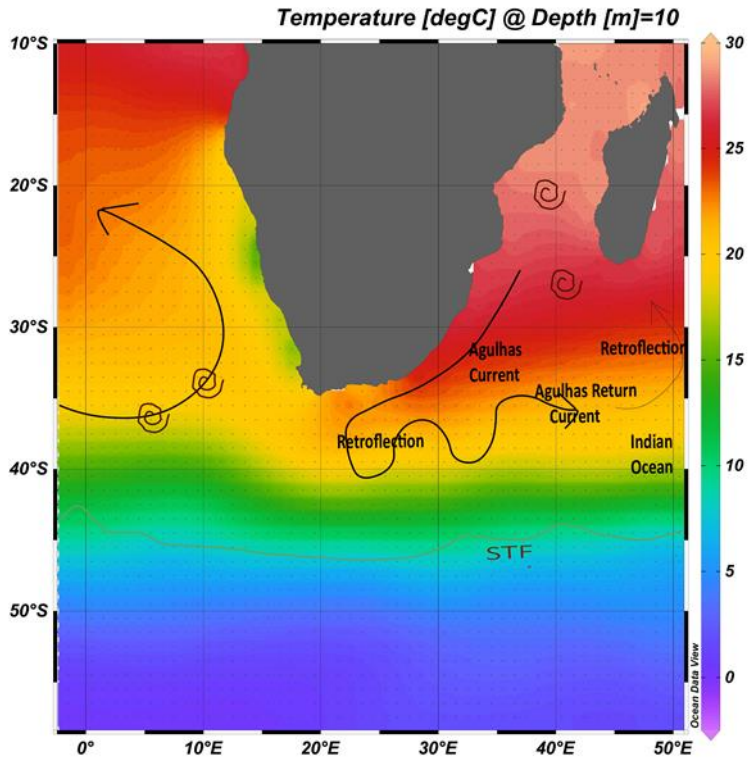

Fig. 1.2 Agulhas leakage and position of STF (after Calley et al., 2011)

These fronts correspond to water mass boundaries. In SO these Water masses are classified into four layers as Subantarctic Surface Water (SASW), Antarctic Intermediate Waters (AAIW), Circumpolar Deep Water (CDW), and Antarctic Bottom Water (AABW) which are mostly identified by salinity, potential temperature, and potential density. In context of paleoceanography, studies on SO water masses suggests a decoupling between intermediate and deep water changes in the SO over the last glacial inception. Studies have suggested succession of ocean-atmosphere feedbacks, in reaction to the early cooling observed in the high southern latitudes. Surface cooling at the Marine Isotope Stage (MIS) 5.5–5.4 transition would be associated with an equator ward shift of oceanic surface fronts and the westerlies, which moved away from the Antarctic divergence. The Southern Ocean circulation of MIS 5.4 is mostly characterized by an increased formation of cold and poorly ventilated AABW, which expanded northward and reached shallower depths. During MIS 4, a further expansion of cold and poorly ventilated AABW and a northward shift in the boundary between AAIW and CDW suggest that the deep Southern Ocean circulation was already close to glacial conditions (Govin et al., 2009). The formation of SO water masses (deep water masses) are significantly impacted by sea ice distribution in SO (Talley et al., 2011).

1.5. Sea Ice

Sea ice is an important parameter of the climate system that influences energy and gas balances, and deep ocean convection (Ackley et al., 1980). It also reflects a large proportion of solar radiation back to space that would otherwise be absorbed by the ocean. Sea ice maintains a tenuous existence at the interface of the ocean and atmosphere, and is highly sensitive to temperature changes. Sea ice has an influential effect on the carbon and nutrient cycling and also on the ecosystem functioning. During sea ice formation the brine which is rejected is enriched in CO_2; and the sea ice which serves as a blanket inhibits any kind of exchange of CO_2 between the atmosphere and the ocean surface (Crosta et al., 2022). During summer, the melting sea ice forms an enriched biological layer which draws down the CO_2 from the atmosphere (Arrigo and Dijken, 2008; Rysgaard et al., 2011, Vancoppenolle et al., 2013; Crosta et al., 2022). The presence of sea ice can also have direct or indirect effects on other mechanisms of the Antarctic marine ecosystem by food chain functioning as phytoplanktons which are attached to the sea ice or related to costal polynyas serves as a food to the zooplanktons (Eicken, 1992; Norkko et al., 2007; Loeb et al., 2015, Ainley et al., 2017; Labrousse et al., 2018; Rossi et al., 2019). Sea ice also serves as home to many algaes for resting and breeding (Fraser et al. 1992; Ancel et al. 1992; Labrousse et al., 2017). Thus sea ice integrates elements of the ocean and atmosphere circulation, as it is a result of ocean-atmosphere exchanges of heat, freshwater and momentum, and therefore the understanding the sea ice changes will help to understand Antarctic climate as a whole (W.R. Hobbs et al 2016).

The satellite records has assessed the Antarctica's seasonal sea ice cover ever since 1979 (Fig. 1.3). The records points towards a high spatial variability in the seasonal to annual trends in sea ice concentration, thickness and extent (Parkinson and Cavalieri, 2012, Yuan et al., 2017, Wang et al., 2021). Slightly increased sea ice extent has been marked for the period between 1979 and 2014 (Simmonds, 2015; Parkinson, 2019). It is estimated that this slight increase was in response of differential trends in the different parts of the Antarctica. A significant sea ice extent decrease was marked in Amundsen and Bellinghausen seas offset by an enormous increase in the western Ross Sea (Zwally et al., 2002; Holland and Kwok, 2012; Fan et al., 2014; Jena et al., 2018; Parkinson, 2019; Crosta et al., 2022).

Year 2016 noted an exceptional decrease in the Antarctica's sea ice extent (Parkinson et al., 2019) and this was notably seen in the Ross and Weddell seas (Hao et al., 2021). This change has been attributed to combination of several factors such as weakened Southern Hemisphere

Westerly Winds, increased advection of warmer masses of air and the oceanic warming over a decade (Doddridge and Marshall, 2017; Nicolas et al., 2017; Stuecker et al., 2017; Turner et al., 2017; Alkama et al. 2020; Eayrs et al. 2021; Sabu et al., 2021).

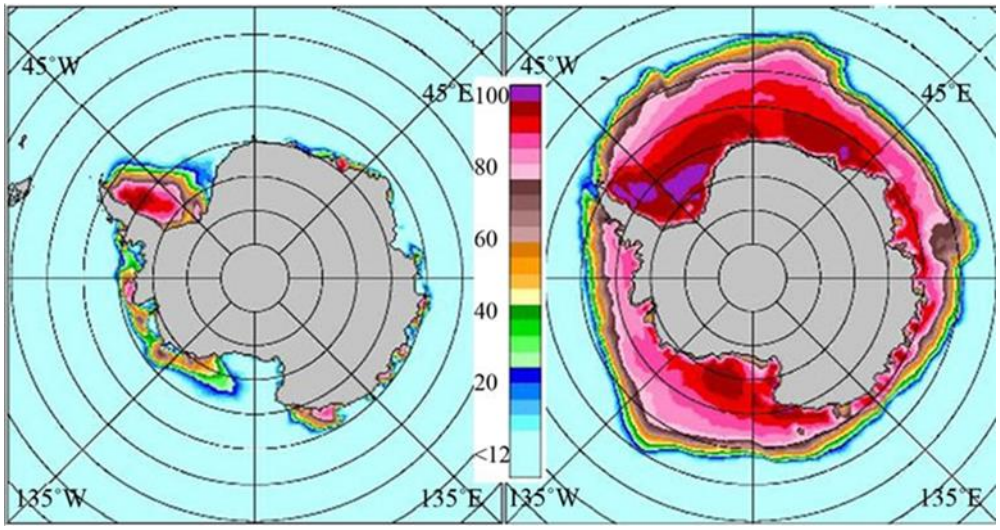

Fig. 1.3: A Maps of Southern Hemisphere sea ice concentration from February and September, averaged over the years 1979–2010, as derived from SMMR, SSMI, and SSMIS satellite observations. (Image source Parkinson and Cavalieri, 2012)

Due to limited understanding of the controlling factors of the Antarctic sea ice over a decadal to multi decadal time scale due to limitations of the satellite data, a longer understanding interms of geological time scale is met by the proxy records. A longer understanding of the sea ice extent which is offered by paleoclimate data is important to document the variability in the sea ice, the governing factors for their distribution, and other feedback mechanisms from decadal to glacial-interglacial timescales. Past sea ice changes are reconstructed using proxies such as fossil diatom communities and certain biomarkers archived in marine sediments, and geochemical tracers in polar ice cores.

1.6 Diatoms

The Diatoms are unicellular organisms belonging to the class Bacillariophyceae. They possess yellowish brown chloroplast with pigmentation of chlorophyll *a* and *c*; *β-carothene,* fucoxanthin, diatoxanthin,and diadinoxanthin (Jeffrey, Mantoura, & Wight, 2005). Due to large variation of the pigments, the diatoms are able to capture wide range of wavelength spectrum. Their valves have two sides in which the cell is encapsulated in an amorphous silica box, called the frustule. Some diatoms even have the typical petri dish structure. Their size ranges from 2 µm to 1-2 mm. They are divided into two orders which is defined based on the

shape of the frustule: Centrales (round diatoms) and Pennales (elongated diatoms) (Fig. 1.4). The diatom frustules are ornamented with presence of pores which are also called as areolae; processes which can be labiate, strutted, internal or external. The taxonomy of the diatoms is largely based on what is the shape of the diatom and what is the ornamentation on the frustule (Pfitzer, 1871; Simonsen, 1979; Round, Crawford, & Mann, 1990; Hasle & Syversten, 1996).

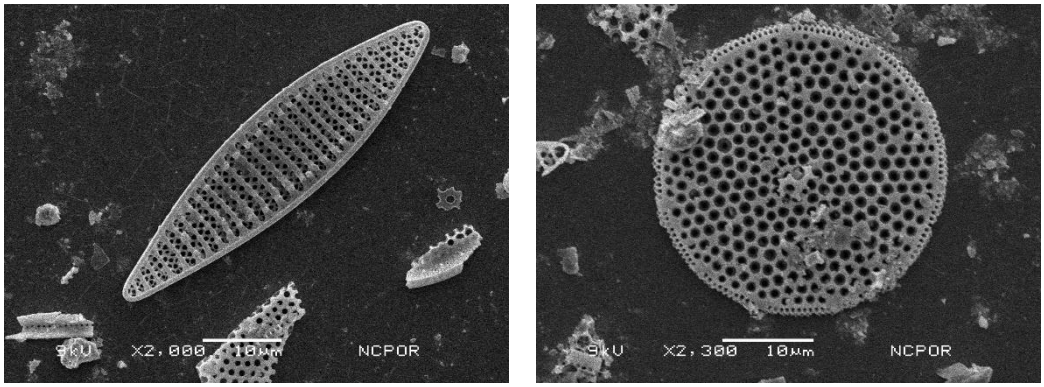

Fig. 1.4 Scanning Electron Microscope (SEM) image of pennate diatom, *Fragilariopsis kerguelensis* and centric diatom *Azpetia tabularis*

They reproduce by means of vegetative fission at a rate of 0.1 to 8 times per day. Due to this they are able to have a high mass of biota. Diatoms also reproduce sexually at a given threshold. Due to vegetative reproduction the size of hypovalves decreases at that time diatoms goes for sexual reproduction thus reviewing the full size of a vegetative cell. Some species undergoes resting spore formations i.e when the conditions are unfavourable (depleted nutrients, low sunlight, etc).

Diatoms are found in all type of aquatic environment but they are restricted to the photic zone. They play an important role in global cycling of silcic acid and carbon, they contribute up to 75% of the primary production of the SO (Treguer et al., 1995). They are major contributors to the carbon export to the deep ocean through the biological carbon pump (Buesseler 1998). Owing to the specific morphology of the diatoms (i.e. organic matter embedded into the siliceous frustule) and ecology, diatoms find various applications in numerous ways to infer paleo-oceanographic conditions containing methods which are based on micropaleontology (diatom identification) and geochemistry (i.e. biogenic content, organic biomarkers isotope geochemistry). Diatoms are very important tool to reconstruct past sea ice estimates (Armand, 1997, 2000; Crosta et al., 1998a, b; Armand and Leventer, 2003; Gersonde et al., 2005) and

past Sea Surface Temperature (SST) (Pichon et al., 1992a; Labeyrie et al., 1996). A quantitative interpretation of Sea ice extent and SST is achieved through transfer function. The size distribution of diatoms highly influences carbon sequestration efficiency because they sink faster and dissolute slowly therefore large cells export large amount of the carbon to the ocean floor (Smetacek 1999; Kemp et al., 2000). Diatom size is a useful indicator for reconstructing past changes in water quality, macronutrient concentration, past food web interactions and biogeochemical cycling (Finkel et al., 2009). Larger diatom frustules tend to occur in productive water (Margelef, 1969;). Nitrogen and phosphorus, both are limiting factors for the growth of diatoms of different species at different time and location.

Significant amount of work on SO SST and sea ice reconstruction is done using diatom as a proxy (Gersonde and Zielinski 2000; Crosta et al., 2004; Ferry et al., 2015). Proxies for Antarctic sea ice reconstruction are largely dependent on the diatom frustules preserved in sediments, aerosol proxies such as sea salt derived sodium present in Antarctic ice cores and highly branched isoprenoids (hydrocarbon compound synthesized by sea ice diatoms). Earlier studies on paleo sea ice in Atlantic sector of SO suggests northward extension of summer sea ice limit (65-70°S) upto present winter sea ice edge (56-60°S), while the winter sea ice limit extended upto Polar Frontal Zone (50-45°S) during glacial period (Gersonde and Zielinski 2000). First records on Mid-Brunhes century-scale SST and sea ice from the Atlantic Sector of SO indicated that the present day Antarctic Zone was seasonally covered by sea ice during MIS12 and 10 (glacial period) (Kunz-Pirrung et al 2002). A rare study (Gersonde et al., 2003) based on multiproxy approach (Diatom, radiolarian and foraminiferal assemblages) estimated summer SST and sea ice extent in Atlantic and West Indian sector of SO during the last glacial environment. Northward shift of zonal bands of ACC and also relative expansion of water realm south of the SAZ by ∽5° in latitude was indicated by the study (Gersonde et al., 2003).

A study from Indian sector of SO concludes that the winter sea ice limit reached its maximum extent upto ∽56°S during the glacial periods. This study also indicates that SST as the major parameter governing the advanced and retreat of sea ice during MIS transitions. But particularly during glacial stages, the advance of sea ice is mainly a positive feedback of ice on albedo, air temperature and meridional wind stress (Crosta et al., 2004). Similarly, a quantitative study by Gersonde et al., 2005 from Atlantic, Indian and Pacific sector of SO reveals maximum winter sea ice extended in the Atlantic and Indian sector close to 47°S showing northward displacement by 7–10° in latitude in the various sectors of SO. Whereas

the Summer SST indicated a northward displacement of the Antarctic cold waters between 5° and 10° in latitude in the Atlantic and Indian sectors. Observations from southtwest Pacific Sector of SO suggests expansion of winter sea ice during Antarctic cold reversal. The glacial sea ice expansion was concomitant with the northern migration of the ACC, PF SAF and or STF (Ferry et al., 2015).

Xiao et al., in 2016 investigated a series of sediment core from the Atlantic and Western Indian sector of SO and concluded that the last glacial summer SSTs of modern PF were 1-3° colder than modern conditions and Winter Sea Ice (WSI) expanded to modern PF. A study by Verana et al., 2016 contributes to the development of a coherent circum-Antarctic picture of temperature and sea-ice distribution during the Last Glacial Maxima (LGM). The result indicates major circum Antarctic cooling in the area of modern SAZ. This implies a surface water temperature range of the glacial ACC reduced by 3°C vs. modern conditions.

Apart from paleo sea ice research various other studies have focused on reconstructing the position of SO fronts during past climate which suggested that frontal positions were displaced northwards during glacial intervals (Carter and Cortese, 2009; Kohfeld et al., 2013). Reconstruction of fronts also provides details regarding the position of the Southern Hemisphere (SH) Westerly Winds (De Deckker et al., 2012; Kohfeld et al., 2013). Among these observations there is some work carried out in understanding significant relationship between the STF position and volume of Agulhas Leakage (Bard and Rickaby, 2009). Literature suggests that during warming the westerlies shifts southward which expands the oceanic gateway between the African continent and the STF and in turn increases the leakage from the Indian Ocean to the Atlantic. Similarly, a northward shift, as inferred from palaeorecords during glacial periods, would reduce the leakage (Beal et al., 2011).

However most of the studies pertaining to past reconstruction of the Antarctic sea ice are restricted to the LGM (Armand, 1997; Burckle and Mortlock, 1998; Crosta et al., 1998, Xiao et al 2016) and are non-quantitative reconstructions. Only exception to this are some studies from the SO that cover pre-LGM times (Gersonde and Zielinski, 2000; Kunz-Pirrung et al., 2002, Ferry et al 2015, Crosta et al 2004). Even the understanding of the past frontal positions and their interaction with the ocean circulation based on SST reconstruction are limited. Hence an attempt is made to understand the paleo sea ice extent and frontal positions and their interaction with the ocean circulation. Down core studies based on diatom taxonomy, absolute

abundance, relative abundance, diatom morphometry has been carried out. Therefore following objectives are formulated to address the above issue.

1.6. Objectives

- Quantitative reconstruction of Sea Ice Extent (SIE) and Sea Surface Temperature (SST) changes during the past glacial – interglacial period in Southern Ocean (SO) using fossil diatom.
- Understanding the latitudinal variation of SO fronts and SIE in response of diatoms to the changes in past climate.
- Studying the changes in diatom paleoproductivity and valve size in response to variation in SIE, SO fronts and nutrient conditions.

CHAPTER – 2

MATERIAL AND METHODOLOGY

2.1 Southern Ocean

The Southern Ocean (SO) is a region of extremes. It is exposed to the strongest wind on earth, the largest ice shelf and the widest range of seasonal sea ice (Wunsch 1998; Scambos et al. 2007; Thomas and Dieckman 2003). These interactions between the atmosphere, oceans and cryosphere have a strong impact on dynamics throughout the formation of the entire climate system. SO (Fig. 2.1) plays a key role in having global control over water mass formation, carbon sequestration, freshwater distribution, etc. due to its unique geographical condition which allows the exchange of water masses over the major oceanic basins (Rintoul et al., 2001, Tchernia 1980). SO habitat is characterized by topographic and oceanographic features. The zonal delimitation can also be seen with respect to distribution of habitat from north to south which is marked by seasonally variable sea ice, and oceanographic fronts with their distinct physical, biological and chemical characteristics (Constable et al., 2014). The bathymetry of the SO strongly steers the main circulation features eg presence of Ross gyre, Weddell gyre, Kerguelen Plateau, etc. These topographic features thus creates four natural sectors of the Southern Ocean – the Atlantic, Indian, West Pacific and East Pacific sectors as defined by constable et al., 2014.

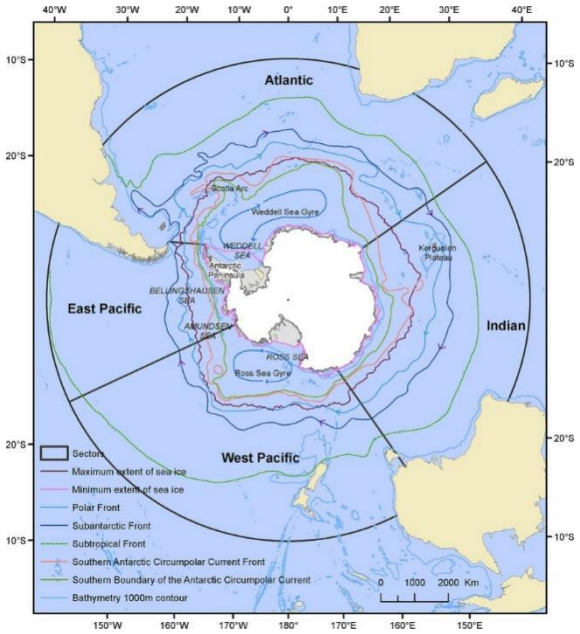

Fig. 2.1 Sectors of Southern Ocean (After: Constable et al., 2014)

2.2 Study Area: Indian sector of SO

To attain the thesis objectives, two sediment cores, SK 200/33 and MD 12 3401 CQ; from the Indian sector of SO are studied. See Table 2.1 for core details. The proposed study area is subdivided by Oceanographic fronts and winter/summer sea ice extent into a series of latitudinal bands/zones. From south to north these are as follows:

1. The sea ice zone (SIZ) (Treguer and Jacques, 1992) is bound by the summer sea ice extent to the North and thus characterized by permanent sea ice coverage. The area between the winter and summer sea ice limit is referred to as seasonal SIZ.
2. The Permanent Open Ocean Zone (POOZ) is bounded by APF to the north and the winter sea ice to the south. The APF is divided in two branches, one located north and the other located south of the Conrad Rise (Sokolov and Rintoul 2009b) (Fig. 2.2).
3. The Polar Frontal Zone (PFZ) is bounded to the north by the SAF and to the south by the APF (Orsi et al., 1995; Belkin and Gordon, 1996).
4. The Sub-Antarctic Zone (SAZ) is the area situated between the STF and SAF (Pollard et al., 2002).

Understanding the structure and location of the major fronts of the SO is of considerable importance. It has a direct influence on physical and biological processes of the SO. They play significant role in global atmospheric interaction and therefore it is important to monitor variability in position of the fronts. Hence two sediment cores are studied from different frontal location for paleoceonographic studies which is based on diatoms.

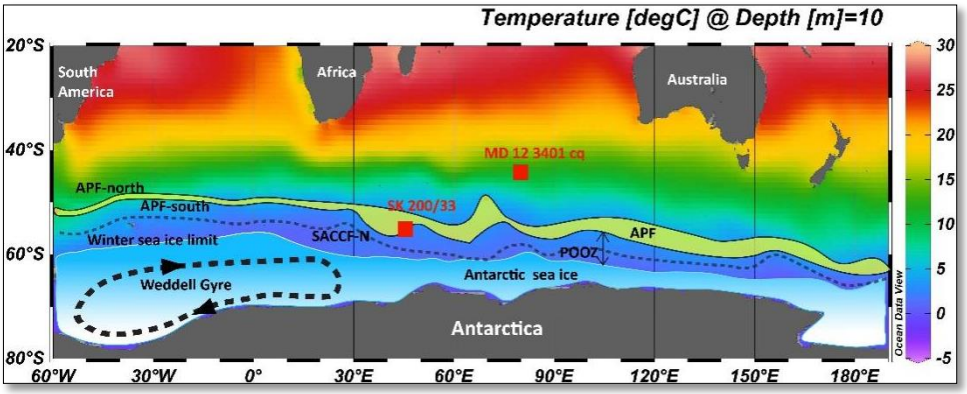

Fig. 2.2: Sediment core location of SK 200/33 and MD 12 3401 cq

2.3 SEDIMENT SAMPLING

2.3.1 SK 200/33

Sediment core SK 200/33 was obtained on-board ORV *Sagar Kanya* in 2004 from 55˚01'S-45˚09'E, at a water depth of 4204 m. The core site is located in the SW Indian sector of the SO within the Permanently Open Ocean Zone (POOZ), sea-ice free region, where mean summer SST is ~2 ˚C (World Ocean Atlas 2013, Lorcarnini et al., 2013) (Fig. 2.2). The present core site is bound by the Antarctic Polar Front (APF) to the north and Southern ACC Front (SACCF) and WSI limit to the south (Comiso et al., 2003; Sokolov and Rintoul, 2009b; Cavalieri and Parkinson, 2008). Several definitions of the APF exist such as the northernmost extent of the subsurface 2 ˚C temperature minimum (Orsi et al., 1995) or the zone of maximum sea-surface height (Sokolov and Rintoul, 2009a). Unfortunately, these quantities cannot be reconstructed through diatom transfer functions. The APF is also a region where a steep gradient in surface isotherms between ~2.5 and ~4 ˚C has been observed (Lutjerhams et al., 1984; Park et al., 2014). In the SW Indian sector, the APF has been evidenced by a steep gradient in SST between 2.7 and 5.5 ˚C (Anilkumar et al., 2006; Luis et al., 2009; Belkin and Gordon 1996). Following this definition, the APF is located at ~48-52 ˚S along the 45 ˚E longitude in the SW Indian sector of the SO (Anilkumar et al., 2006; Luis et al., 2009). Similarly, the SACCF is defined as a steepening of the isotherms between 1 and 2 ˚C and is positioned at 57-60˚S in this sector (Sokolov and Rintoul, 2009a). The sediment core is composed of alternating layers of light olive-grey colour diatom-rich sediments and yellowish-clayey sediments (Thamban et al., 2005). The top 100 cm of the core were utilised in the present study and were subsampled at every 1 cm interval for diatom census counts.

2.3.2 MD 12 3401 cq

The sediment core MD 12 3401 cq is retrieved onboard Marion Dufresne (2012) from 44˚40.73S Latitude and 80˚23.58E Longitude by calypso from a water depth of 3400m. The core is 821cm long spanning 58kyr, however in this study it is studied till 388cm spanning last 28.5kyr. The core location is positioned in the SAZ wherein it is bound to the north by STF and to the south by SAF. The Kergulen Island which encompasses the region between 46 to 68˚S and 62 and 85˚E acts as a major topographic obstacle for ACC in this area.

Table 2.1: Sediment core details

Core id	Latitude	Longitude	Water depth (m)	Core length (cm)	Age (kyr)	Cruise
SK 200/33	55˚01'S	45˚09'E	4204	100	156	ORV Sagar Kanya 200 (2004)
MD12 3401 cq	44˚40.73' S	80˚23.58'E	3400	821	40	Marion Dufrense (2012)

2.4 CHRONOLOGY – explained in respective chapters (chapter 4, 5 and 6)

2.5 Sample Preparation

Cleaning of the sediment samples and preparation of permanent slides for light microscopy were performed according to the method described by (Batterby 1986; R. Gersonde; U. Zielinski 2000 and Crosta et al., 2020) with some modifications (Dr. Xavier Crosta, University of Bordeux, France). Around 0.3-1g (depending on diatom concentration) of the raw freeze dried sediment were leached with H_2O_2 to remove the organic matter coating the valves, and with HCl to remove carbonates, at a temperature around 60°C in a beaker. Centrifugation of the solution containing the diatom valves was carried to ensure better recovery of small diatoms. From the diluted residue, 1–2 drops were taken into a prefilled petri dish (containing cover slip and water), and wool wire was used to evacuate the water (Pichon et al., 1987; Rathburn et al., 1997). The coverslip was glued to slide when it was dry (overnight) using Naphrax as a Mounting medium. Two slides were prepared per sample (Koc Karpuz & Schrader, 1990; Zielinski, 1993) in two different Petri dishes to avoid artifacts on subsamples during processing (Pichon et al., 1987; Rathburn et al., 1997).

2.6 Taxonomic notes

Identification of diatoms was carried out at 1000 x magnification on a Nikon Eclipse Ti inverted polarising microscope. The major taxonomic references includes Hustedt (1930), Round et al., 1990, Fryxell, 1979,1986, Armand and Zielinski, 2001, Pichon et al., 1992, Armand, 1997, Adrian Cefarelli, 2010, Crosta et al., 2005) with consulting additional personal sources (Dr. Xavier Crosta, University of Bordeux, France).

2.7 Diatom counts

From each sample, 350 diatom valves (175 diatom valves per slide) were counted at ×1000 magnification using a Nikon Eclipse Ti-U inverted microscope. This provides an accurate representation of the diatom diversity, and therefore provide better confidence in the paleoceanographic reconstructions (Allen, Pike, Pudsey, & Leventer, 2005). Each valve was identified to species level using taxonomic identification guidelines by Hasle and Syvertsen (1997), Scott and Merchant (2005), Round et al., 1990 and Cefarelli et al., 2010. The relative abundance of each species was determined as its ratio to the total diatom assemblage. In addition to the relative diatom abundance, the diatom absolute abundance (DAA) per gram of sediments was also calculated using the equation presented in Crosta et al., 2008. Diatoms were counted for every 1cm interval (SK 200/33) and every 4cm (MD 12 3401 cq) throughout the sediment core.

The diatom species from the core which are having similar environmental conditions were grouped together as determined by Q mode factor analysis (Table 2) (Crosta et al., 1998a). The diatom species are grouped into four groups as:

a. 'Sea ice group' which is represented by the species thriving in sea surface temperature range of -1 to 1°C and is indicative of 8 -11 months of sea ice/yr.

b. 'Water Stratification group' which is represented mainly by Chaetoceros group of diatoms which flourish in temperature range of 0 to 2° C and represents 5-9 months/yr of sea ice cover.

c. 'Permanent Open Ocean Zone group' (POOZ group) characterized by open ocean group of diatoms. They are found abundantly in temperature range of 2 to 10° C and represents sea ice cover of 1 to 7 months/yr.

d. 'Sub Antarctic Zone group' (SAZ group) which comprises of species blooming in warm water. They prefer to proliferate in 11 to 14° C temperature range and if found in abundance represents no sea ice cover.

The total abundance of the diatom was calculated using following formula and the abundance was expressed as Total abundance × 10^6 valves/g of the sediment.

$$\boldsymbol{Abundance} = \frac{\boldsymbol{no.of\ valves}}{\boldsymbol{no.of\ field\ of\ view}} \times \frac{\boldsymbol{surface\ area\ of\ petridish}}{\boldsymbol{surface\ area\ of\ field\ of\ view}} \times \frac{\boldsymbol{dilution}}{\boldsymbol{volume\ of\ drop}} \times \frac{\boldsymbol{no.of\ drops}}{\boldsymbol{weight\ of\ the\ sample}}$$

Table 2.2: Diatom groups used in the present study, after Crosta et al. (2004).

Sea ice group	POOZ group	Water Stratification group	SAZ group
Actinocyclus actinochilus, F. curta, F. cylindrus, F. obliquecostata, F. ritscheri, F. sublinearis	*F. kerguelensis, F. rhombica, F. separanda, Rhizosolenia styliformis gp, Thalassionema nitzschioides, Thalassiosira gracilis, T. lentiginosa, T. oliverana, Thalassiothrix sp., Trichotoxon reinboldi*	*Chaetoceros resting spores, Rhizosolenia antennata, Thalassiosira antarctica*	*Azpetia tabularis sp., Hemidiscus cuneiformis, Thalassionema nitzschoides var. lanceolata, T. eccentrica, T. oestrupii gp*

2.8 Transfer function for SST and sea ice estimation

The transfer function (Crosta et al., 2004) provides the quantitative estimates of SIE and SST. A transfer function is a statistical method that analyses census counts of fossil assemblages to produce absolute values of surface properties by comparing fossil samples to a subset of modern samples having definite modern conditions. It produces the calibrated quantitative evaluations of parameters of environment like surface temperature of ocean or air (Hillaire-Marcel, C., & De Vernal, A. (Eds.). (2007), *Proxies in Late Cenozoic Paleoceanography*. Elsevier.). The WSI conditions and summer SST were reconstructed by applying the modern analog technique (MAT) to diatom assemblages as fully detailed in Crosta et al. (2020). The modern dataset is composed of 249 surface sediment samples, for which the modern summer (January till March) SST were interpolated from 10 m of water depth on a 1˚*1˚ grid from the World Ocean Atlas 2013 (Locarnini et al., 2013) using Ocean Data View (Schlitzer, 2002). The monthly sea-ice concentration was interpolated on 1˚*1˚ grid using the numerical atlas of Schweitzer (1995) covering the 1978-1994 period.

The measurement of annual sea ice duration is denoted by the number of months per year during which each core top location remains covered by sea ice. This yearly sea ice duration is calculated by summing up the monthly sea ice values. Specifically, regions with 0 t o15% sea ice concentration are considered ice free areas and are assigned 0 months of sea ice duration per year. Locations with the sea ice concentrations ranging from 15 to 40% are categorised as having unconsolidated sea ice and are attributed 0.5 months of sea ice duration per year. Finally the areas with sea ice concentration of 40 to 100% are classified as having consolidated ice and assigned 1 month of sea ice duration per year. The core-tops cover the whole SO from the Antarctic coast to the Subtropical Zone, essentially in the Atlantic and Indian sectors (Armand

et al., 2005). The core-tops were visually evaluated for dissolution (preservation of the valves, fragmentation, and presence of diatoms covering the whole range of sizes). The core-tops have been, as much as possible, assessed for their age through radiocarbon dating or isotopic control and only sub-recent to recent core-tops were included in the modern database. The species database is composed of the relative abundance of 32 diatom species. The MAT used here was implemented from the "bioindic" package (Guiot and de Vernal., 2011) built on the R-platform (http://cran.r-project.org/). For each fossil sample, the selection of the five most similar analogues was done using the chord distance. Quantitative estimates of summer SST, Winter sea ice concentration (WSIC) and Winter sea ice duration (WSID) represent a distance-weighted mean of the climate values associated to the selected modern analogues (Guiot et al., 1993). The MAT approach yields a determination coefficient (R2) of 0.96 and a root mean square error of prediction (RMSEP) of 0.96 ˚C for summer SST, a R2 of 0.92 and a RMSEP of 10.2 % for WSIC, and a R2 of 0.96 and a RMSEP of 0.86 month/year for WSID. The linear correlation coefficient (R) between WSID and SST in the modern database is -0.78 (n = 138 samples presenting non-zero sea-ice values), yielding a determination coefficient of 0.60. This indicates that 60% of the modern distribution of the yearly sea-ice duration is explained by changes in SST, therefore suggesting ocean temperature is the prime factor driving the sea-ice field but that other processes (air temperatures, winds, ocean currents, mechanical breakup, etc) are almost equally important, especially at short spatial-temporal scales.

There are two types of uncertainties associated with MAT (Modern Analog Technique): One is global error of prediction: This error is based on the modern dataset and has been found to be approximately 1°C for SST (Sea Surface Temperature) and 0.9 months per year for SIP (Sea Ice Presence). Both of these errors demonstrate a high correlation with an R-squared value of 0.96. Second is sample specific error: MAT is unique among other transfer functions like Imbrie and Kipp Method (IKM) and weighted average partial least squares (WAPLS) as it allows for sample-specific error assessment. The other methods work on global error. Thus MAT provides a more comprehensive understanding of the prediction errors associated with individual samples.

2.9 Diatom size measurements

The *F. kerguelensis* and *T. lentiginosa* absolute abundance (valves/g of sediments) (Fig. 2.3) were calculated (350 valves were counted per sample) following the equation detailed in Crosta et al., 2008. Lengths of the apical and transapical axes of *F. kerguelensis* and diameter of *T. lentiginosa* were measured manually on the computer screen using the Nuclear Inelastic

Scattered (NIS) Element imaging software connected to the Nikon Eclipse E 600 POL microscope at 1000X magnification (Fig. 3). Reproducibility of the measurements is around 0.1 µm. Sizes of these two diatoms were measured every 1 cm from 0 to 100 cm providing a ~1700 years cm^{-1} mean temporal resolution. In each sample, 70 specimens of each species were measured and the mean length, width and diameter were calculated out of the 70 measures and are believed to be representative of the species mean morphometric parameters at each depth interval. The fluxes of *F. kerguelensis* and *T. lentiginosa* were calculated through the equation Flux (valves $cm^{-2}ka^{-1}$) = Absolute abundance (valves g^{-1} of sediments) × Density of the dry sediments (g/cm^3) × Sedimentation rate (cm/ka).

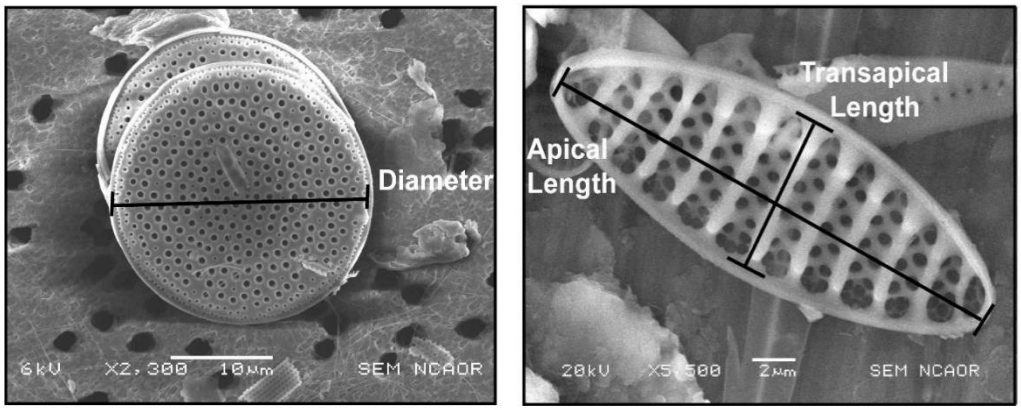

Fig. 2.3: Scanning electron microscope images of *Fragilariopsis kerguelensis* and *T. lentiginosa* used for morphometric analysis.

2.10 Biogenic silica analysis

Biogenic silica was extracted from the bulk sediment by using 2M Na_2CO_3 at 80°C for 5 h following the procedure of Mortlock and Froelich (1989). The extraction was preceded by a H_2O_2 leaching (10%) and an acid leaching using 1N HCl for 30 min, each at room temperature. The dissolved silica concentration was measured by molybdate-blue spectrometry using BioTek® Synergy 2 Spectrophotometer. This method is particularly suited for opal-rich sediments, as is the case in this study. Since the determination of biogenic silica is tightly related to the extraction procedure, great care was taken in the present study to use a reproducible and consistent protocol throughout the analysis. Duplicate measurements were conducted producing an accuracy better than ±1%.

CHAPTER – 3

ANNOTATED INDEX OF KEY DIATOM SPECIES

3.1 The Diatom

Diatoms which are unicellular organisms belongs to the major group of eukaryotic algae who shares a close ancestry with Heterokont (Sims et al., 2005; Young 2010). They are one of the most common phytoplanktons. They grow abundantly in aquatic ecosystem with the availibility of light and nutrients. Although tiny in their size, these organisms are responsible for the 20 percent of the primary production globally. Owing to the silica frustules, diatoms poses splendid fossil evidences which suggests their evolution during the Jurassic period of Mesozoic era. The subsequent diversification is seen in the Cretaceous. The three major clades are Coscinodiscophyceae (radial centrics), Mediophyceae (polar centrics + radial *Thalassiosirales*) and Bacillariophyceae (pennates) appeared in the Jurassic, early Cretaceius and late Cretaceous respectively (Kooistra et al., 2007, Medlin 2016).

The aim of this chapter is to list out the abundant diatoms from their specific groups i.e. Sea ice diatom group, Permanently open ocean zone diatom group (POOZ), water stratification group and subantarctic zone diatom group (SAZ) according to their taxonomic description referring to different authors. The diatom groups are presented with Light Microscope (LM) and Scanning Electron Microscope (SEM) images.

Diatom species having similar environmental preferences based on Q mode factor analysis were grouped together (Crosta et al., 1998a, Crosta et al., 2005a; Armand et al., 2005; Romero et al., 2005). The diatom groups used hereafter are: The Sea-ice diatom group, POOZ diatom group, water stratification diatom group and SAZ diatom group.

3.2. The Sea-ice diatom group

The group is represented by the species thriving in SST range of -1 to 1˚C and sea-ice duration of 8-11 months/year. These species includes *Actinocyclus actinochilus, Fragilariopsis curta, Fragilariopsis cylindrus, Fragilariopsis ritscheri, Fragilariopsis obliquecostata, Fragilariopsis sublinearis*.

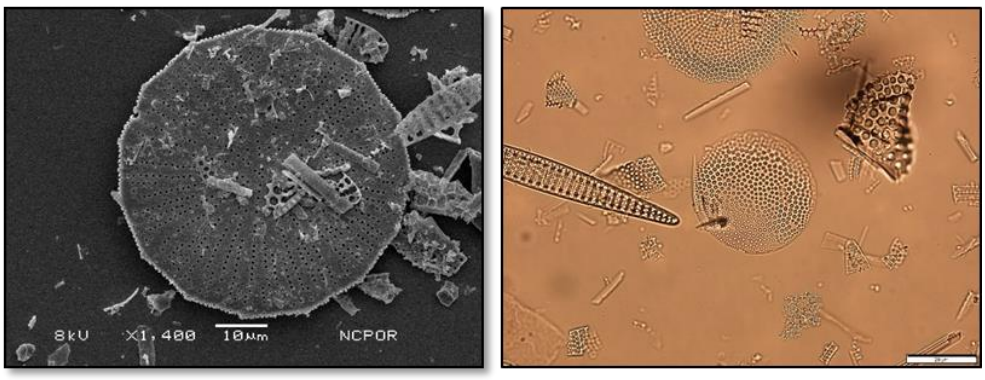

Fig. 3.1: SEM (left) and LM (right) image of *Actinocyclus actinochilus*

Actinocyclus actinochilus *(Ehrenberg) Simonsen*

Description: The cells are solitary, varying from cylindrical to disc-shaped. The valve is flat, with rounded edges, and measures 20-112µm in diameter. Aerosols may occasionally appear curved or incomplete, and the areolation shows variability. Approximately 5-11 aerosols are present within a 10 µm space, each surrounded by a thick border. A labiate process can be found at a distance of 10 µm, about 9-15 µm apart, and laterally dilated. At times, pseudonodules are observed near the flat part of the valve surface and the junction of the mantle. The valve envelope typically showcases around 13-21 streaks in the 10 µm range (refer to Fig. 3.1). When *Actinocyclus actinochilus* accounts for over 2% of the total, it indicates a sea ice duration exceeding 7 months per year (Armand et al., 2005). *Actinocyclus actinochilus* is commonly reported in sedimentary records and distributed in coastal waters near Davis Station, East Antarctica, the Weddell Sea, as well as the Indian and Atlantic sectors of Antarctica, and the Kerguelen Islands. References for figures: Villareal and Fryxell (1983), Figs. 21–24; Zielinski (1993), Pl.1 Figs. 1 and 3.

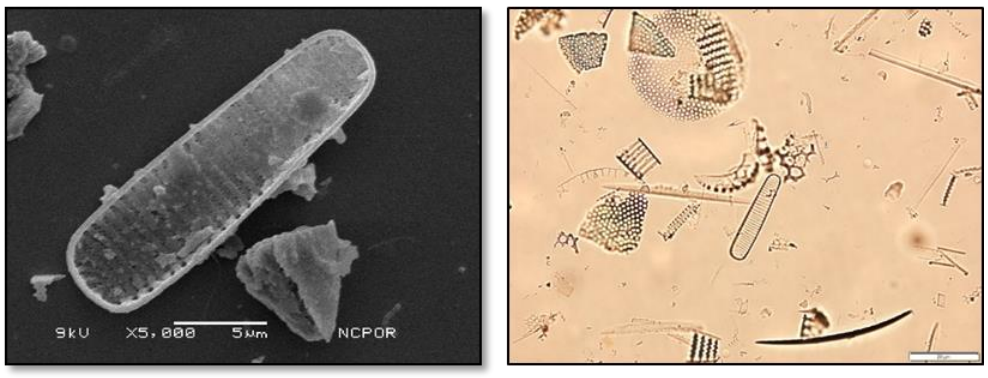

Fig 3.2: SEM (left) and LM (right) image of *Fragilariopsis curta*

Fragilariopsis curta (Van-Heurck)

Description: F. curta (Fig. 3.2) cells tend to form chains, but they can also occur as single cells. They have rounded poles, with one pole broader than the other. The apical axis measures 10-42 µm, and the transapical axis ranges from 3.5-6 µm. Approximately 9-12 transapical striae are present within an area of 10 µm. The interstitial membrane contains perforations in the form of areolae. F. curta is most abundant in Prydz Bay, the Ross Sea region, and along the George V Coast. They are also distributed throughout the Southern Ocean, including locations near Davis Station and in the coastal waters off Syowa Station, East Antarctica. References for figures: Hustedt (1958), Pl. 11, Figs. 140–144; Hasle (1965), Pl. 12, Figs. 2–5, Pl. 13, Figs. 1–6.

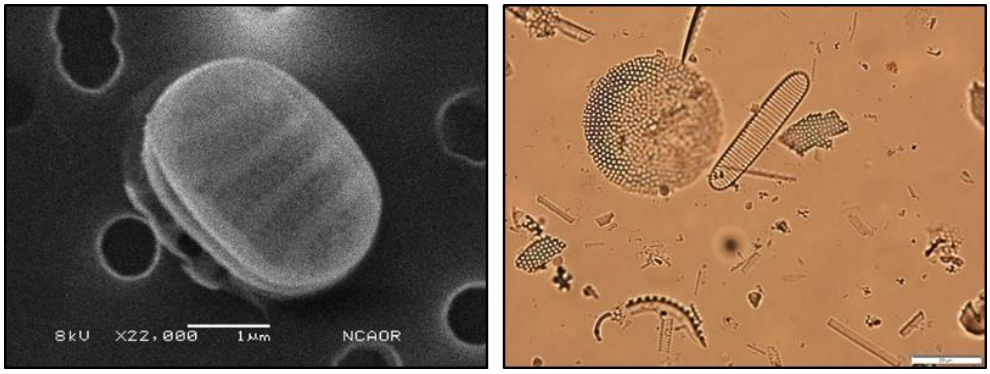

Fig 3.3: SEM (left) and LM (right) image of *Fragilariopsis cylindrus*

Fragilariopsis cylindrus (Grunow) Krieger

Description: The cells of *Fragilariopsis* cylindrus can occur either as solitary entities or in chain formations, attaching themselves via the valve surfaces (Fig. 3.3). In a valve view, they appear linear with rounded ends. The apical axis measures 3-48 µm, while the transapical axis ranges from 2-4 µm. The transapical striae are straight, with approximately 13-17 present in a 10 µm area. The interstitial membranes exhibit perforations with the presence of tiny areolae, which can be scattered or arranged in 2-3 rows. Canal raphe and fibrulae structures are also present.

When *Fragilariopsis cylindrus* reaches a maximum abundance of 2.9%, this occurrence is linked to February sea surface temperatures between 0.5 and 1 ˚C. An abundance of over 2% indicates a sea ice duration exceeding 7.5 months per year. It is well-established that

Fragilariopsis cylindrus predominantly occupies sea ice-covered environments, with the highest reported abundances along the Antarctic coast (Armand et al., 2005). The sea ice near Davis Station, East Antarctica, serves as the type locality for this species. Additionally, they can be found in the Southern Ocean, Arctic Ocean, Weddell Sea, and Benguela Current regions. References for figures: Hustedt (1958), Pl. 11, Figs. 145–146; Hasle (1965), Pl. 12, Figs. 6–12; Pl. 14, Figs. 1–10.

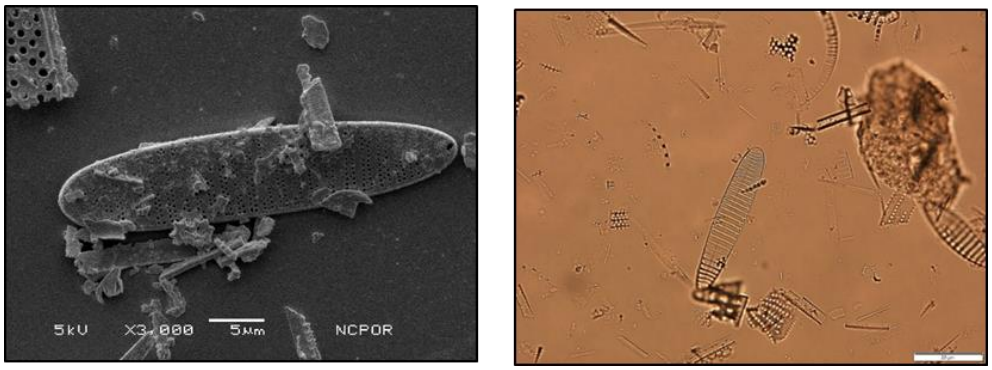

Fig 3.4: SEM (left) and LM (right) image of *Fragilariopsis ritscheri*

Fragilariopsis ritscheri *hustedt*

Description: The cells of *Fragilariopsis ritscheri* can occur in chain formations or as solitary entities (see Fig. 3.4). In a valve view, the smaller cells appear linear to elliptical, while the larger cells are linear to lanceolate, broader at one pole. The apical axis measures 22-60 µm, and the transapical axis ranges from 8-9 µm. The transapical striae at the center of the cell are straight, whereas those at the valve poles are curved. The striae adjacent to the broader pole are more oblique compared to the narrower pole. The interstitial membranes are perforated with the presence of 2-3 rows of alternating poroids. Canal raphes are also present, but their distinctness may vary.

Fragilariopsis ritscheri occurs in low abundances, i.e., <3%, in sea ice regions, with some seemingly expatriated occurrences observed in the South Atlantic PFZ. Observations in the literature suggest that the species is found with increasing abundances north of the Antarctic Divergence (DeFelice and Wise, 1981; Zielinski and Gersonde, 1997). The highest reported abundance of *F. ritscheri* to date is 3.28% in the Ross Sea (Cunningham and Leventer, 1998), whereas Zielinski and Gersonde (1997) observed a maximum of 2.6% in the South Atlantic

sector (Armand et al., 2005). References for figures: Hustedt (1958), Pl. 11 Figs. 133–136; Hasle (1965), Pl. 1, Fig. 20; Pl. 4, Figs. 1–10; Pl. 15, Figs. 12–13; Pl. 17, Fig. 8.

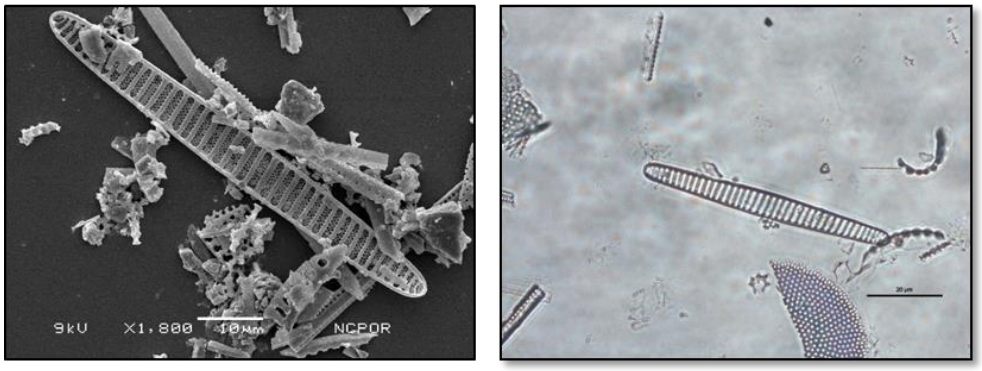

Fig 3.5: SEM (left) and LM (right) image of *Fragilariopsis obliquecostata*

Fragilariopsis obliquecostata *(Van Heurck) Heiden* from *Heiden et Kolbe.*

Description: The cells of *Fragilariopsis obliquecostata*, when viewed from the valve, exhibit a linear to lanceolate shape and are predominantly found as solitary entities (refer to Fig. 3.5). The apical axis measures between 57-110 µm, while the transapical axis ranges from 8-10 µm. The transapical striae are typically straight, numbering around 6.5 to 8 in a 10 µm area, but they can also appear curved or oblique at the poles. The canal raphe is significantly eccentric, and central nodules are absent in this species.

Fragilariopsis obliquecostata is most abundant in the Ross Sea and the Prydz Bay Region. Lower abundances are observed in the marine sediments of the Antarctic Peninsula and along the George V Coast. Locations with over 7 months per year of sea ice cover, where highly consolidated ice conditions prevail during winter (65–90%), are associated with the highest abundances, while the influence of summer sea ice concentrations on species distribution seems to be less significant. According to temperature–abundance plots from earlier literature (Armand et al., 2005), this species shows a preference for summer temperatures ranging from -1.3 to 2˚C, with the maximum abundance occurring within temperatures between -1 and 0 ˚C. The highest abundances of the species have been reported in the Weddell Sea (16.9%, Zielinski and Gersonde, 1997) and the Ross Sea (13.59%, Cunningham and Leventer, 1998). Figure references: Hasle (1965), Plate.7, Figs. 2–7; Zielinski (1993), Plate. 5, Figs. 15-17.

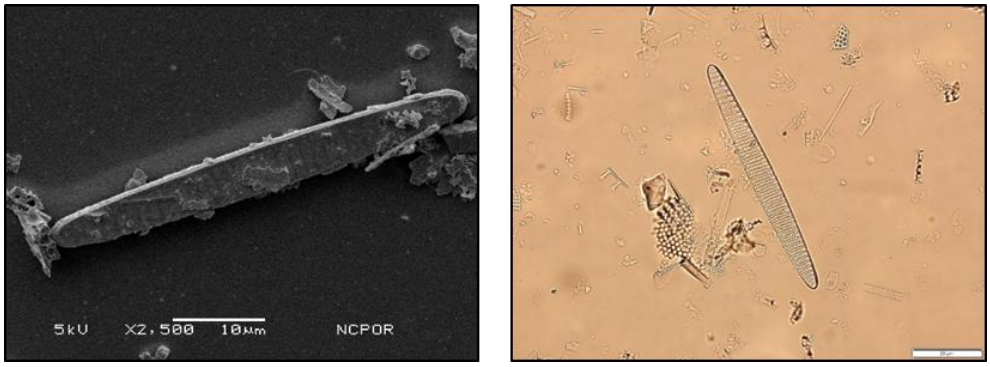

Fig 3.6 SEM (left) and LM (right) image of *Fragilariopsis sublinearis*

Fragilariopsis sublinearis *Van Heurck.*

Description: The cells of *Fragilariopsis sublinearis* are solitary and exhibit a linear to lanceolate shape. In the valve view, they possess obtuse apices (see Fig 3.6). The apical axis ranges from 30-90 µm, while the transapical axis measures 5.5-8 µm in length. The transapical striae are broad and straight, with 1-3 striae near the valve poles that can be either oblique or curved. The interstitial membrane of perforations is rarely visible, potentially comprising of two rows of small alternating poroids. Fibulae are present in the same number as the striae.

Fragilariopsis sublinearis exhibits maximum abundance associated with February sea surface temperatures ranging from -1.3 to 2.5 °C (refer to Table 1, Fig. 4A). In cases where abundances of *Fragilariopsis sublinearis* exceed 2%, it indicates a sea ice duration greater than 7.5 months per year. Geographically, the major abundances of *Fragilariopsis sublinearis* are almost exclusively located in Prydz Bay, Ross Sea, and along Wilkes Land, within the maximum February sea ice extent. *F. sublinearis* shares a similar distribution in the Antarctic Zone with *Fragilariopsis ritscheri* and *Fragilariopsis obliquecostata* (Kozlova, 1966; Hasle, 1965; Hasle, 1976; Tanimura, 1992; Zielinski and Gersonde, 1997). Like the latter species, Fragilariopsis sublinearis is considered to have heightened abundance in sediments south of the Antarctic Divergence (Armand et al., 2005). Figure references: Hasle (1965), Plate. 7, Fig.1; Plate. 11, Figs. 1–10; Plate. 12, Fig. 1; Zielinski (1993), Plate. 5, Figs. 25–26.

3.3. The POOZ diatom group

The group is characterized by open ocean diatoms. They are found abundant within the SST range of 2 to 10 ˚C and sea-ice cover of 1 to 7 months/year. These species includes *Fragilariopsis kerguelensis*, *Fragilariopsis rhombica*, *Fragilariopsis separanda*,

Thalassiosira gracilis, Thalassiosira lentiginosa, Thalassiosira oliverana, Thalassiothrix antarctica, Trichotoxon reinboldi.

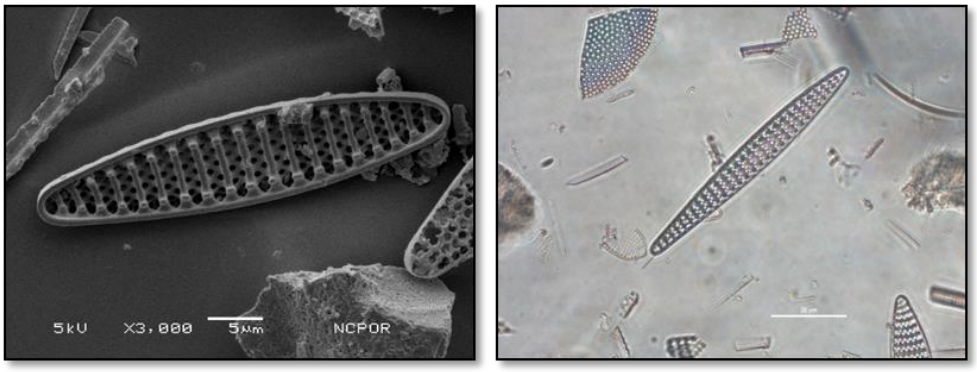

Fig 3.7: SEM (left) and LM (right) image of *Fragilariopsis kerguelensis*

Fragilariopsis kerguelensis *(O'Meara) Hustedt.*

Description: The cells of *Fragilariopsis kerguelensis* can be found either as solitary entities or forming ribbon-shaped colonies, which are attached by the valve surfaces (refer to Fig 3.7). When observed from the girdle view, these valve surfaces appear curved at the ends, while in the valve view, the cells exhibit an elliptical shape. The apical axis measures 10-76 µm, and the transapical axis ranges from 5-11 µm in length. The transapical striae are coarse and straight. Interstitial membranes punctuate with the presence of two rows of alternating areolae. *Fragilariopsis kerguelensis* shows maximum abundances between 70–83% and is typically observed in a zone constrained between the maximum summer sea-ice edge and the Polar Front. Their occurrence in relation to modern sea surface temperatures (SST) reveals that they are most abundant under February SSTs of 1–8 ˚C. Abundance gradually decreases above 8 ˚C, reaching less than 5% at 19 ˚C, while abundances sharply decline below 0˚C and above 20˚C. *Fragilariopsis kerguelensis* is considered endemic to the waters of the Southern Ocean. The geographic distribution indicates that they are dominant assemblages in the open ocean zone (Crosta et al., 2005). However, along the Antarctic coast, many researchers have reported a lack of high abundances of *Fragilariopsis kerguelensis* (Crosta et al., 2005). Figure references from Hustedt (1958), plate 10, figures 121–127; Hasle (1965), plate 4, figures 11–18.

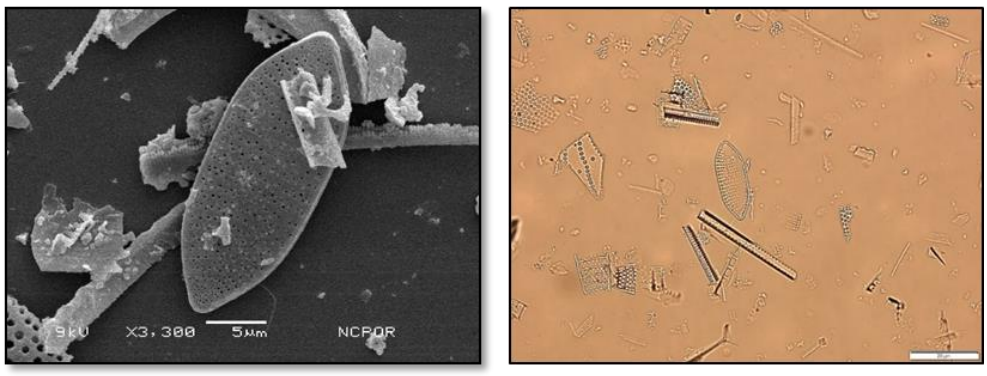

Fig 3.8: SEM (left) and LM (right) image of *Fragilariopsis rhombica*

Fragilariopsis rhombica *(O'Meara) Hustedt.*

Description: The cells of *Fragilariopsis rhombica* exhibit an elliptical to circular shape and taper towards the poles. The apical axis measures 8-53 µm, with a transapical axis ranging from 7-13 µm. The transapical striae are curved towards the poles but straight at the center. The interstitial membrane consists of one or two rows of poroid areolae, and a central nodule is typically absent (see Fig 3.8). *Fragilariopsis rhombica* is often found in abundances between 1–3% in sediments close to the Antarctic coast. The dispersion of this diatom in the sediments is related to the summer sea ice's northern side limit, with few sporadic occurrences observed between this limit and the winter sea ice edge, along with rare observations extending into the Subantarctic Zone (SAZ). The species' favored temperature range in February is -1.3 to 11.5 ˚C, with the majority of elevated abundances occurring between -1 and 1 ˚C. Regarding annual sea ice cover, the major abundances of the species were observed in regions where sea ice persists for 7–9 months of the year (Armand et al., 2005). *Fragilariopsis rhombica* is distributed in coastal waters near Davis Station, East Antarctica, as well as in the Southern Ocean, Bellingshausen Sea, and South Orkneys regions. References for figure are in Hustedt (1958), Plate. 10, Figs. 113–120; Hasle (1965), Plate. 10, Figs. 2–6; Plate. 9, Figs. 1–6; Plate. 4, Fig. 19; Plate. 1, Fig. 6.

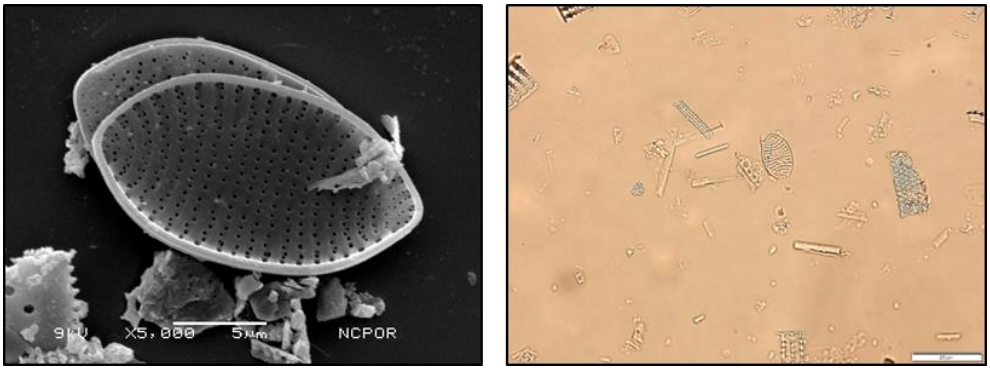

Fig 3.9: SEM (left) and LM (right) image of *Fragilariopsis* separanda

Fragilariopsis separanda *Hustedt*.

Description: The cells of *Fragilariopsis separanda* are solitary and vary in shape from elliptical to lanceolate in their valve view when they are small. However, when they are large, they appear linear with tapering ends (see Fig 3.9). The apical axis measures 10-33 µm, and the transapical axis ranges from 8-13 µm in length. The interstitial membrane exhibits perforations with one or two rows of poroids near the margin. The canal raphe contains broad fibulae with narrow openings between them.

Fragilariopsis separanda is most dominant in the Ross Sea and Prydz Bay regions, generally observed around the Antarctic coast. The species is distributed throughout the Southern Ocean, primarily north of the winter sea ice extent. This indicates the species' ability to be more easily transported in bottom water currents, particularly evident in the Southwest Pacific sector, south and east of New Zealand.

The highest abundances of *Fragilariopsis separanda* are associated with the February sea surface temperature (SST) signature of -0.5 to 0 ˚C. Previous literature points towards the species exhibiting the highest maximum abundances at offshore locations rather than in-shore coastal environments (Armand et al., 2005). Figure references taken from Hustedt (1958), Plate. 10, Figs. 108–112; Hasle (1965), Plate. 9, Figs. 7–10; Plate. 10 Fig. 1.

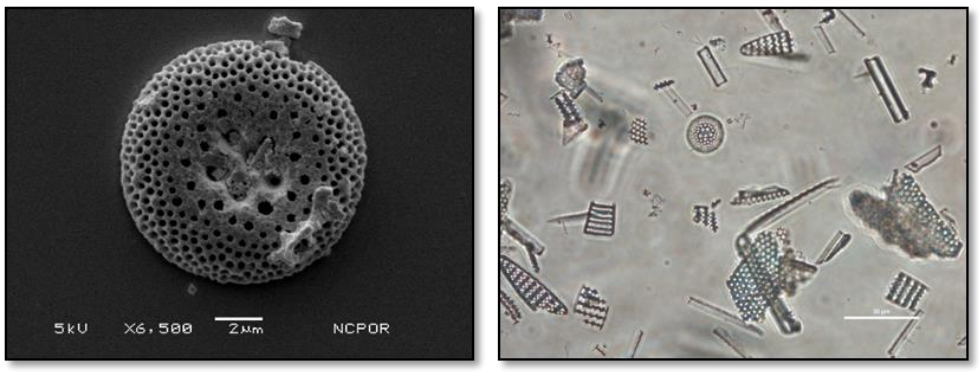

Fig 3.10: SEM (left) and LM (right) image of *Thalassiosira gracilis*

Thalassiosira gracilis *(Karsten) Hustedt.*

Description: The cells of this species can occur as solitary entities or in chain formations. They are highly silicified, featuring thin chitinous strands extending from the central strutted process (refer to Fig 3.10). The valves are flat and circular, measuring about 5-28 µm in diameter. Coarse areolations are present, with approximately 8-12 in the central 10 µm area, and the number increases towards the margin. The loculate opens externally through a simple foramen and internally through a finely pored velum. The margin is adorned with a single ring of processes, approximately 3-4 in a 10 µm area. Labiate processes are solitary and located at about one-third of the distance from the valve center to the margin.

These diatoms are distributed in the Atlantic sector of the Atlantic, Pacific, and Indian Oceans, as well as in the sub-Antarctic waters of the Southern Ocean. Their highest abundances are associated with February sea surface temperatures (SST) between 1 and 2 ˚C. The abundance shows a steady decline from these high points, reaching around ~8 ˚C. With the exception of the highest abundance point in the Antarctic Peninsula, the distribution with respect to sea ice parameters indicates an increasing occurrence with longer sea ice duration, reaching a maximum of 8.5 months per year. Abundances then decrease with continued presence of sea ice. During summer sea ice conditions, this species group appears to be most strongly associated with open-ocean settings, showing a decline in abundance in regions with unconsolidated sea ice (Crosta et al., 2005). Figures are found in Hustedt (1958), plate 3, figures from 4–7; Fryxell and Hasle (1979), figures from 12–22. Additionally, in Hustedt (1958), plate 3, figures from 8–10; and Fryxell and Hasle (1979), figures from 23–28.

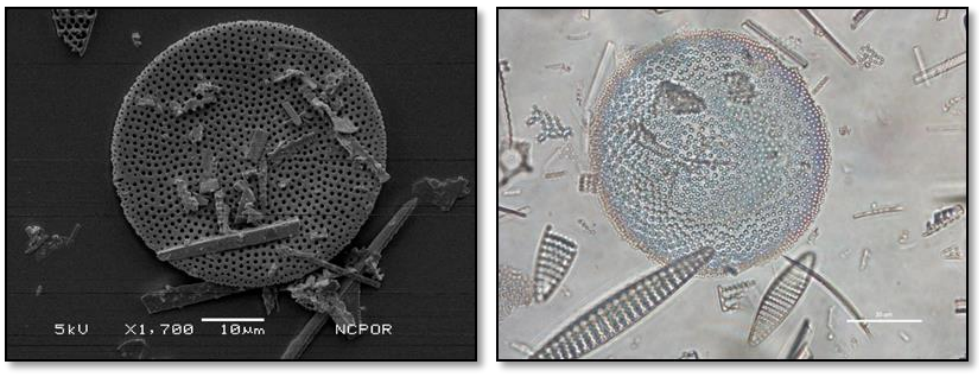

Fig 3.11: SEM (left) and LM (right) image of *Thalassiosira lentiginosa*

Thalassiosira lentiginosa *(Janisch) Fryxell.*

Description: The cells of *Thalassiosira lentiginosa* exhibit a discoid shape, appearing solitary and narrowly rectangular when viewed through the girdle (see Fig 3.11). The valves are circular and flat, measuring 29-120 µm in diameter. Fasciculate areolation is evident, with 7-9 areolae present in a 10 µm area over the valve face. The external opening is through a foramen, while the internal opening is via cribrum. The valve face displays evenly scattered strutted processes resembling small areolae (visible on SEM). Additionally, a marginal, internal slit-like opening is also identifiable.

Thalassiosira lentiginosa demonstrates its highest abundances from the maximum winter sea-ice edge to the Subantarctic Front (SAF). Beyond this range, their occurrences decrease in the Subantarctic Zone (SAZ) and the Subtropical Zone. The relationship between the relative abundances of *Thalassiosira lentiginosa* in modern sediments and summer sea surface temperature (SST) follows a similar pattern to that of *Fragilaripsis kerguelensis*, exhibiting a stable maximum abundance of 30% between 1 and 8 ˚C. The relative abundances decrease from 8 ˚C and reach trace levels near 18 ˚C. Abundances are notably low below 1 ˚C. *Thalassiosira lentiginosa* displays an inverse relationship with sea ice cover, showing high occurrence between 0 and 4 months of sea ice presence per year, and declining towards prolonged sea ice duration. During summer, the species appears to be associated with open-ocean conditions near the sea-ice edge (Crosta et al., 2005). Figures are located in Hustedt (1958), plate 4, figures 22– Johansen and Fryxell (1985), figures 49 and 50.

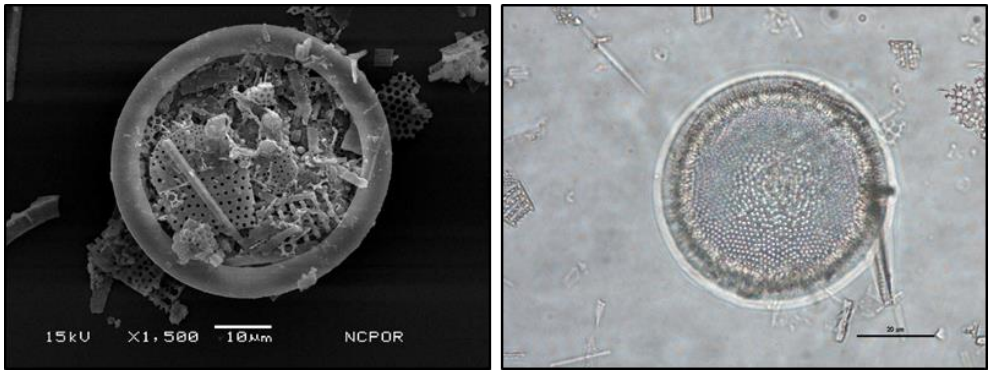

Fig 3.12: SEM (left) and LM (right) image of *Thalassiosira oliverana*

Thalassiosira oliverana *(O'Meara) Makarova et Nikolaev.*

Description: The cells exhibit a discoid shape, while the valves are circular and measure approximately 23-60 µm in diameter. A total of 7-8 areolae, varying in size from fine to coarse, are found within a 10 µm area, arranged in a radiating to irregular pattern. The marginal band is notably broad and characterized by the presence of small areolations. Additionally, there are strutted processes located in a marginal ring within the aforementioned marginal band. Near the margin, a labiate process of significant size is present. According to previous literature, the species *Thalassiosira oliverana* (Fig 3.12) appears to have a widespread distribution in sediments of the Southern Ocean, with the exception of the Antarctic coast where its abundances are reduced and sometimes even rare. Typically, the species is found in higher concentrations along the maximum winter sea-ice edge and the Polar Front, similar to *Fragilariopsis kerguelensis* and *Thalasiosira lentiginosa*. This geographic distribution spans a wide range of sea surface temperatures (SST), particularly with the highest abundances (4-5%) observed in February when SST is between 2 and 4˚C (Crosta et al., 2005).

The occurrence of *Thalassiosira oliverana* has been found to be inversely related to sea ice cover, showing a general reduction from open ocean conditions towards areas with prolonged sea ice cover, which is also evident in winter sea ice concentration. The species is prominently dominant in locations where open ocean conditions transition to sea-ice edge during the summer season. It is distributed across both Antarctic and subantarctic waters, as depicted in figures found in Fenner et al. (1976), plate 14, figures 1-5, and Akiba (1982), figures 1-5.

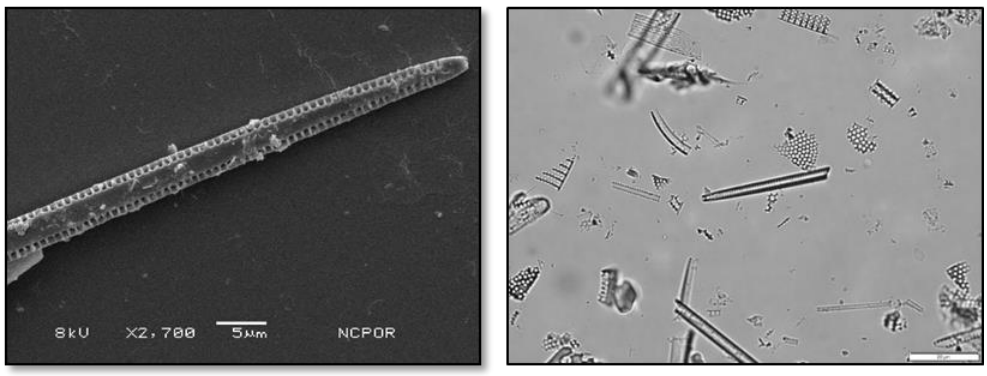

Fig 3.13: SEM (left) and LM (right) image of *Thalassiothrix antarctica*

Thalassiothrix Antarctica A. Schimper ex Karst.

Description: The cells of *Thalassiothrix* display a straight, needle-like morphology, often appearing slightly curved or sigmoidal when viewed from the side. They form radiating colonies that are connected by bending at one end of the frustule, while the head poles remain separate. The specimens are typically fragmented into multiple parts. The apical axis of the cells measures between 420 and 5680 µm, while the transapical axis ranges from 1.5 to 6 µm. One end of the frustule is rounded, featuring two projecting spines at the apex of the rounded head pole. A single marginal row contains the areolae, and there is a row of fine spines pointing towards the head pole. Labiate processes are present at each apex. *Thalassiothrix* (Fig 3.13) is most commonly found north of the wintertime sea ice limit, with decreasing occurrences towards the Subantarctic Front (SAF), though occasional high abundances are noted in the Subantarctic Zone (SAZ). Conversely, the species is less abundant in the seasonal sea ice zone and the coastal regions of Antarctica. The distribution of *Thalassiothrix* in relation to modern summer sea surface temperatures (SST) shows a peak abundance between 1 and 3˚C, with a general decline in warmer temperatures.

The occurrence of *Thalassiothrix* appears to be closely linked to sea ice parameters, as evidenced by a notable decrease in abundance from open ocean conditions to regions with extended annual sea ice cover. Comparing the species distribution to September sea ice concentration reveals higher abundances in ice-free regions and much lower abundances in regions with compact sea ice during winter (Crosta et al., 2005). This species is predominantly found in the waters of the Antarctic Ocean, including the South Atlantic, Pacific, and Indian waters. Refer to figures 26–59 in Hasle and Semina (1987) for visual representations.

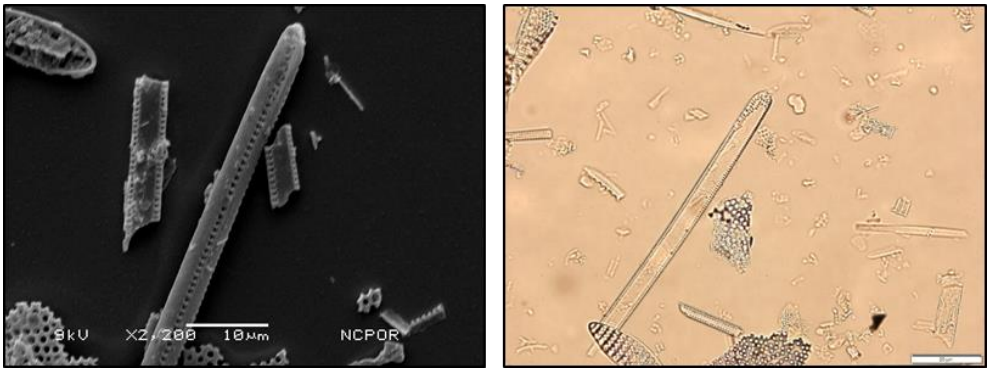

Fig 3.14: SEM (left) and LM (right) image of *Trichotoxon reinboldi*

Trichotoxon reinboldi (Van Heurck) F. Reid and Round.

Description: These organisms exhibit a needle-like appearance, being arcuate and progressively pointed towards the poles. They can occur individually or in colonies. The cells have an apical axis ranging from 800 to 3600 µm and a transapical axis measuring 3 to 10 µm. The poles lack any spines, and the mantle is adorned with striae that slightly extend into the valve face. The face of the cells is scattered with external criba, and a Labiate process is located at each pole. These species are endemic to the Antarctic Ocean. *Trichotoxon reinboldi* (Fig 3.14) is a species that is poorly represented in the global sedimentary assemblage, typically occurring in low abundances, usually less than 1%. However, there are exceptions to this, observed in a few core-tops in the Atlantic sector of the Southern Ocean near the winter sea ice edge. These higher abundances correspond to modern summer sea surface temperatures (SST) of 1–2 ˚C, and the species is not encountered in areas with a summer SST below 0 ˚C. Additionally, the species has demonstrated the ability to tolerate unconsolidated sea ice conditions, but it is notably abundant in sediments where open ocean conditions prevail (Crosta et al., 2005). *Trichotoxon reinboldi* is endemic to the Southern Ocean, with higher abundances found in the Weddell Sea and the Indian Ocean sector of Antarctica. For visual representations, refer to figures 67–70 in Hasle and Semina (1987).

3.4. The ‘Water Stratification diatom group’

The group mainly comprises of *Chaetoceros* resting spores which flourish in a SST range of 0 to 2 ˚C and sea-ice cover of 5-9 months/year. These species includes ***Chaetoceros resting spores*** **and** ***Thalassiosira Antarctica***

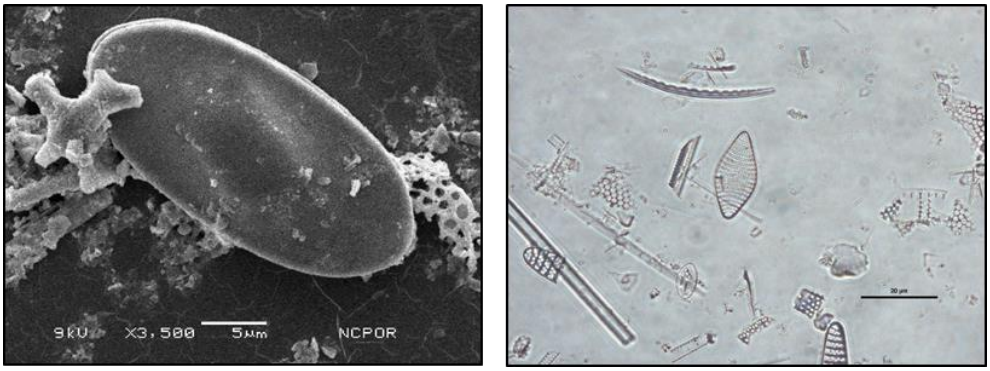

Fig 3.15: SEM (left) and LM (right) image of *Chaetoceros resting spores*

Chaetoceros, a widely found diatoms genus in modern seas, thrives in various environments, from temperate coastal areas to polar regions. Within this genus, there are approximately 180 marine plankton species, including about 75 species that exist as resting spores or survival stages (Stockwell and Hargraves, 1984). These resting spores can dominate the water, accounting for up to 91.8% of its abundance when the sea surface temperature (SST) ranges from -0.5 to 1.5˚C. They are distributed throughout the circumpolar sediments, showing little regard for zonal boundaries. The Antarctic Peninsula region and the Ross Sea host the highest concentrations of these spores, particularly during February when the SST ranges from -1.3 to 3.5˚C. Observations have revealed that *Chaetoceros* resting spores *(Fig* 3.15) are frequently present in areas where sea ice covers the water for over 3 months annually, with the ideal coverage being between 3 to 9 months per year, reaching a maximum abundance of 7 m/yr. However, in the POOZ and SAZ sediments, the occurrences of these spores generally remain below 5%, except in the vicinity of the Crozet–Kerguelen islands (Armand et al., 2005).

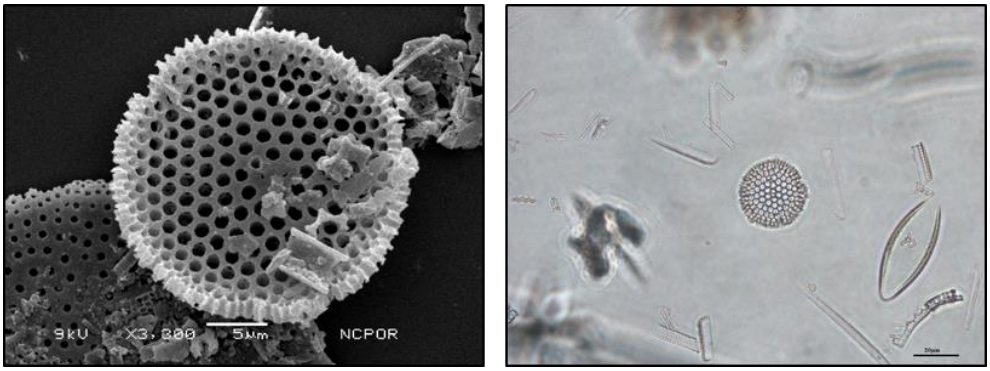

Fig 3.16: SEM (left) and LM (right) image of *Thalassiosira antarctica*

Thalassiosira antarctica G. Kartst.

Description: The cells form a chain interconnected by chitinous strands that emerge from the central cluster of the strutted process. Larger cells exhibit lower silicification. The valves' circular diameter measures approximately 14-56 µm and follows a convex shape as it decreases in size. The areolation is radial, and the size of the areolae is about 17-20 µm. The outer opening features a simple hole, while the inner opening passes through a uniformly porous soft palate. The number of strutted processes can range from 2 to many. The labiate process is large, solitary, sessile, and located in the outer ring of valves with a marginal ring. The interior opening of the labiate process aligns with the valve's radius, whereas the external opening is elongated and similarly oriented. These organisms are well distributed in the South Atlantic region, specifically in the area of the South Shetland; Southern Ocean, and in Arctic waters. Based on previous studies, the maximum relative abundance recorded for *Thalassiosira antarctica* (Fig 3.16) is 31.8% (Armand et al., 2005). These peak abundances are associated with February sea surface temperatures (SST) ranging from 0 to 0.5˚C. When the abundances of T. antarctica exceed 10%, it indicates that the sea ice persists for over 6 months per year.

Geographically, this species occurs in almost all sites south of the maximum winter sea ice zone, with the highest abundances found in Prydz Bay and along Wilkes Land. Occasional occurrences of the species are also observed in the South Atlantic and the Indian Ocean sectors. Relevant figures can be found in the following sources: *Thalassiosira antarctica*: Hasle and Heimdal (1968), Figures from 7–13; Johansen and Fryxell (1985), Figures from 37–39.

3.4 The ‘SAZ diatom group’

It comprises of species that are abundant in warm waters where SST range between 11 and 14 ˚C and are absent in sea-ice regions. The species included in this group are *Azpetia tabularis, Hemidiscus cuneiformis* and *Thalassiosira oestrupii*.

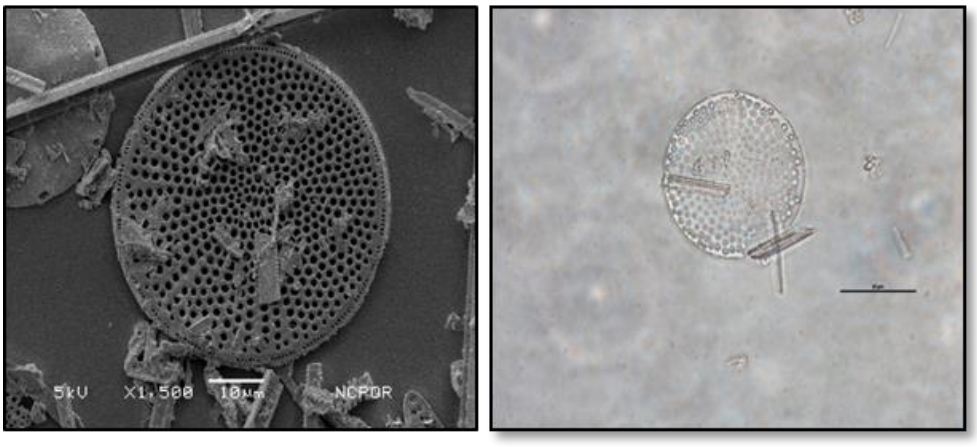

Fig 3.17: SEM (left) and LM (right) image of *Azpetia tabularis*

Azpetia tabularis tabularis var. tabularis *(Grunow) G. Fryxell and P.A. Sims.*

Description: The cell exists as a singular entity, and its valve exhibits a circular shape with a flat apical axis spanning between 16 to 17 µm. The areolae are slightly fasciculate and arranged in radial rows. Around 5 to 10 areolae are situated near the center within a range of 10 µm, while approximately 16 areolae occur within the same space at the edges. The labiate processes are positioned on the marginal ring, appearing as singular, large structures located at the end of the central ring. *Azpeitia tabularis* (Fig 3.17) is a diatom typically found in tropical to subtropical regions and is currently distributed across all oceans, including Subantarctic areas. It is commonly found in the coastal waters of East Antarctica, the Arctic Ocean, and the Antarctic Ocean. *Azpeitia tabularis* displays its highest occurrence north of the Polar Front in sediments of the Southern Ocean (Romero et al., 2005). Notably, maximum abundances of approximately 24% are observed in warmer sea surface temperatures (SSTs) of around 13˚C in February and 11˚C in August. Interestingly, the distribution of Azpeitia tabularis is only minimally influenced by sea-ice concentrations, as occurrences below 5% have been observed even during periods of September sea ice concentration (Romero et al., 2005). Relevant figures can be found in the following sources: Hustedt (1930) figure in 230a; Fryxell et al. (1986).

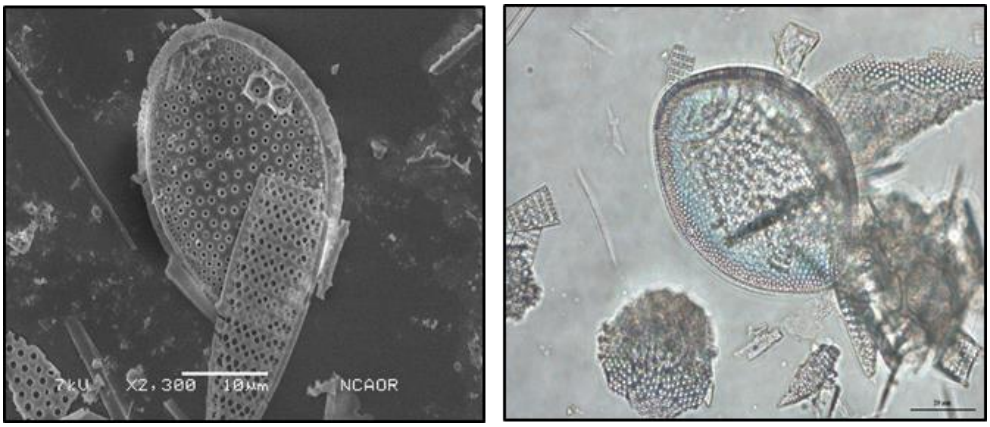

Fig 3.18: SEM (left) and LM (right) image of *Hemidiscus cuneiformis*

Hemidiscus cuneiformis Wallich

Description: The cells of *Hemidiscus cuneiformis* are wedge-shaped and exist independently. The valves exhibit a flat, nearly semi-circular form, characterized by a pronounced convex dorsal edge. The ventral edge, on the other hand, is slightly convex and often displays a median bulge on its ventral side. The dimensions of the diatom include an apical axis ranging from 40 to 174 µm and a longitudinal axis approximately measuring between 30 to 90 µm. Arranged in irregular radial fascicles, the areoles present short parallel lines extending towards the center of the valve, while irregular or tangential sectors extend towards the margins and poles. Notably, no central translucent area or rosette is observed. The valve exhibits a small spine on its ventral edge, along with a partially occluded pseudonodule at the center of the edge. Additionally, the diatom has 1 to 2 labiate processes, and its girdle is simple without an interclary strap.

Hemidiscus cuneiformis (Fig 3.18) is typically associated with warm-water environments (Hasle and Syvertsen, 1996; Semina, 2003); however, it is not frequently found in high numbers. It has also been noted as a rare component of diatom assemblages in the Arabian Sea and Indian Ocean (Simonsen, 1974). Existing literature indicates its presence in sediments underlying warm-temperate waters from the Pacific, Indic, and Atlantic Oceans (Romero et al., 2005). The occurrence of *Hemidiscus cuneiformis* in temperate-to-warm waters is closely linked to both February and September sea surface temperatures (SST), with the highest abundances associated with SST above 11˚C. Therefore, the presence of *Hemidiscus cuneiformis* is unrelated to sea-ice cover. Relevant figures can be found in the following sources: Hustedt (1930) figure 542; Fryxell et al. (1986).

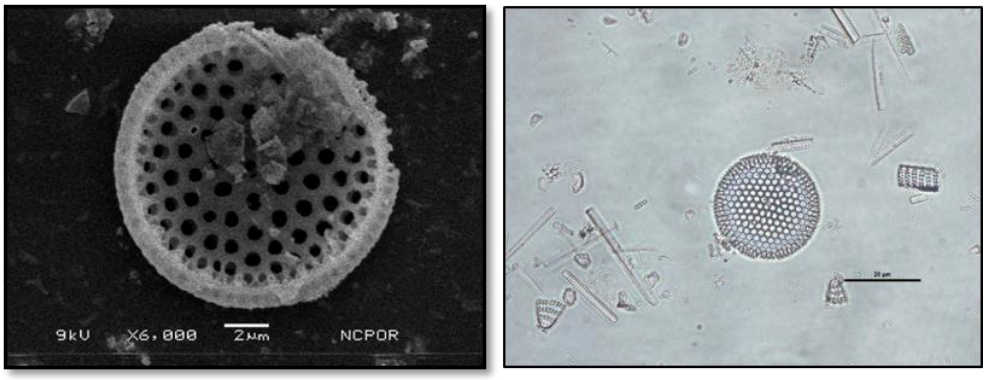

Fig 3.19: SEM (left) and LM (right) image of *Thalassiosira oestrupii*

Thalassiosira oestrupii var. oestrupii *(Ostenfeld) Hasle.*

Description: The cells of *Thalassiosira oestrupi var. oestrupii* form chains bound together by chitinous threads originating from the strutted processes. In girdle view, these cells appear discoid to rectangular in shape. The valves, circular and ranging from 7 to 60 µm in diameter, exhibit a flat to slightly curved surface. Areolation, characterized by coarse and eccentric patterns, varies in distribution from the center to the margin. The strutted processes possess internal extensions and are trifulate and operulate. One process is positioned in an off-centered manner, while another forms a marginal ring of processes. In contrast, the labiate processes are not marginal; they exist in solitary form and are internally flattened, aligning parallel to the valve's margin .This diatom species, *Thalassiosira oestrupi var. oestrupii* (Fig 3.19), holds easy identification features. Despite being a cosmopolitan species, with a preference for tropical to temperate waters, it has been occasionally recorded as far north as the Norwegian Sea and as far south as the Wedell Sea (Fryxell and Hasle, 1980). *Thalassiosira oestrupii var. oestrupii* is well-preserved in both surface and downcore sediments.

Its relative abundance decreases southward, with the highest relative occurrence of approximately 5% observed in the Atlantic Ocean, approximately 5% north of the Subantarctic Front (SAF), and only trace amounts seen in the Indian Ocean (Romero et al., 2005). Surprisingly, there is no discernible relationship between sea-ice cover and the presence of *T. oestrupii.* Like most tropical/subtropical diatoms, the contribution of *Thalassiosira oestrupii var. oestrupii* sharply increases at temperatures around 1 ˚C. Relevant figures can be found in the following sources: Fryxell and Hasle (1980) figures from 1–3, 6–7, and 12–19.

CHAPTER – 4

ANTARCTIC SEA-ICE AND PALEOPRODUCTIVITY VARIATION OVER THE LAST 156 000 YEARS IN THE INDIAN SECTOR OF SOUTHERN OCEAN

4.1 Introduction

Antarctic sea ice is the most seasonal feature on Earth. Its annual cycle modulates the radiative balance of the SO (Comiso, 2010), the heat-gas exchange between the ocean and the atmosphere (Delille et al., 2014; Ferrari et al., 2014), the global oceanic circulation (Abernathey et al., 2016) along with the SO productivity (Arrigo and Thomas, 2004). Of special interest is that all these processes affect the partitioning of carbon between the ocean and the atmosphere (Kohfeld et al., 2017). More precisely, Antarctic sea-ice expansion during glacial periods is thought to be the main process for lowering of the atmospheric CO_2 concentration via its direct insulation effect (Ferrari et al., 2014), its impact on the carbon storage in abyssal SO waters (Bouttes et al., 2011) and on the regional and distal productivity (Moore et al., 2000; Matsumoto, 2007; Jaccard et al., 2013). Hence, it is necessary to document the past changes in Antarctic sea-ice extent in all SO basins to better understand its interactions with climate drivers on a multi-millennial timescale.

Most reconstructions of past Antarctic sea-ice dynamic are either qualitative or restricted to the last 30,000-40,000 years (Burckle and Mortlock, 1998; Crosta et al., 1998a,b; Gersonde and Zielinski, 2000; Gersonde et al., 2005; Collins et al., 2012; Ferry et al., 2015; Xiao et al., 2016). Only few quantitative studies cover the last glacial-interglacial cycle (Kunz-Pirrung et al., 2002; Crosta et al., 2004; Esper and Gersonde 2014a; Nair et al., 2019). These studies suggested that the winter sea-ice (WSI) limit was located 5-10 degrees of latitude northward during the last glacial stage relative to its modern position. The northward shift probably resulted from a congruent shift in the Southern Hemisphere Westerlies Winds (SWW) and ACC along with a drop in atmospheric and oceanic temperatures (Martinson, 2012; Kohfeld et al., 2013; Bostock et al., 2015; Nair et al., 2019). However, there are currently not enough studies to document potential regional differences and therefore robustly assess drivers of past sea-ice dynamic and its feedbacks on the climate system.

The narrow ecological preferences of diatoms is studied to infer past oceanographic conditions such as SST and WSIC and WSID, and compared these with paleoproductivity records (Nair et al., 2019 in the under-studied Indian sector of the SO over the past 156,000 years. Quantitative estimates of both SST and WSIC-WSID are provided through the MAT and are compared to similar records from the Atlantic and southwestern (SW) Pacific to evaluate whether sea-ice dynamic was comparable in each SO basin over the past ~156,000 years.

4.2 Chronology

Core SK 200/33 age control is provided by five Accelerator Mass Spectrometry (AMS) radiocarbon dates measured on the bulk organic matter at the University of Arizona (Table 4.1). In the absence of carbonate tests in SO and coastal Antarctic sediments, radiocarbon dating is commonly performed on bulk organic carbon (Leventer et al., 2006; Crosta et al., 2007; Borchers et al., 2016; Mezgec et al., 2017; Tesi et al., 2020). The ^{14}C age of bulk organic carbon from the SO sediments are known to be older than the expected ages by few hundred years due to the presence of dead carbon (Andrews et al., 1999; Zheng et al., 2002; Costa et al., 2007). However, the good correspondence between the ^{14}C ages and the age model derived from the tuning of SK 200/33 records to Antarctic climate records suggests that the radiocarbon chronology is robust enough to interpret multi-millennial changes (Fig. 4.1b). The radiocarbon dates were calibrated to calendar ages using Calib 6 Software (Stuiver et al., 2005) after applying a reservoir age correction of 850 years ± 20 as recommended for this region (Bard, 1988; Berkman and Forman, 1996; Dutta, 2008). Core chronology beyond the radiocarbon ages was obtained by tuning the SST and winter sea ice duration (WSID) records of SK 200/33 to the temperature record of EPICA Dome C (EDC) ice core (Jouzel et al., 2007; Table 1, Fig. 4.1a), assuming synchronous climate changes in the SO and over Antarctica (Pahnke et al., 2005; Wolff et al., 2006; Fischer et al., 2010; Jaccard et al., 2013; Nair et al., 2019; Thöle et al., 2019). Additional tie-points were obtained by tuning the magnetic susceptibility signal from core SK 200/33, which truthfully records terrigenous input at the core site (Thamban et al., 2005), to the EDC dust record (Lambert et al., 2008). Figure 4.1b shows the final age model that is based on linear interpolation between the control points. The top 100 cm of the core cover the period between ~6730 years before present (6.73 ka BP) and 156 ka BP, therefore encompassing Marine Isotope Stage (MIS) 1 to late MIS 6.

SI No.	Sediment core depth (cm)	Lab No.	$\delta^{13}C$	Radiocarbon age (years BP)	Calibrated ages (2σ) range (years)	Age (cal. ka BP)
1	1	AA102622	-23.9	8276 + 43	7473-7180	7.3
2	7	AA102623	-22.7	13488 + 76	14571-14046	14.22
3	19	AA102625	-22.9	14131 ± 78	15526-14991	15.2
4	27	AA102626	-23.4	19460 ± 170	21937-21039	21.4
5	35	AA102627	-22.8	22420 ± 250	25330-24184	24.53
6	37	Tuning to SST, sea ice, MS & EDC records.				30
7	40	Tuning to SST, sea ice, MS & EDC records.				38
8	45					53
9	49	Tuning to SST, sea ice, MS & EDC records.				58
10	60					68
11	64	Tuning to SST, sea ice, MS & EDC records.				84
12	68					104
13	74	Tuning to SST, sea ice, MS & EDC records.				108
14	83					130
15	85	Tuning to SST, sea ice, MS & EDC records.				146
16	99					156

Table 4.1: SK 200/33 core chronology. The age control is provided by five Accelerator Mass Spectrometry (AMS) dates measured on the bulk organic carbon and, beyond radiocarbon ages, the ages are obtained by tuning SK 200/33 SST, sea ice and magnetic susceptibility (MS) records to the temperature and dust records of EPICA Dome C ice core (Jouzel et al., 2007).

a)

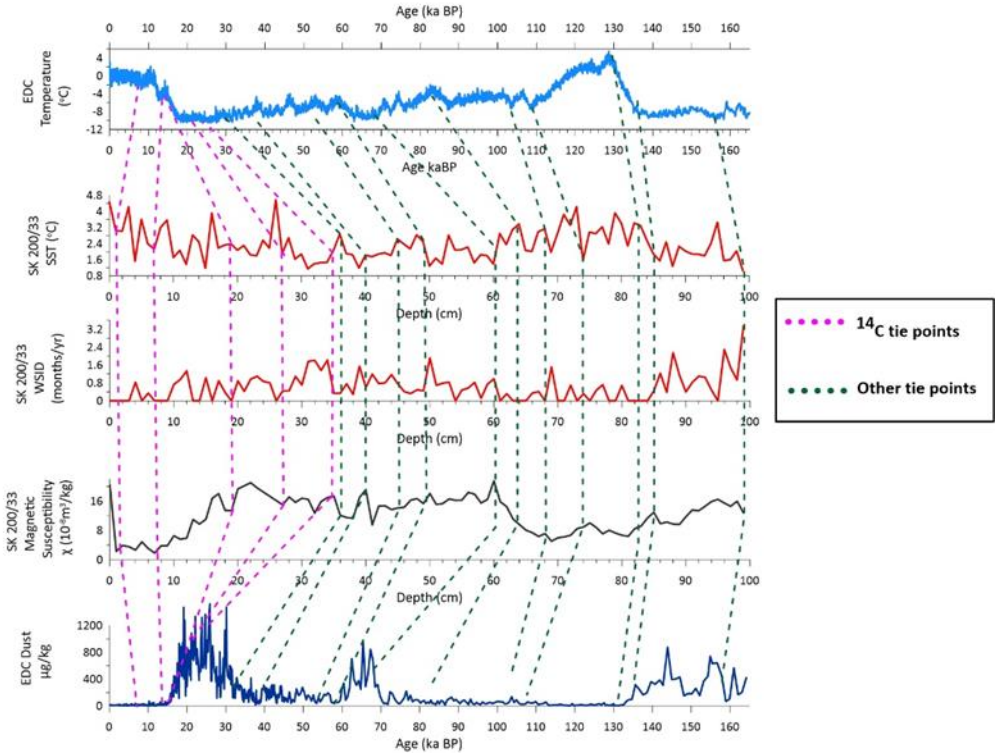
Age (ka BP)
EDC Temperature (°C)
Age kaBP
SK 200/33 SST (°C)
Depth (cm)
SK 200/33 WSID (months/yr)
Depth (cm)
SK 200/33 Magnetic Susceptibility χ (10⁻⁶m³/kg)
Depth (cm)
EDC Dust µg/kg
Age (ka BP)
14C tie points
Other tie points

b)

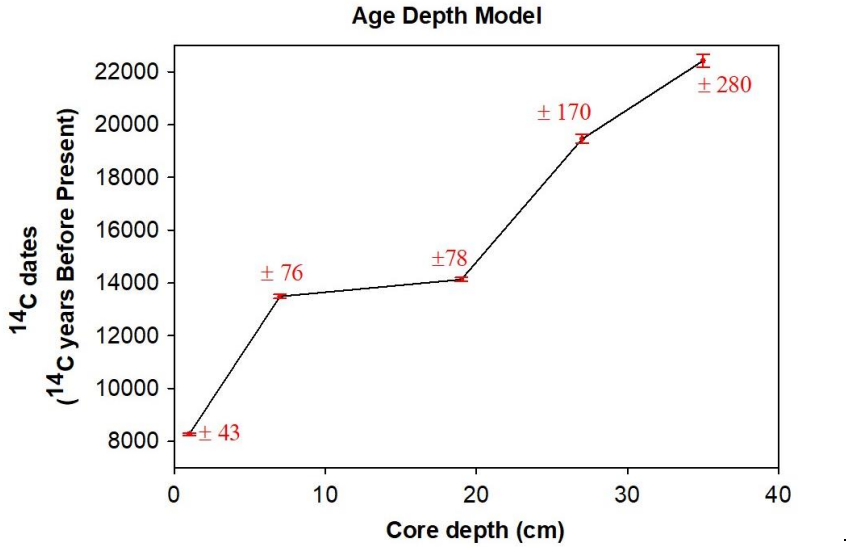
Age Depth Model
14C dates
(14C years Before Present)
Core depth (cm)
± 43
± 76
±78
± 170
± 280

c)

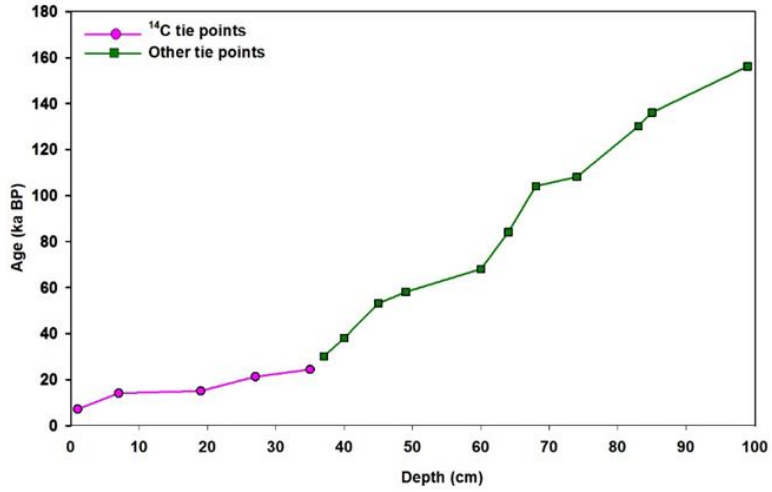

d)

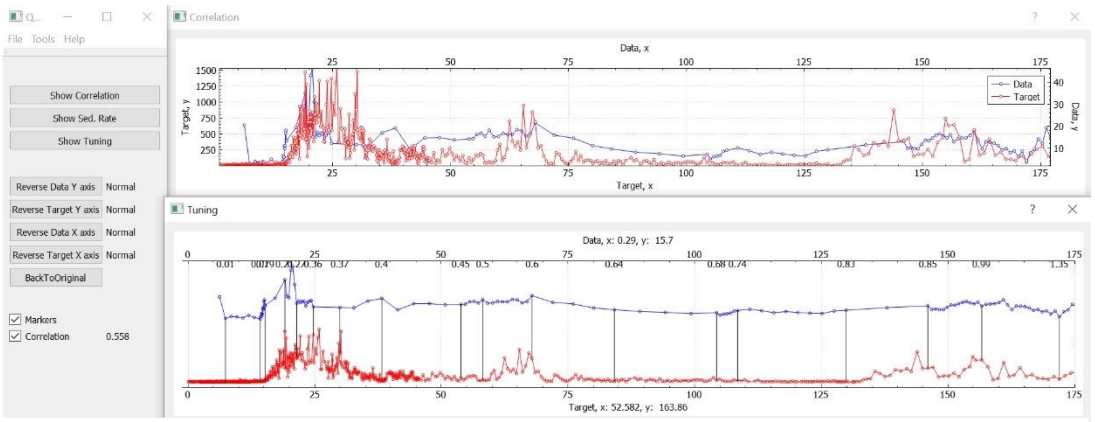

e)

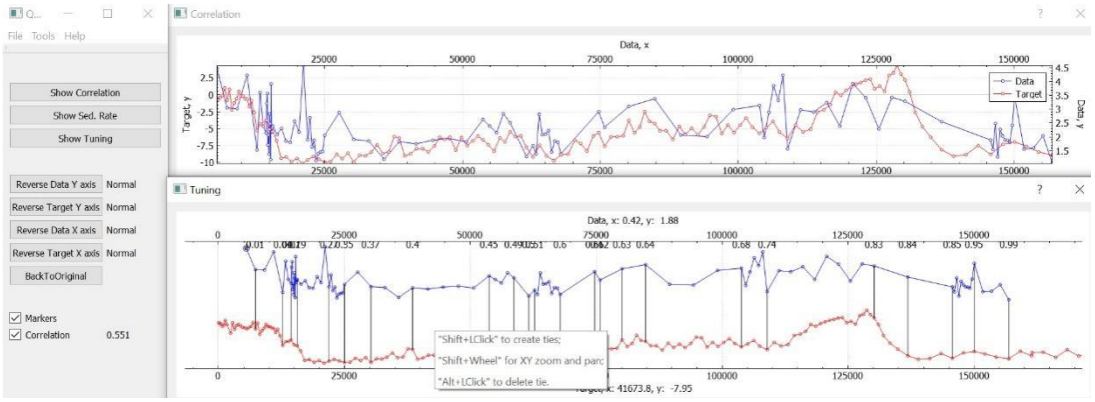

Fig. 4.1: Age model for sediment core SK 200/33. a) Age tuning of SK 200/33 based on AMS radiocarbon dates (dotted pink lines) and other tie-points (dotted green lines) linking sea-surface temperature (SST, red curve), winter sea-ice duration (WSID, red curve) and magnetic

susceptibility (black curve) from SK 200/33 with the temperature records of EPICA Dome C (EDC) ice core (Jouzel et al., 2007) and EDC dust data (Lambert et al., 2008). b)14C age depth model with uncertainities c) Age-depth model showing ^{14}C tie points (pink circles) and tuned age points (green squares). d) Age tuning of SK 200/33 based on magnetic susceptibility and EDC dust data using QAnalseries software. e) Age tuning of SK 200/33 based on SST and EDC ice core data using QAnalseries software.

4.3 Results

4.3.1 Down-core variations in diatom assemblages

The sea-ice diatom group (refer chapter 3 for the details of the diatom group) represents the second most abundant group in the core SK 200/33 with the relative abundances ranging from 0 to 8 % over the last 156 ka (Fig. 4.2a). The highest occurrences (> 3 %) of this group were observed during the glacial stages (MIS 2-4 and 6) and the lowest abundances (0-2 %) were found during the interglacial periods (MIS 1 and 5). Similarly, the water stratification group was more present during the glacial stages, when abundances were 0-5 % than in the interglacial periods when abundances were lower than 1% (Fig. 4.2b). The POOZ group dominated the diatom assemblages in the core during the last 156 ka, with relative abundances varying between 81 and 97 % (Fig. 4.2c). The maximum occurrences of the POOZ group were observed during the interglacial periods (> 95 %), while minimum proportions (< 95 %) were recorded during the glacial stages. The abundance of SAZ diatom group varied between 0 and 4 % with higher proportions (2-4 %) during the interglacial stages and deglaciations, while lower abundances (0-2 %) were recorded during the glacial periods (Fig. 4.2d). The total diatom abundance was highest (180-370 $\times 10^6$ valves/g of sediments) during interglacial periods and deglaciations whereas lowest values (< 180 $\times 10^6$ valves/g of sediments) were observed during the glacial periods (Fig. 4.2e).

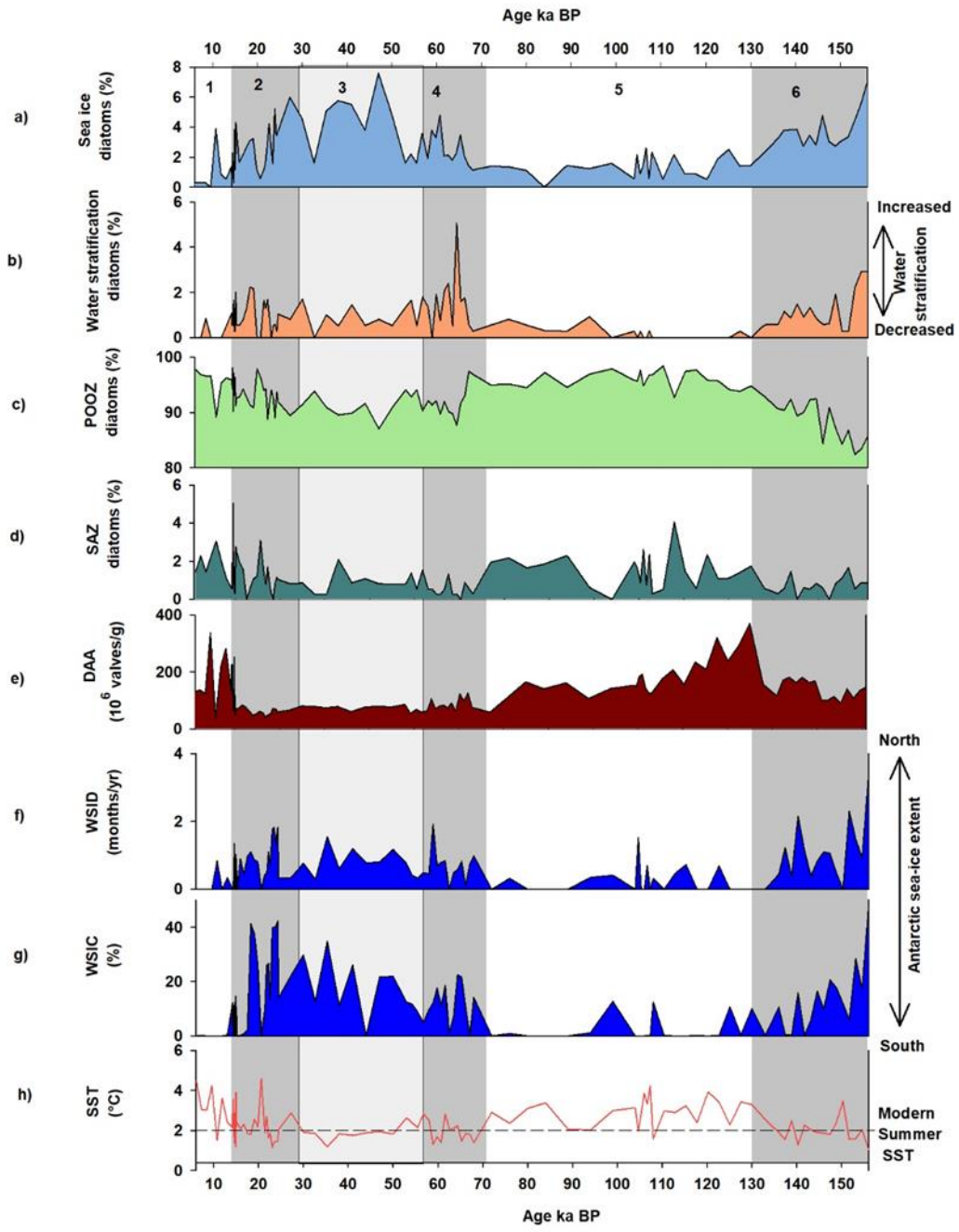

Fig. 4.2: Relative abundances of the diatom groups encountered in core SK 200/33 along with reconstructed summer SST, WSIC in percentages and WSID in months/year. a) Sea-ice diatom group, b) Water stratification diatom group, c) POOZ diatom group, d) SAZ diatom group, e) diatom absolute abundance (DAA) in 10^6 valves/g of sediments, f) WSID in months/year, g) WSIC in percentage, h) SST (˚C). Glacial periods are highlighted by grey bands and the number (1 to 6) indicates MIS stages (Lisiecki and Raymo, 2005).

4.3.2 Down-core variations in summer SST and WSI

In the core SK 200/33, WSIC estimates vary between 20-40 % during the glacial stages while the interglacial periods were generally ice free. The highest WSIC values were reconstructed during the mid to late MIS 6, MIS 4 and MIS 2 (Fig. 4.2g). The WSID record mimics the WSIC record. WSID estimates vary between 0 and ~2 months/year with generally higher values in the glacial stages compared to the interglacial periods (Fig. 4.2f). The highest values were recorded during the mid to late MIS 6 and during the MIS 3-2. The interglacial periods generally showed no sea-ice presence except for a brief statistically non-significant events at ~95 and 115 ka BP during MIS 5.

The summer SST values vary between 1 and 4 ˚C over the last 156 ka (Fig. 4.2h). Summer SST of 2 to 4 ˚C were estimated during the interglacial periods while SST of 1 to 2 ˚C were generally estimated during the glacial stages, except for the short-lived warmer peak at 20 ka BP during the MIS 2. The interglacial SSTs were higher than the modern SST (2 ˚C) at the core site.

4.4 Discussion

4.4.1 Latitudinal shifts in Antarctic winter sea-ice extent and hydrological fronts in the Indian sector

At present time, core SK 200/33 is located in the POOZ, north of the SACCF and WSI edge but 2-3˚ of latitude to the south of the southern APF (Fig. 4.3). The most recent diatom assemblages, dated from the early-mid Holocene, preserved in the core are strongly dominated by the POOZ diatom group (Fig. 4.2c), with few percent of SAZ diatoms (Fig. 4.2d), and the absence of sea-ice diatoms (Fig. 4.2a). These assemblages resulted in SST estimates of ~ 4 ˚C (Fig. 4.2g), which are ~ 2 ˚C higher than the modern regional SST of ~ 2 ˚C. These results are in agreement with previous studies showing warmer conditions during the early-mid Holocene than during the late Holocene in the Indian sector of the SO from Antarctica (Masson et al., 2011), coastal Antarctica (Cremer et al., 2007; Verleyen et al., 2011), Polar Frontal Zone (Katsuki et al., 2012; Xiao et al., 2016) to SAZ (Crosta et al., 2005b; Nair et al., 2019) realms. Very similar diatom assemblages were recorded in core SK 200/33 during the MIS 5.5 as during the early-mid Holocene, and similarly resulted in SST estimates above 2 ˚C and absence of winter sea ice. At the basin scale, the MIS 5.5 has been shown to be even warmer than the early Holocene (Masson et al., 2011; Capron et al., 2014; Crosta et al., 2020), with reduced winter sea-ice extent in data (Chadwick et al., 2020) and models (Holloway et al., 2017).

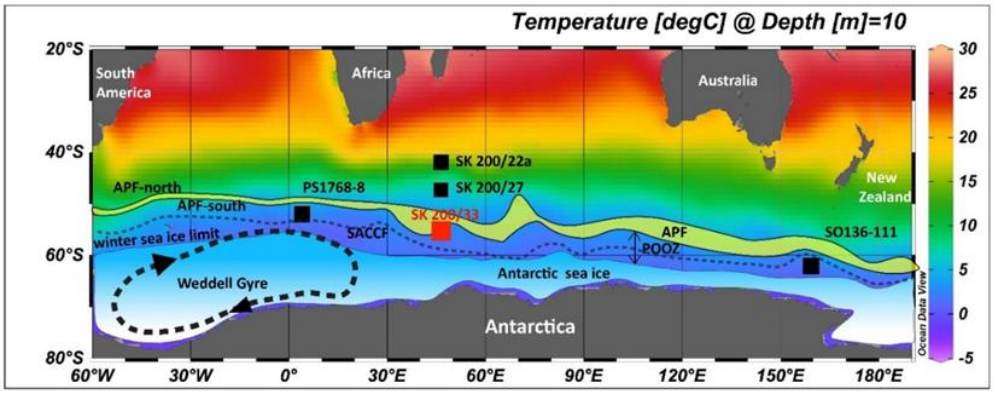

Fig. 4.3: Study area showing core site SK 200/33 location (red square) along with the locations of the published sea-ice records used here (black squares, SK 200/27 (49˚S, 45˚E; Nair et al., 2019), core SK 200/22a (43˚S, 45˚E; Nair et al., 2019), SO136-111 (56˚40'S, 160˚14'E; Ferry et al., 2015) and core PS1768-8 (52˚35.6′S, 4˚28.6′E; POOZ Esper and Gersonde., 2014b)). The position of the Antarctic Polar Front, both northern and southern branches (APF-north and APF-south), is marked based on Anilkumar et al. (2006), Luis et al. (2009) and Belkin and Gordon (1996) while the position of the Southern Antarctic Circumpolar Current Front (SACCF) is marked based on Sokolov and Rintoul. (2009a,b). Modern winter sea-ice limit is marked based on Comiso et al. (2003). The mean summer sea-surface temperature data is taken from the World Ocean Atlas 2013 (Locarnini et al., 2013) and has been gridded with the Ocean Data View software (Schlitzer, 2002).

The new data, along with regional climate data, suggest that the hydrological fronts and WSI edge were located to the south of their modern position during the early-mid Holocene and MIS5.5 in the SW Indian sector of the SO. More precisely, SST of 2-4 ˚C during these periods in core SK 200/33 suggest that the south APF branch, now lying ~3˚ of latitude to the north, was located in the vicinity of the core site (Fig. 4.6). The result also suggests that the SACCF was displaced to the south, closer to the Antarctic continental slope, which may have allowed more Circumpolar Deep Water to upwell onto the Antarctic shelf and to participate to the retreat of regional ice-shelves (Leventer et al.; 2006; Mackintosh et al., 2011). Surprisingly, SST of ~2-3 ˚C were also estimated during the early Holocene in core PS2606-6, located at 53˚S in this sector (Xiao et al., 2016) and in core SK 200/27, located at 49˚S (Nair et al., 2019; Fig. 4f) while SST of 4-5 ˚C were estimated in core SK 200/22a located at 43˚S (Nair et al., 2019; Fig. 4.4d). Taken at face value, these reconstructions would indicate a northward migration of the northern APF branch, probably till at ~43˚S, during the early Holocene while

the southern APF branch shifted southward by 3˚ of latitude and was lying at ~55˚S. Such oceanographic changes, although not inconceivable, appear at odds with other SO sectors where all hydrological fronts were suggested to be to the south of their modern position during warmer-than-present climate (Bianchi et al., 2004; Chadwick et al., 2020). However it is noted that early-mid Holocene SST in core DCR1-PC were 8-10 ˚C (Crosta et al., 2020; Fig. 4.4e), slightly higher than modern SST at the core site, which suggests that the northern APF branch did not reach the core site at ~46 °S and was probably located south of its present location at ~50˚S (Durgadoo et al., 2008). Therefore it is proposed that the lower-than-modern SST reconstructed during the early Holocene in cores SK 200/22a and SK 200/27 result from the northward transport of SIZ and POOZ diatoms to the core sites, probably by bottom currents that are deflected by the presence of the Conrad Rise (Oiwane et al., 2014). As such, it is believed that the new results from core SK 200/33, obtained from a more stable region, represent a better image of past SST and sea-ice dynamics than the ones inferred from the SK 200/22a and SK 200/27 core. Based on SK 200/33 and DCR1-PC results it is proposed that the northern and southern APF were lying at around 49˚S and 55˚S, respectively, during the early-mid Holocene and MIS 5.5, that the SACCF migrated southward by a couple of degrees of latitude and that winter sea ice was less extended. It was not possible to capture here the reduction in sea-ice extent, which would request additional cores to the south.

The diatom assemblages were rather different during the glacial periods than during the interglacial periods, with a decrease in the POOZ and SAZ groups and a concomitant increase in the water stratification and sea-ice groups (Fig.4.2). This resulted in SST estimates generally below the modern value of 2 ˚C and in pervasive WSIC estimates of 20-40 % and WSID up to 2 months per year (Fig. 4.4), in line with regional studies that displayed glacial SST 2-4 ˚C lower than interglacial ones (Xiao et al., 2016; Nair et al., 2019; Crosta et al., 2020) and glacial WSIC ~50% higher than Holocene ones (Xiao et al., 2016) when southern hemisphere climate was globally cooler (EPICA, 2004). These results suggest a northward expansion of the Antarctic cold realm with the SACCF positioned in the vicinity of core SK 200/33 (55˚S) and the APF and the WSI edge both located north of core site. It is challenging to locate precisely the position of the APF and winter sea ice extent (WSIE) during the last glacial period with few records. However, the data in hands suggest that the south APF branch was lying north of core SK 200/27 (49˚S), close to DCR1-PC at 46 °S (Crosta et al., 2020; Fig. 4.4e) and that its northern branch may have reached core SK 200/22a (43˚S) (Nair et al., 2019) (Fig. 4.6). The data also suggest that WSIE was lying north of core PS2606-6 (53 ˚S), maybe as north as core

SK 200/27 in which very little sea ice is estimated during the last glacial (Fig. 4.4b). As Gersonde et al. (2005) positioned the WSIE at ~50˚S in the SW Indian sector of the SO, it is believed that the high values of sea-ice duration episodically estimated in core SK 200/22a during the MIS 2 (Fig. 4.4a) result from the advection of either floating ice or ice-related diatoms by bottom currents.

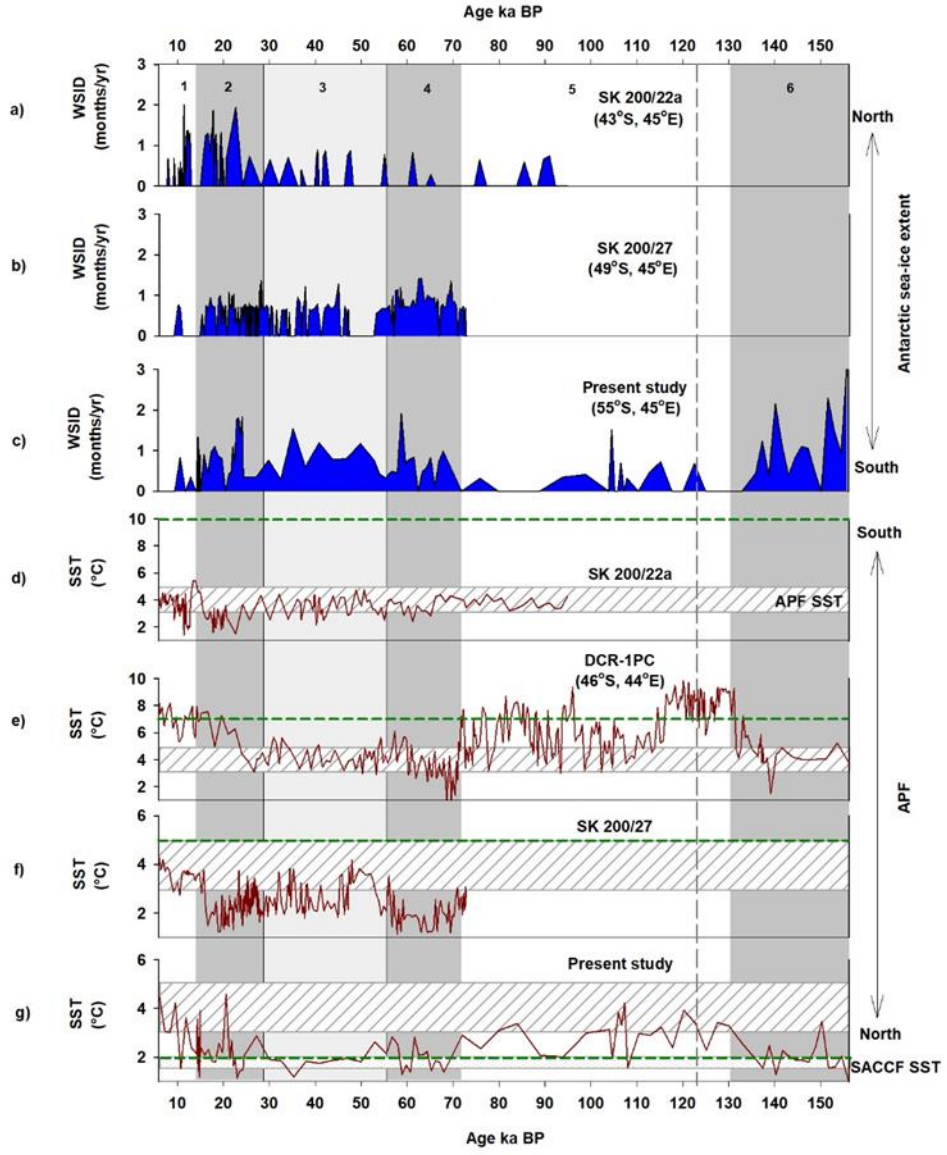

Fig. 4.4. Comparison of winter sea-ice records with summer sea-surface temperature (SST) records from the Indian sector of the Southern Ocean. Winter sea-ice duration (WSID) from sediment cores a) SK 200/22a (Nair et al., 2019), b) SK 200/27 (Nair et al., 2019), c) SK 200/33 (present study), SST from sediment cores d) SK 200/22a (Nair et al., 2019), e) Core DCR-1PC (Crosta et al., 2020), f) SK 200/27 (Nair et al., 2019) and g) SK 200/33 (present study). The striped band represents the APF temperature range, dotted band represents the SACCF

temperature range, green line symbolizes the modern temperature at the respective core sites. Glacial periods are highlighted by grey bands and the number (1 to 6) indicates MIS stages (Lisiecki and Raymo, 2005). The vertical dotted grey line represents the MIS 5.5.

The new results obtained in core SK 200/33 provide for the first-time insight into several glacial periods in this sector of the SO. Despite high-amplitude variability in each glacial period, there appears to be no significant differences between mean climate conditions in MIS 2, MIS 4 and MIS 6 (Fig. 4.4), in agreement with hemispheric climate inferred from ice cores (EPICA, 2004). Disregarding millennial-scale variability that was not tackled here, the new records suggest that the SACCF, the APF and the WSIE have been located at rather similar respective positions during the MIS 2, MIS 4 and MIS 6. The latitudinal shifts of WSI and the hydrological fronts recorded here can be related to the growth and decay of the Antarctic cryosphere along with changes in SST and westerly winds highlighting the importance of large-scale processes on sea ice history at the glacial-interglacial timescale (Neil et al., 2004; Carter and Cortese, 2009; Martinson, 2012; Kohfeld et al., 2013).

4.4.2 Zonal comparison of winter sea ice in the Southern Ocean

The new SST and sea-ice records obtained from core SK 200/33 is compared with an array of records to evaluate whether oceanographic conditions, especially sea-ice dynamics, varied accordingly in the three basins of the Southern Ocean over the last 156 ka. Generally, the SST records from the three basins reveal a similar glacial-interglacial pattern and timing over the past 156 ka (Fig. 4.5). The oceanic warming across the last two deglaciations is estimated at 2-3 ˚C in all three cores, in agreement with studies from the POOZ and polar frontal zone (PFZ) focusing on the last deglaciation (Gersonde et al., 2005; Esper and Gersonde, 2014b; Xiao et al., 2016). Glacial SST are lower in core PS1768-8 (Atlantic POOZ; Esper and Gersonde, 2014b) than in core SK 200/33 (SW Indian POOZ, this study) by 1-2 ˚C (Fig. 4.5), suggesting a cooler Atlantic sector. Across terminations, SST rose 2000-3000 years later in the Atlantic sector than in the SW Indian and SW Pacific sector. Keeping in mind potential chronological issues, this might indicate sustained influence of cold surface waters transported northward by the Weddell Gyre into the western Atlantic POOZ, therefore delaying the increase in SST. Similar to SST records, the pattern of WSI changes are rather similar in the three cores, with a rapid retreat during the late glacial (18-20 ka BP). However, the new data suggest that sea-ice retreat possibly occurred earlier in the SW Indian core than in the other sectors across Termination II with little sea-ice surviving at 53 ˚S after 140 ka BP, when dust fluxes decreased

drastically in EDC (Jouzel et al., 2007) (Fig. 4.5). Such results suggest that the drop in SWW intensity reduced the longitudinal extent of the Weddell Gyre, decreasing its influence on the SW Indian sector as soon as 140 ka. A significant anti-correlation between WSI and SST is evidenced in all three cores (R = 0.5 to 0.7; supplementary Fig. 4.9). A similar anti-correlation between proxy records of sea-ice and air temperatures has been also evidenced (Wolff et al., 2006; Röthlisberger et al., 2010). Such anti-correlations indicate a strong control of oceanic and atmospheric temperatures on past sea-ice dynamics at the multi-millennial timescale.

If pattern and timing in WSIC appear rather similar between the three sectors over the past 156 ka, the amplitude in WSIC variations between glacial and interglacial periods is higher (0-85%) in the Atlantic core than in the other two cores (0-40%) (Fig. 4.5a-c). It is here proposed that the higher glacial WSIC along with the higher amplitude glacial-interglacial changes in the Atlantic (Xiao et al., 2016) than any other sectors (this study; Ferry et al., 2015) have resulted from the advection of cold coastal Antarctic waters and sea ice from the Weddell Sea by the Weddell Gyre into the Atlantic southern ACC (Fig. 4.6). Today, the non-circular shape of Antarctic sea ice, with a regional maximum in sea-ice extension north of the Weddell Sea (Comiso et al., 2003; Nicholls et al., 2009; Holland and Kwok, 2012), is believed to result from intense sea-ice formation in the inner embayment and subsequent transport by the Weddell Gyre that extends until 60˚S and 20˚E (Olbers et al., 1992). Although less pronounced, another maximum in sea-ice extension can be observed today north of the Ross Sea in the SW Pacific sector (Comiso et al., 2003; Nicholls et al., 2009; Holland and Kwok, 2012). In this region, a large sea-ice extension was similarly reconstructed off the Ross Gyre for the last glacial maximum time slice (Benz et al., 2016). This suggests that more intense Weddell and Ross gyres during glacial times enhanced the northward transport of sea ice and cold waters, further facilitating sea-ice freezing at lower latitudes of SO and allowing high sea-ice concentration and cover in the SW Atlantic and SW Pacific sectors. The comparison of the new SST and sea-ice records with SO climate records therefore suggests that, though oceanic and atmospheric temperature changes determined the pacing of sea-ice history over the last 156 ka BP, winds and ocean currents drove the amplitude of the changes between the basins.

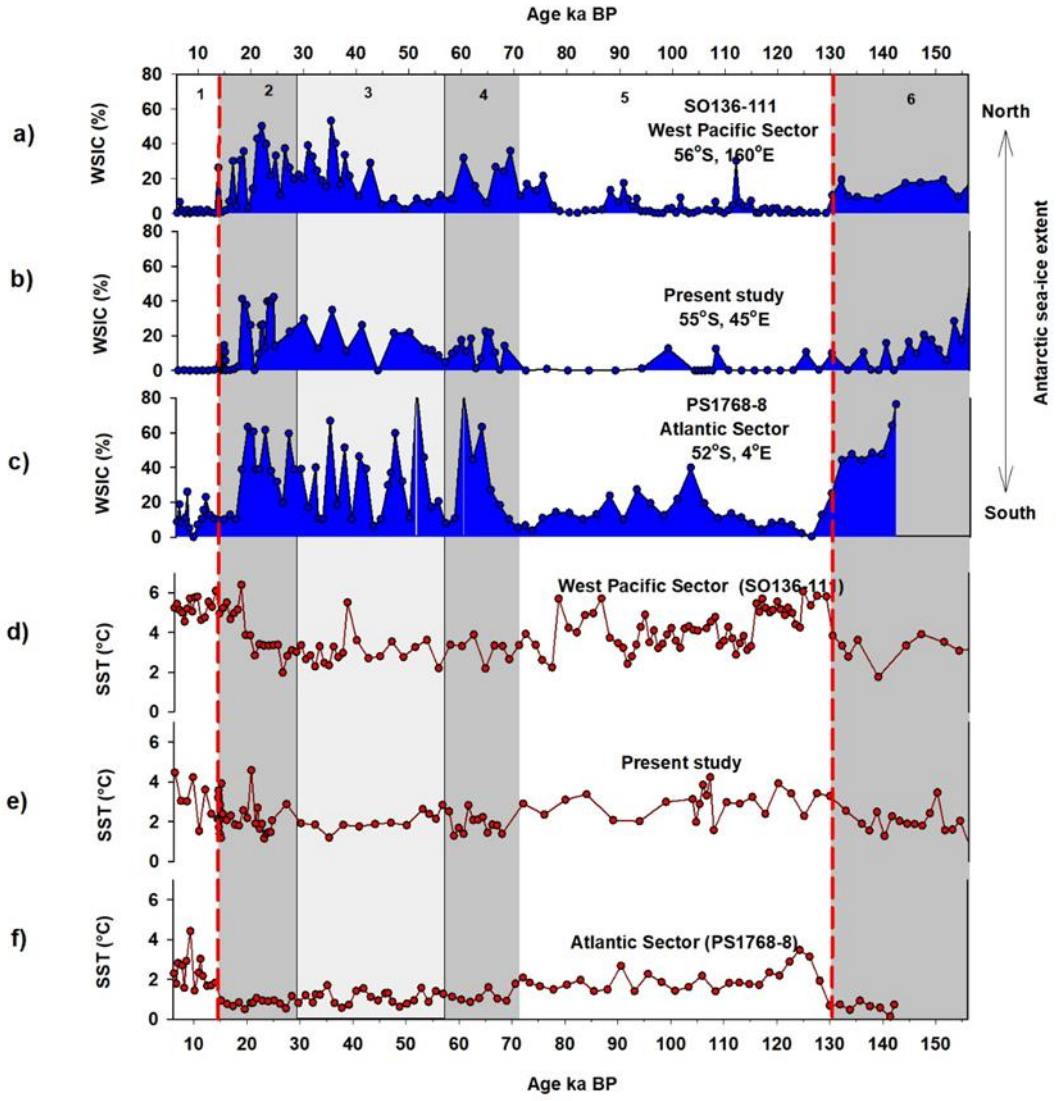

Fig. 4.5. Comparison of winter sea-ice concentration (WSIC, in percentages) with summer sea-surface temperature (SST) records from different sectors of the Southern Ocean. a) WSIC from SO136-111 (Crosta et al., 2004), b) WSIC from SK 200/33 (present study), c) WSIC from PS1768-8 (Esper and Gersonde, 2014b), d) SST from SO136-111 (Crosta et al., 2004), e) SST from SK 200/33 (present study) and f) SST from PS1768-8 (Esper and Gersonde, 2014a). Glacial periods are highlighted by grey bands and the number (1 to 6) indicates MIS stages (Lisiecki and Raymo, 2005). Red colour line indicates the Terminations (T I and T II).

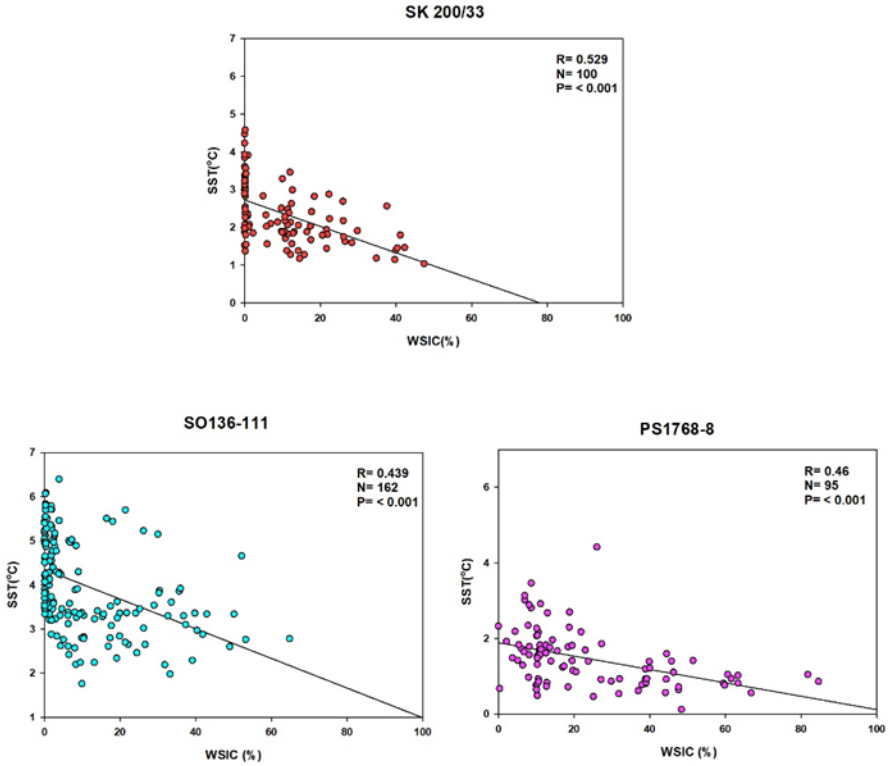

Fig 4. 9 Correlation between winter sea-ice concentration (WSIC, in percentages) and sea-surface temperature (SST, in degree Celsius) for the sediment core SK 200/33 (present study), SO136-111 (Crosta et al., 2004) and PS1768-8 (Esper and Gersonde., 2014b).

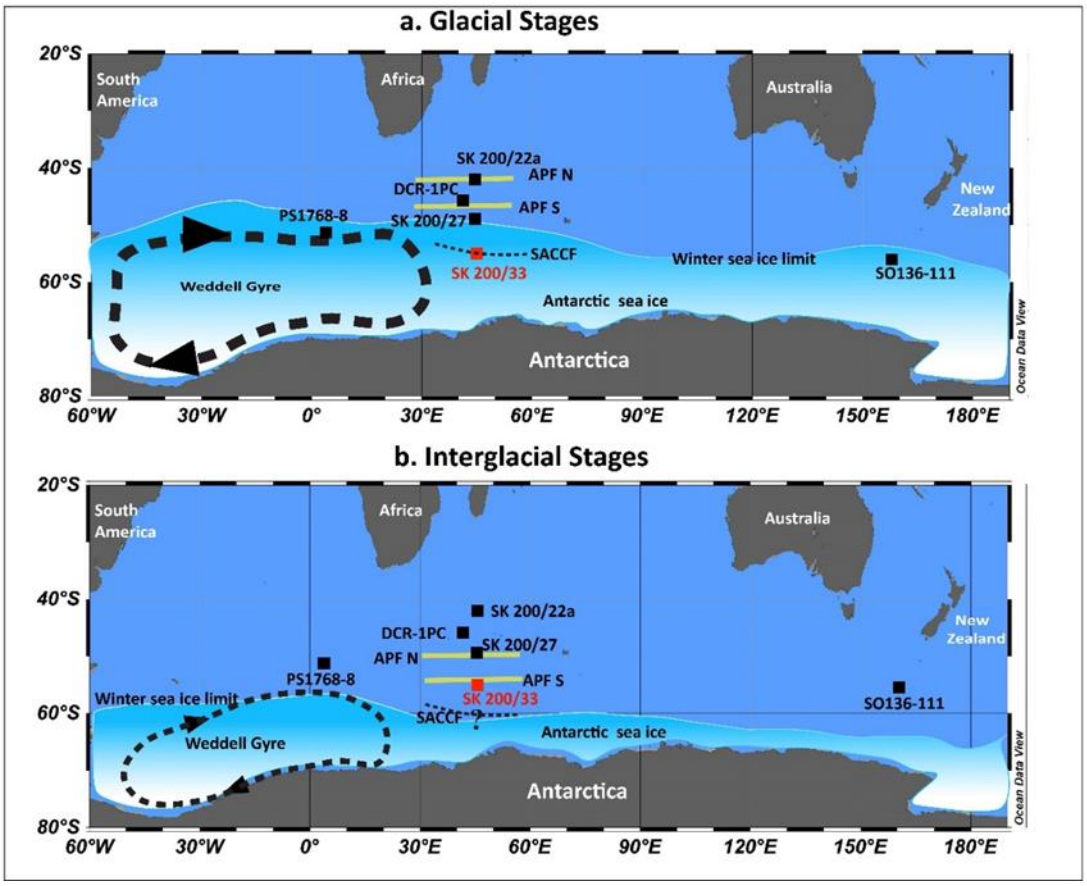

Fig. 4.6. Schematic representation of sea-ice extent and hydrological fronts position during a) Glacial stages, b) Interglacial stages. The Antarctic winter sea-ice limit during glacial periods is marked based on the observations from the present study, Crosta et al. (2004), Gersonde et al. (2005) and Esper and Gersonde (2014b). The APF is inferred based on Crosta et al. (2020) and SACCF is located based on the present study (SK 200/33 - red square). For the interglacial periods, the location of the APF is marked based on the present study and Nair et al. (2019) and the SACCF is marked based on the present study. As very little information exist for the position of the winter sea-ice limit during interglacial periods, we have marked here its mean modern location as presented in Comiso et al. (2003), Xiao et al. (2016) and Gersonde et al. (2005). Supporting datasets are marked as black squares.

4.4.3 Latitudinal changes in SW Indian sector paleoproductivity

The comparison of biogenic silica and DAA records from the three SK cores across the main hydrological features allows to assess changes in productivity in the SW Indian sector of the SO over the last climatic cycle. The POOZ site SK 200/33 registered a decrease in DAA and opal during glacial periods as compared to interglacial periods (Fig. 4.7a, b). These results are in agreement with records from the Atlantic POOZ (Fig. 4.7c; Esper and Gersonde, 2014b;

Jaccard et al., 2013), the Indian POOZ (Bareille et al., 1998) and the Pacific POOZ (Chase et al., 2003). The drop in biological productivity during the last glacial period has been attributed to the large expansion of the WSI cover (Chase et al., 2003) through several processes.

First, the greater sea-ice cover reduced the phytoplankton growing season preventing large and highly silicified diatoms to develop (Burckle and Cirilli, 1987; Cortese and Gersonde, 2007). Second, the increased sea-ice cycle (Gersonde et al., 2005) injected more low salinity meltwater (Shin et al., 2003) leading to a more stratified glacial water column, which restricted the nutrient supply from mid-depth waters to surface waters in the POOZ (François et al., 1997; Sigman et al., 2010; Jaccard et al., 2013) (Fig.4.8a).

Contrastingly, core SK 200/22a, from the SAZ, recorded a rise in productivity, as indicated by the different proxies, during glacial stages as compared to interglacial periods (Fig. 4.7f, g). The highest productivity is inferred to have occurred during MIS 2. High productivity in SAZ surface waters has been suggested to result from several synergistic processes. First, as lower productivity prevailed in the glacial POOZ, a larger fraction of nutrients remained unused and were transported northward in to the SAZ. Second, the northward migration of the APF and SAF, along with the northward shift of SWW, increased the upwelling into the SAZ enhancing the nutrient stocks there (Sigman et al., 2010) (Fig.4.8b). Third, the increase in dust iron supply from South America enhanced diatom growth rate and silica uptake (Brzezinski et al., 2002; Jaccard et al., 2013). However, the latter process may not have been dominant in the SW Indian sector of the SO that lies at the end of the dust plumes from South America and South Africa (Lamy et al., 2014). It is therefore suggested that the zone of high productivity, located today at around 50-55 ˚S in this region (Ragueneau et al., 2000), migrated at least until 43˚S during glacial periods of the last climatic cycle. In core SK 200/27 from the APF, productivity proxies do not display a clear glacial-interglacial pattern. DAA and biogenic silica seem to present lower values during MIS 2 and MIS 4 as in the southernmost core but, though DAA increased across the last deglaciation into the Holocene, biogenic silica values do not see any clear trend during this period (Fig. 4.7d, e). It is suggested that the apparent high variability in paleoproductivity proxies in core SK 200/27 result from the rapid and repeated latitudinal variations of the APF and associated nutrient supply. More records from this highly dynamic are however necessary.

The results show contrasting productivity conditions across the APF, with the rise recorded in the SAZ potentially compensating for the decrease observed in the POOZ in the SW Indian

sector of the SO during glacial periods (Supplementary fig. 4.10). The results also show an expanded sea-ice cover in this sector. Results therefore give support to previous studies, mainly from the Atlantic sector and from modelling, suggesting a strong role of the SO on the atmospheric CO_2 glacial drop via the combined action of (1) increased productivity in the SAZ (Kumar et al., 1995; Anderson et al., 1998; Matsumoto et al., 2002; Jaccard et al., 2013), (2) greater sea-ice extent lidding the surface ocean and reducing the outgassing of CO_2 (Ferrari et al., 2014) and (3) reduced vertical diffusion of deep CO_2-rich waters due to denser bottom waters (Bouttes et al., 2011; Galbraith and de Lavergne, 2018; Marzocchi et al., 2019). However, because only a handful of sea-ice and biological productivity data exist in the SW Indian Sector SO, most of them at low resolution, it is still extremely difficult to understand the transient role of sea ice in controlling the atmospheric CO_2 concentrations over the glacial-interglacial times (Kohfeld et al., 2017), especially on a millennial timescale that may bear essential information on the sea ice-carbon feedbacks over the next decades.

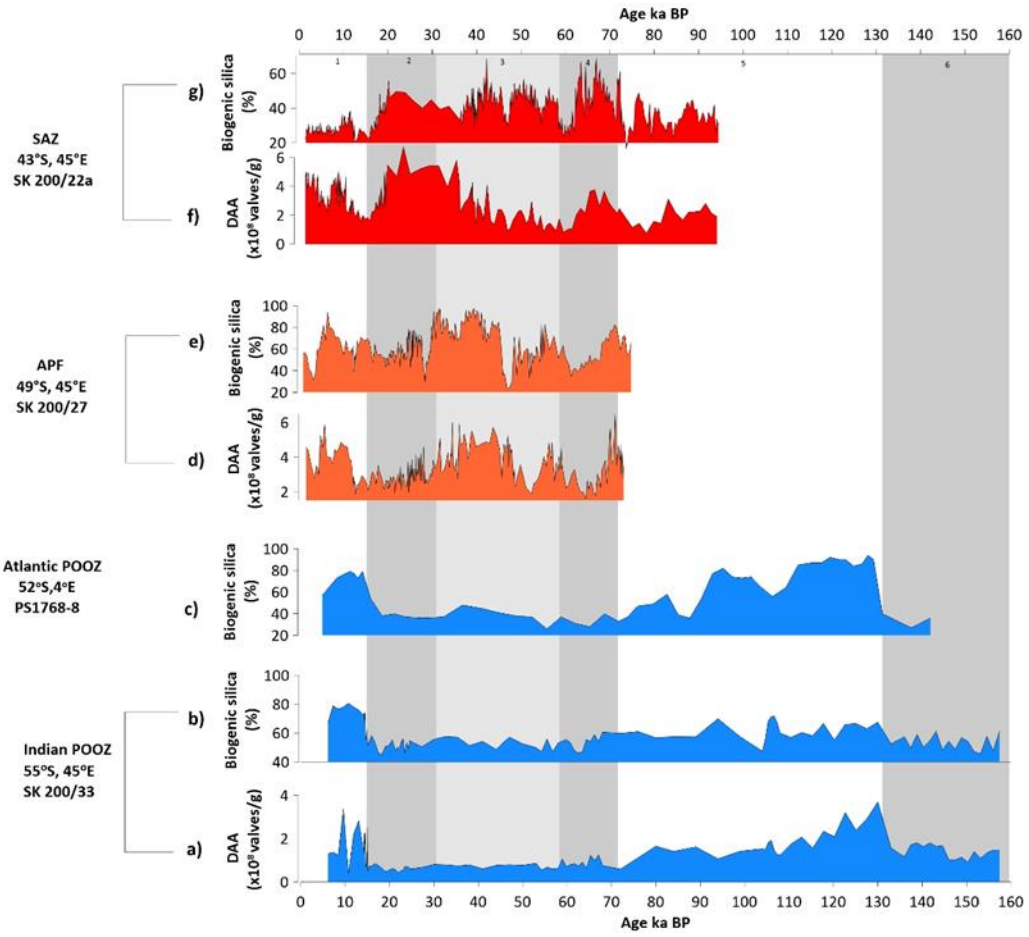

Fig. 4.7. Comparison of the diatom absolute abundance (DAA, $\times 10^8$ valves/g) and biogenic silica (%). a, b) Indian Permanently Open Ocean Zone (POOZ, SK 200/33, present study), c) Atlantic POOZ (PS1768-8, Esper and Gersonde, 2014b), d, e) Indian APF (SK 200/27, Nair et al., 2019), f, g) Indian SAZ (SK 200/22a, Nair et al., 2019). Glacial periods are highlighted by grey bands and the number (1 to 6) indicates MIS stages (Lisiecki and Raymo, 2005).

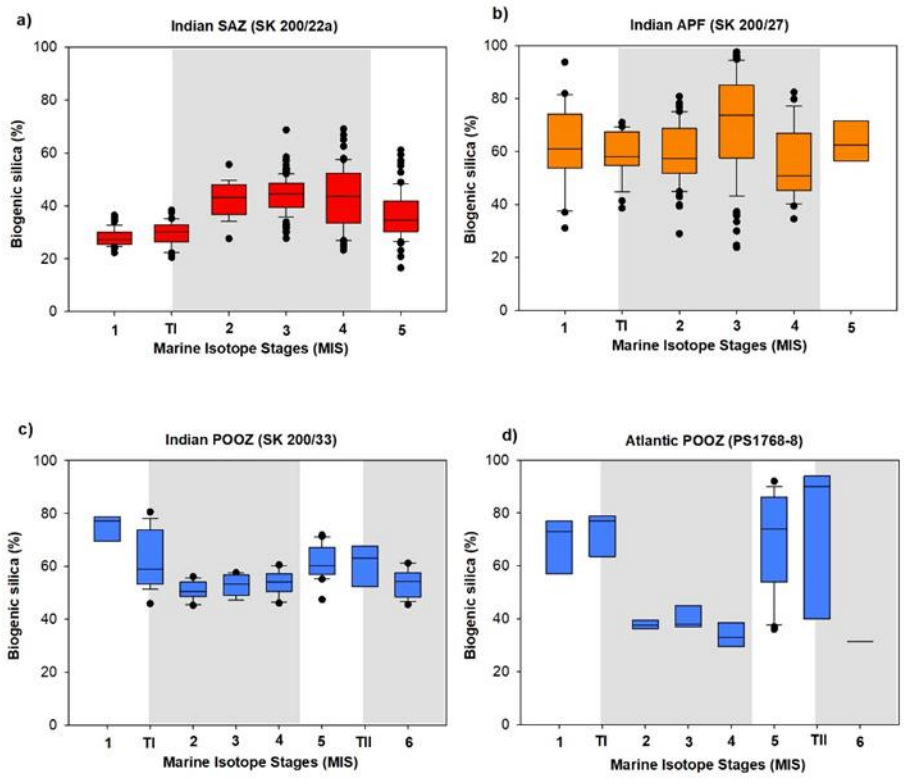

Fig 4. 10: Box and whisker plot showing variation of biogenic silica (%) for sediment cores from different latitudes. a) SK 200/22a (Nair et al., 2019); b) SK 200/27 (Nair et al., 2019); c) SK 200/33 (present study); d) PS1768-8 (Esper and Gersonde., 2014b).

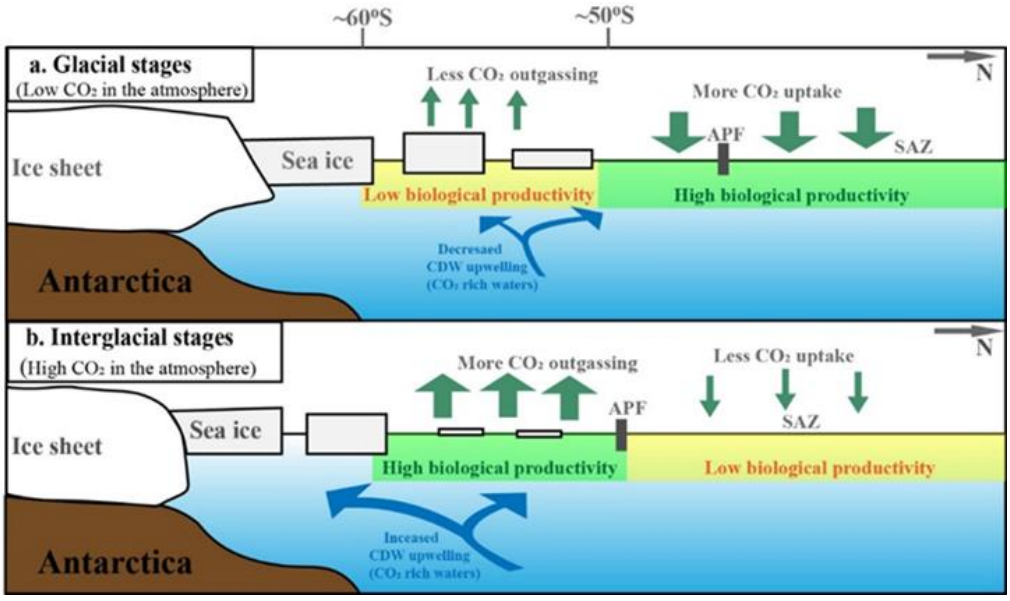

Fig. 4.8: Schematic representation of past variability of sea ice and its potential impact on Southern Ocean biological productivity during a) glacial stages and b) interglacial stages. APF - Antarctic Polar Front, SAZ – Sub-Antarctic Zone, CDW - Circumpolar Deep Water, N - North. Brown squares indicate the core location of SK200/33, SK200/27 and SK200/22a.

4.5 Conclusion

The diatom assemblages preserved in sediment core SK 200/33 allowed to estimate SST and WSI conditions in the POOZ of the SW Indian sector of the SO over the past 156 ka. The new records suggest SST of ~1-2 ˚C and WSID of ~2 months/year during each glacial period, with very little difference in between the mean values during each glacial period. The combination of the new data with published regional SST and WSI data suggests that all hydrological features migrated northward by few degrees of latitude during each glacial period and allows to place the SACCF at ~55˚S, the WSI edge close to 49˚S and the mean APF at 46˚S. The comparison of the new records with SST and WSI records from the Atlantic and Pacific sectors evidences higher amplitude changes in sea ice in the Atlantic sector compared to the other sectors during the last climatic cycle. Such behaviour is attributed to the influence of Weddell Gyre that transported sea ice farther to the north. All these data suggest that, though oceanic and atmospheric temperature changes determined the pacing of sea-ice history over the last 156 ka, winds and ocean currents drove the amplitude of the changes between the basins. The new records also evidence a decrease in paleoproductivity in the POOZ of the SW Indian sector in response to greater sea-ice cover and associated hydrological changes, namely reduced phytoplankton growing season, greater surface water stratification and lower nutrient input.

Despite the challenge of developing robust chronologies, it is extremely important to provide additional sea-ice records from the under-studied southern POOZ to obtain a more exhaustive view of sea-ice dynamic and, therefore, to better understand the transient role of sea ice in global climate at different timescales over glacial-interglacial cycles. Oxygen and temperature measurements play a crucial role in paleoceanography. Oxygen isotope analysis of foraminifera (d18Oforam) is widely used for reconstructing various environmental variables such as water temperature, salinity, and ice volume. However, this method has limitations due to factors like ice volume changes and regional conditions affecting carbonate oxygen isotope values. Therefore, additional information about past seawater conditions is often required. In some regions, like the North Pacific and Southern Ocean, the scarcity of coccolithophores and foraminifera in sediment records poses challenges. Diatom microfossils offer an alternative, with their oxygen isotopes (d18Odiatom) providing insights into SST, sea-ice extent, and paleoproductivity. Thus, the use of transfer functions may offer more reliable estimations of SSTs in various locations.

CHAPTER – 5

GLACIAL-INTERGLACIAL FLUX AND SIZE VARIABILITY OF FRAGILARIOPSIS KERGUELENSIS AND THALASSIOSIRA LENTIGINOSA FROM THE INDIAN SECTOR OF THE SOUTHERN OCEAN

5.1 Introduction

The Southern Ocean covers ~20% of the world's ocean, however, it is responsible for ~40% of the global oceanic uptake of atmospheric CO_2 via direct solubilisation of CO_2 in cold waters and CO_2 uptake by phytoplankton (Caldeira and Duffy, 2000; Orr et al., 2001; Mikaloff Fletcher et al., 2006; DeVries, 2014). A large fraction of the Southern Ocean's primary productivity is contributed by diatoms with efficient export and burial of biogenic silica and organic carbon to the sea-floor (Tréguer et al., 1995; Ragueneau et al., 2000). Among the hundreds of diatom species present in Southern Ocean phytoplankton, *Fragilariopsis kerguelensis* and *Thalassiosira lentiginosa*, two strongly silicified species, have been shown to be the most effective opal carrier to the seafloor (Shukla et al., 2013, 2016). These species are especially abundant in the water column around the Antarctic Polar Front (APF) (Hasle, 1969; Fenner et al., 1976) and can reach up to 70% and 40% of the total diatom assemblages, respectively, in the underlying modern sediments (Zielinski and Gersonde, 1998; Crosta et al., 2005a; Esper and Gersonde, 2014). The contribution of these species to the diatom assemblages decreases both northward in the Subantarctic Zone and southward in the seasonal sea-ice zone (Zielinski and Gersonde, 1998; Crosta et al., 2005a; Esper and Gersonde, 2014). Similarly, these species experience large latitudinal variation in valve mean sizes whereby they build larger frustules close to the APF and smaller ones both north and south (Cortese and Gersonde, 2007; Shukla et al., 2016). This finding is counter-intuitive to the mean size reduction induced by asexual cell division in which, repetitive divisions during bloom conditions should led to small size diatom communities (Round et al., 1990; Kloster et al., 2019). Other processes are therefore overwhelming size reduction due to the vegetative divisions. It is believed that diatoms growing at optimal conditions grow larger initial cells (Round et al., 1990; Assmy et al., 2007) therefore contributing to larger mean size of the communities. The production of larger initial cells, via sexual reproduction, is indeed facilitated by more efficient uptake of silica along with more efficient internal transport and deposition of silicic acid when diatoms grow at their optimal temperature range (Martin-Jézéquel et al., 2000). This range is 1-8°C for *F. kerguelensis* and *T. lentiginosa* as shown by very high abundances of these species in surface sediments (Crosta et al., 2005). However, temperature is not the sole parameter affecting diatom mean valve size. Iron fertilization experiments have shown that diatoms growing in iron-rich waters are bigger than in the surrounding areas (Boyd et al., 2002; Assmy et al., 2007). This is especially true for *F. kerguelensis* whereby the overall species abundances (Armand et al., 2008), the auxospore abundances (Assmy et al., 2006) and mean chain lengths and valve sizes (Gall et al., 2001) are higher within the iron-rich patch than in the surrounding waters.

Much less is known for *T. lentiginosa,* but iron-fertilization experiments did not show a significant response of *T. lentiginosa* to iron addition, with similar abundances in and out of an iron-rich patch (Assmy et al., 2007). *T. lentiginosa* are even more abundant outside the natural iron-rich region off Kerguelen Islands and thrive in low nutrient conditions (Armand et al., 2008).

Based on these findings, diatom size variations were used in several paleo-studies to infer past diatom physiology and past oceanic changes. Depending on the region and timescale studied, it was shown that iron, SST and sea ice were the most important variables to explain *F. kerguelensis* and *T. lentiginosa* past size variations (Cortese and Gersonde, 2007; Crosta, 2009; Cortese et al., 2012; Shukla et al., 2013, 2016; Nair et al., 2015). In the Polar Frontal Zone (PFZ), glacial-interglacial *F. kerguelensis* size variations were probably controlled by iron and silica availability with a secondary control by SST (Cortese and Gersonde, 2007; Cortese et al., 2012; Shukla et al., 2013, 2017; Nair et al., 2015), while in the iron-rich marginal ice zone of coastal Antarctica, Holocene *F. kerguelensis* size variations were largely controlled by sea ice and SST conditions (Crosta, 2009). Conversely, *T. lentiginosa* glacial-interglacial size variations probably responded to changes in SST (Shukla et al., 2016). However, all these studies cover 40,000 years before present (40 ka BP) at maximum and none of them were performed in the POOZ of the Indian sector of the Southern Ocean far away from iron leached from the Antarctic Peninsula (De Jong et al., 2012) or aeolian dust-born iron (Lamy et al., 2014).

In this study, the first continuous records of *F. kerguelensis* and *T. lentiginosa* average size and flux over the last 161 ka BP is presented, thus encompassing two climate cycles, in the understudied Indian sector of the POOZ. The first aim is to document whether average size and the flux variations responded similarly in the glacial periods and terminations (and in interglacial periods) of the two last climatic cycles and second to better understand the respective role of iron, silica and SST-sea ice on diatom average size variations. To this end, a comparison is made between the new records and published records from different sectors of Southern Ocean to identify the possible controlling factor for the size variation of these two species.

5.2 Chronology

Chronology of core SK 200/33 was obtained by AMS radiocarbon (^{14}C) dating on the bulk organic matter (due to the absence of foraminifera) in 5 samples from the top 36 cm (Table

5.1). The raw radiocarbon dates were calibrated to calendar ages using Calib software (Stuiver et al., 2005) after applying a mean reservoir age correction of 850 years recommended for this region (Bard, 1988; Berkman and Forman, 1996; Dutta, 2008). Chronological controls beyond the radiocarbon dates were achieved by tuning the SK 200/33 biogenic opal record with the EPICA Dome C temperature records of Antarctic ice core (Jouzel et al., 2007), assuming that the signals preserved in the Southern Ocean sediment cores and Antarctic ice cores are similarly related to large scale climate variability (additional data Fig. 5.8). The final age model is based on linear interpolation between the tuning points (Fig. 5.1). The top 100 cm of the sediment core represents 161 ka BP (Fig. 5.1), encompassing the Marine Isotope Stages (MIS) 1 to late MIS 6, with sedimentation rate ranging from 12 cm ka^{-1} (last deglaciation) to 0.2 cm ka^{-1} (MIS 5).

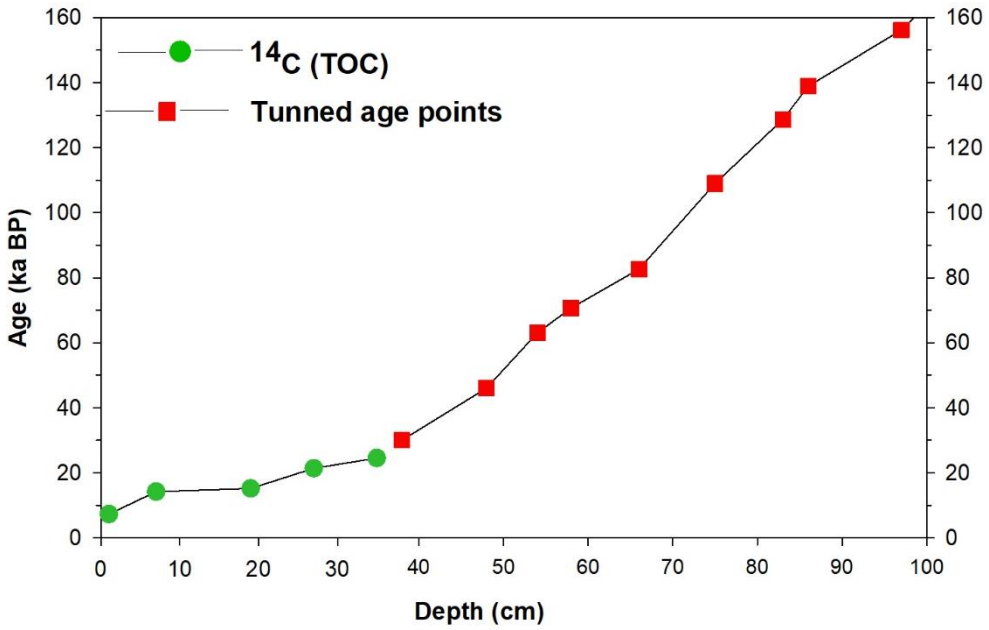

Fig. 5.1: Age model for sediment core SK 200/33 showing radiocarbon control points (green circles) and tuned age points (red square) against the depth of the sediment core.

Depth (cm)	Age (cal. Ka BP)	Dating
1	7.3	14C AMS dating
7	14.227	14C AMS dating
19	15.2	14C AMS dating
27	21.4	14C AMS dating
35	24.53	14C AMS dating
38	30	Opal and EDML
48	46.03	Opal and EDML
54	63.01	Opal and EDML
58	70.68	Opal and EDML
66	82.64	Opal and EDML
75	108.99	Opal and EDML
83	128.66	Opal and EDML
86	138.87	Opal and EDML
97	156.17	Opal and EDML
99	161.32	Opal and EDML

Table 5.1: Data used for constructing the age model for the investigated sediment core SK200/33. The tuned ages are based on correlation of the opal record with the established records of temperature records from Antarctic ice core (EPICA Dome C (EDC); Jouzel et al., 2007).

5.3. Additional data

To place the new measurements in a larger context and better understand drivers of *F. kerguelensis* and *T. lentiginosa* mean size variations, the data is compared with the published valve area (VA), absolute abundance (AA) and SST records from different sectors of Southern Ocean (Fig. 5.2). More precisely, the records from the Atlantic POOZ (core TNO57-13PC4; Shukla et al., 2013, 2016), the Indian Subtropical Front (SSTF, core MD97-2101), Subantarctic Zone (SAZ, core MD88-769), Polar Front (APF, core SK 200/27) (Shukla et al., 2013, 2016, 2017; Nair et al., 2019), and the Pacific APF (core SO136-111; Shukla et al., 2013, 2016) were used (Fig. 5.2).

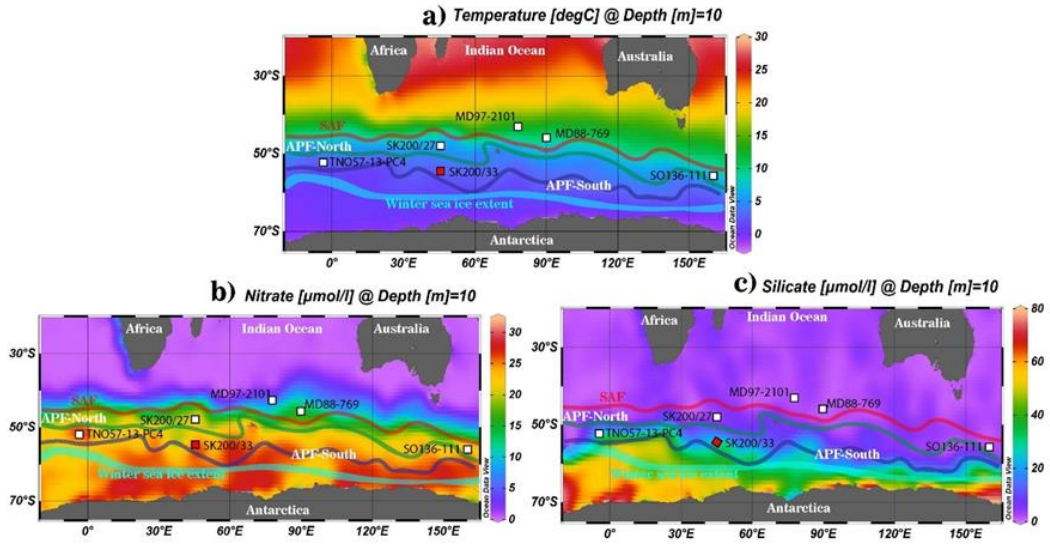

Fig. 5.2. Study area showing the location of the present sediment core site SK 200/33 (red square), along with locations of the other core sites used as a supporting dataset (white squares). The map at the background represents, a) annual mean sea-surface temperature (˚C), b) annual mean nitrate (µmol/l) and c) annual mean silicate (µmol/l) field from World Ocean Atlas 2013 (Locarnini et al., 2013) which have been gridded with the Ocean Data View software (Schlitzer, 2005).The positions of the SAF, APF and winter sea ice is based on (Belkin and Gordon, 1996; Orsi et al., 1995; Comiso, 2003; Pollard and Read, 2001; Pollard et al., 2007: Sokolov & Rintoul, 2009).

5.4 Results

The average size variables such as apical length (AL), trans-apical length (TL), and VA of *F. kerguelensis (Fig 2.3)* covaried for the last 161 ka BP (Fig. 5.4a) with a correlation coefficient (r) of ~0.98 (Additional data Fig. 5.9). The highest (AL of 57 µm; TL of 14 µm; VA of 648 μm^2) and the intermediate (AL of 40µm; TL of 11µm; VA of 345 μm^2) mean sizes, with mean values larger than the recorded averages, were found during the Termination I and the MIS 5 (Fig. 5.4a). Conversely, low values in *F. kerguelensis* size variables (AL<40µm; TL<11µm; VA<300 μm^2), with mean VA below the average value, were recorded during the mid-MIS 6, MIS 4, MIS 3 until late MIS 2 and MIS 1 (Figs. 5.4a and 5.5a). Down-core values in *F. kerguelensis* mean VA display a positive correlation, with a r of 0.5 ($p<0.05$), to down-core variations of *F. kerguelensis* flux. High flux values (50×10^7 valves cm^{-2} ka^{-1}) and intermediate

values (4×10^7 valves cm^{-2} ka^{-1}) occurred during the Termination I and II, respectively (Fig. 5b). Low flux values ($<2\times10^7$ valves cm^{-2} ka^{-1}) flux were recorded both during the glacial (MIS 6 and 4-2) and the interglacial stages (late MIS 5 and 1).

Thalassiosira lentiginosa showed higher than average diameter (>44µm) and VA (>1500µm) during the MIS6, late MIS 5, Termination II, mid-MIS 3 and Termination I when they reached their maximum values (Figs. 5.4d and 5.5b). Conversely, lower than average values (diameter <44µm and VA <1500µm) were observed during most of the MIS 5, MIS 4, early-mid MIS 2 and MIS 1. Downcore variations in *T. lentiginosa* mean VA and flux reveal a positive correlation, with a r value of 0.46 ($p<0.05$). The highest (8×10^7 valves cm^{-2} ka^{-1}) flux of the *T. lentiginosa*, were recorded during Termination I (Fig. 5.4e). The early MIS 2 and 5 were characterized by intermediate ($\sim1\times10^7$ valves cm^{-2} ka^{-1}) flux of the *T. lentiginosa* (Fig 5.5b).

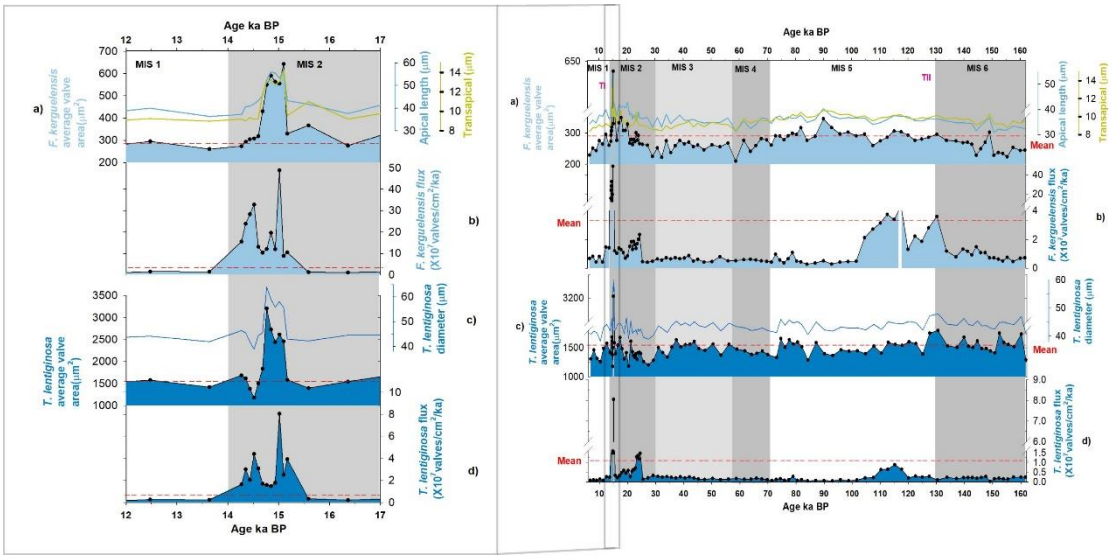

Fig. 5.3: SK 200/33 sediment records for the last 161 ka BP showing the variation of a) *F. kerguelensis* average valve area (µm^2), Apical and transapical length (µm), b)*F. kerguelensis* flux (× 10^7 valves/cm^2/ka), c) Average *T. lentiginosa* valve area (µm2), diameter (µm), d) *T. lentiginosa* flux (× 10^7 valves/cm^2/ka). The red dashed line represents the mean values. The dark grey bands indicate glacial stages, light grey band indicates interstadial and the white bands indicate interglacial stages (Lisiecki and Raymo, 2005).

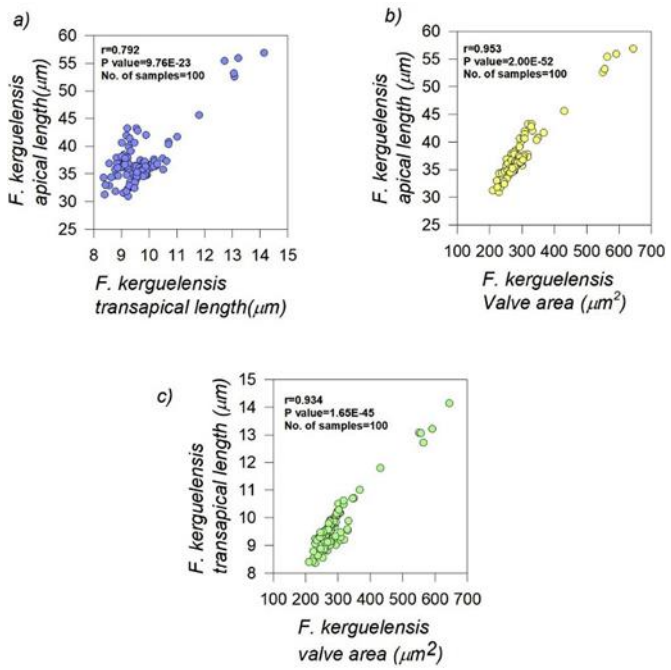

Fig. 5.9: Graph showing the Pearson's correlation between a) *F. kerguelensis* average Apical length (μm) and transapical length (μm), b) *F. kerguelensis* average Apical length (μm) and *F. kerguelensis* average valve area (μm2) and c) *F. kerguelensis* average transapical length and *F. kerguelensis* average valve area.

5.5 Discussion

There are no clear trends in *F. kerguelensis* and *T. lentiginosa* mean VA and fluxes in core SK 200/33. While both mean VA and fluxes are rather similar between full glacials and full interglacials, they appear significantly different during deglacial periods. A scenario is proposed involving sea ice, SST, the SO upwelling and macro- and micro-nutrient supply to Antarctic surface waters to explain these findings.

5.5.1 Terminations

The variation in the *F. kerguelensis* and *T. lentiginosa* mean VA and fluxes in core SK 200/33 over the last 161 ka BP is characterised by a pronounced peak during Termination I (Figs. 5.4 and 5.5), indicating an enhancement in their production and sizes in the southwestern Indian POOZ. The results are consistent with the last deglacial rise in biogenic opal burial in the Atlantic POOZ (Fig.5.6b-f) (Frank et al., 2000; Anderson et al., 2009; Jaccard et al., 2013) and Indian POOZ (Tang et al., 2016), indicating an increase in siliceous productivity during Termination I.

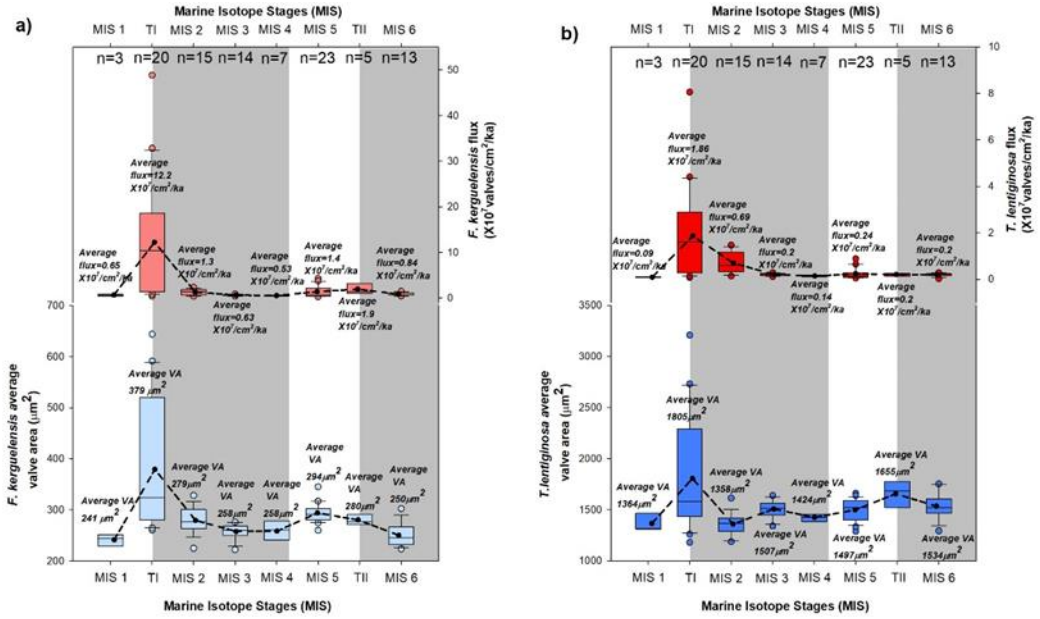

Fig. 5.4: Box and whisker plot showing variation of (a) Left Panel-Average *F. kerguelensis* valve area (µm2) in light blue boxes and *F. kerguelensis* flux (× 10^7 valves/cm^2/ka) in light red boxes, and (b) right panel-Average *T. lentiginosa* valve area (µm2) in dark blue boxes and *T. lentiginosa* flux (× 10^7valves/cm^2/ka) in dark red boxes from Marine Isotope Stage (MIS) 1–6. Grey bands indicate glacial stages and the dashed black lines are the average values.

Also, the size records agree with previous results on diatom biometry from the Atlantic POOZ (Shukla et al., 2013) and are opposite to the ones from the Atlantic and Indian APF and SAZ regions (Cortese et al., 2012; Shukla et al., 2013; Nair et al., 2015, 2019). These dichotomic behaviours of diatom sizes/biometry are related to the interplay of SST, sea ice and nutrient stocks. In the POOZ, the increase in diatom productivity and sizes over Termination I is attributed to greater supply of dissolved Si and Fe to the surface waters of the POOZ by the enhanced deglacial SO upwelling (Fig. 5.6h) (Anderson et al., 2009; Jaccard et al., 2013). To the north of the APF, *F. kerguelensis* and *T. lentiginosa* mean sizes decreased over Termination I to stay low during the Holocene (Fig. 5.7; Fig. 5.8) (Cortese et al., 2012; Shukla et al., 2013; Nair et al., 2015; Nair et al., 2019). They also decreased over the previous three terminations (Cortese et al. 2012). There, such a decrease, accompanied by a drop in the diatom and opal fluxes, was suggested to result from a reduction of aeolian dust to the SO.

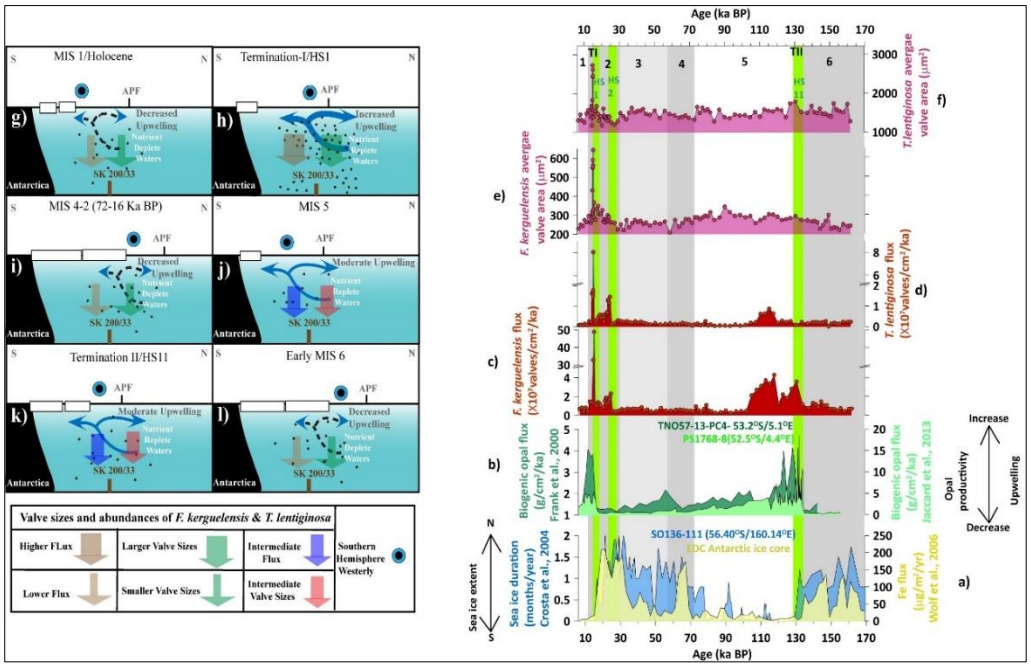

Fig. 5.5: Glacial-interglacial variation of a) Blue graph-Antarctic winter sea ice duration (months/year) reconstructed from the sediment core SO136-111 west Pacific sector of Southern Ocean (Crosta et al., 2004) and yellow graph-Fe flux from EDC, Antarctic ice core (Wolff et al., 2006), b) Biogenic opal fluxes (g/cm2/ka) from Atlantic permanent open ocean zone, indicative of opal productivity (dark green curve-Frank et al., 2000; light green curve-Jaccard et al., 2013), c) *F. kerguelensis* flux (× 10^7 valves/cm^2/ka), d) *T. lentiginosa* flux (× 10^7 valves/cm^2/ka), e) *F. kerguelensis* average valve area (µm2) and f) Average *T. lentiginosa* valve area (µm2). The dark grey bands indicate glacial stages, light grey band indicates interstadial, the white bands indicate interglacial stages and the light green band indicates Heinrich Stadials (HS) (Lisiecki and Raymo, 2005). Left panel represents different schematic scenarios from MIS 1-6 (g–l).

Given the new results, it is proposed that the southward migration of the westerlies winds and associated upwelling also reduced the supply of ocean-derived nutrient to the surface subantarctic waters. The increase in SST also pushed *F. kerguelensis* and *T. lentiginosa* out of their respective ecological range, which reduced their ability to use the low nutrient stocks. Results also indicate that Termination II appears different than Termination I both in terms of *F.kerguelensis* and *T. lentiginosa* VA and fluxes. The increase in VA and flux, at Termination II, was much less than at Termination I (Fig. 5.6). An opposite pattern in CaCO3 burial, with low burial during Termination I and high burial during Termination II, was found at site IODP 1094 in the Atlantic POOZ (Jaccard et al., 2013). These results may indicate different SO

upwelling conditions and associated nutrient levels during the two terminations, maybe linked to different global oceanic circulations with more millennial events (such as Heinrich stadial 1 (HS1) and Younger Dryas) interrupting Termination I more than Termination II (Deaney et al., 2017). Termination I was characterized by intense Northern Hemisphere cooling during HS1 (18-14.6 ka BP). The large-scale reorganization of the global atmospheric circulation (southward shift of trade winds) induced a poleward shift of Southern Hemisphere westerlies, which increased the SO upwelling (Fig. 5.6h) (Anderson et al., 2009: Toggweiler and Lea, 2010) and outgassed CO_2 to the atmosphere (Martinez-Boti et al., 2015). After the Bolling-Allerod warming, a second cooling occurred in the northern Atlantic with a similar influence on SO atmospheric and oceanic circulations. The SO upwelling strengthened again during the Younger Dryess (YD; 12.8-11.5 ka BP), which again resulted in high silica production and burial along with CO_2 outgassing to the atmosphere. Unlike Termination I, only one millennial event scattered Termination II, namely HS11 (~135-129 ka BP). As such the Northern Hemisphere cooling during Termination II was prolonged (Bohm et al., 2015) as compared to Termination I, with important repercussions on the global oceanic circulation (Marino et al., 2015; Deaney et al., 2017) and probably SO upwelling. The lower rate of CO_2 outgassing at Termination II suggests a less intense SO upwelling or a less deep ventilation than during Termination I, probably injecting less nutrients to the Antarctic surface waters. Additionally, although ice cores indicate that Antarctic sea-ice retreat started 135 ka ago (Wolff et al., 2006), in phase with CO_2 increase, marine cores suggest that sea ice still did not reach its interglacial extent by 130 ka BP (Crosta et al., 2004; Esper and Gersonde, 2014). By comparison, it is believed that sea ice reached its interglacial extent by 15-14 ka BP during Termination I (Xiao et al., 2016). As such, a late sea-ice retreat during Termination II may have reduced siliceous productivity and the mean size of the studied species, along with limiting CO_2 outgassing. However, such issues of different upwelling conditions during the two terminations need further investigation.

5.5.2. Glacials

During glacial stages, smaller VA, lower productivity and fluxes of both species were recorded in core SK 200/33 (Figs. 5.4-6) in line with lower opal burial in the Atlantic and Pacific POOZ (Frank et al., 2000; Chase et al., 2003). Size records are in agreement with previous results from the West Pacific APF and Atlantic POOZ (Shukla et al 2013, 2016) and are opposite to the results from north APF regions such as the Indian and Atlantic SSTF, SAZ, APF (Figs. 5.7 and 5.8) (Cortese et al., 2012; Shukla et al 2013, 2016, 2017; Nair et al., 2015, 2019). In the

POOZ, smaller sizes, lower siliceous productivity and burial, despite higher dust flux to the SO (Lambert et al., 2008), probably resulted from greater sea-ice extent (Gersonde et al., 2005) and water column stratification (François et al., 1997). Both processes, along with the northward migration of the Southern Hemisphere Westerly (Figs. 5.6i and 5.l), reduced the SO upwelling and the availability of nutrients in surface waters (Sigman and Boyle, 2000; Jaccard et al., 2013). In addition, core site SK 200/33 appears quite remote from any aeolian dust input (Lamy et al., 2014) leaving the ocean as the main iron source for phytoplankton in this region. In regions north of APF (Figs. 5.7 and 5.8), larger sizes and higher abundances of both species during glacial stages may result from the combination of 1) increased nutrient availability due to the northward shift of fronts and associated upwelling and 2) ecologically ideal SST allowing the effective utilization of available nutrients by both species (Shukla et al., 2013; 2016; 2017).

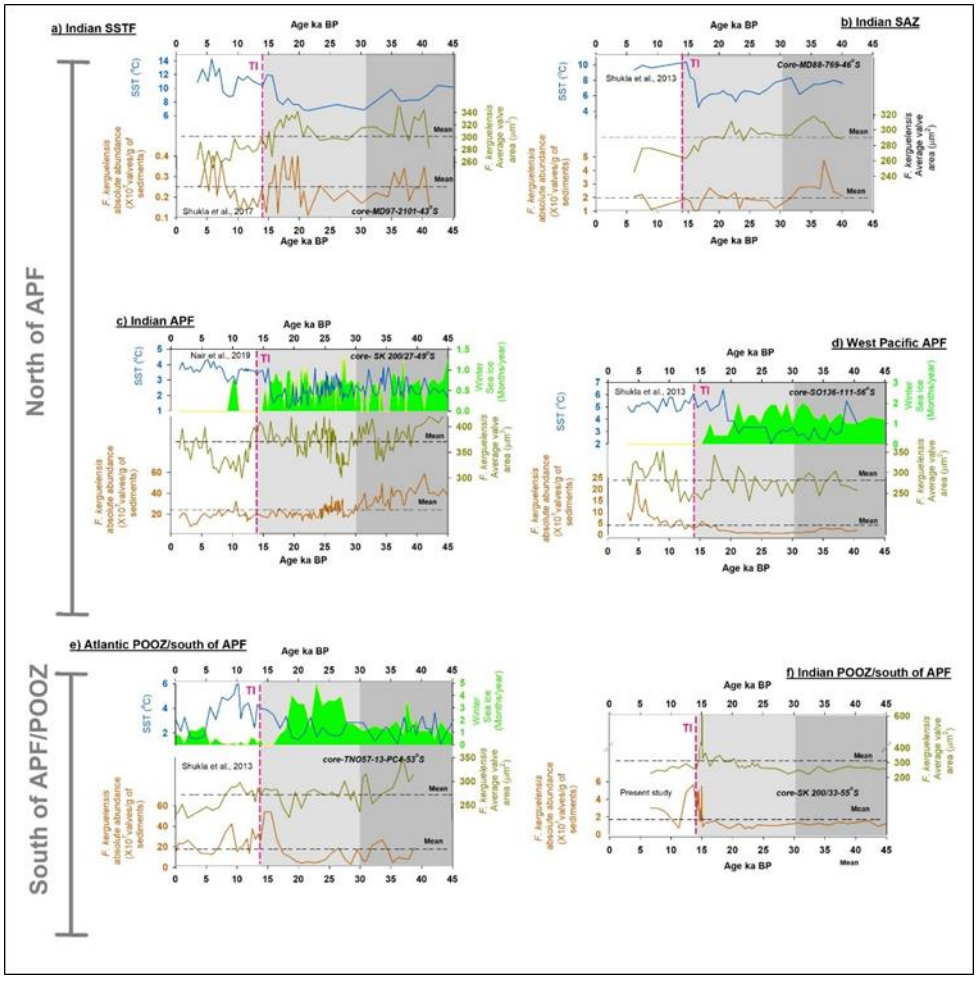

Fig. 5.6: Comparison between SST (blue curve), Average *F. kerguelensis* valve area (olive green curve) and *F. kerguelensis* absolute abundance (orange curve) for the last 45 ka BP from the sediment core records of a) Indian SSTF (Shukla and Crosta, 2017), b) Indian SAZ (Shukla et al., 2013), c) Indian APF (Nair et al., 2019), d) West Pacific APF (Shukla et al., 2013), e) south of APF, Atlantic sector (Shukla et al., 2013) and f) south of APF, Indian sector (present

study). The bright green graph (c–e) represents winter sea ice duration (months/year). The light grey band indicate Marine Isotope Stage (MIS) 2 (glacial stage) and the dark grey band indicate MIS 3 interstadial (Lisiecki and Raymo, 2005). The dashed horizontal line indicates mean values.

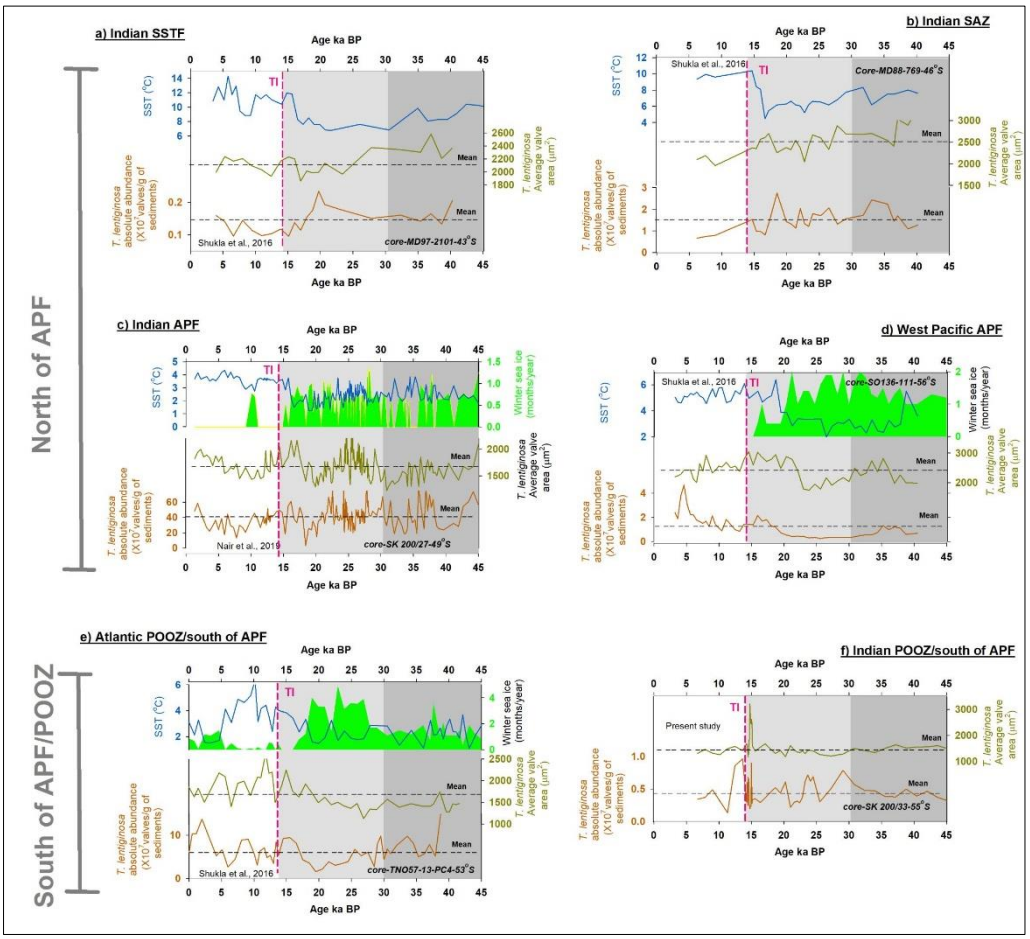

Fig. 5.7: Comparison between SST (blue curve), *T. lentiginosa* valve area (olive green curve) and *T. lentiginosa* absolute abundance (orange curve) for the last 45 ka BP from the sediment core records of a) Indian SSTF (Shukla et al., 2016), b) Indian SAZ (Shukla et al., 2016), c) Indian APF (Nair et al., 2019), d) West Pacific APF (Shukla et al., 2016), e) south of APF, Atlantic sector (Shukla et al., 2016), f) south of APF, Indian sector (present study). The bright green graph (c–e) represents winter sea ice duration (months/year). The light grey band indicate Marine Isotope Stage (MIS) 2 (glacial stage) and the dark grey band indicate MIS 3 interstadial (Lisiecki and Raymo, 2005). The dashed horizontal line indicates mean values.

Slightly smaller sizes of *F. kerguelensis* and lower fluxes of both species during MIS 6 than during MIS 2 (Figs. 5.4 and 5.5) suggest less favourable environmental conditions during the previous glacial period. The few sea-ice records extending back to 150 ka generally indicate

more pervasive sea-ice cover during the MIS 6 than during the MIS 2 (Schneider-Mor et al., 2005; Wolff et al., 2006; Esper and Gersonde, 2014). A longer sea-ice duration may have further weakened the SO upwelling and associated macro- and micro-nutrient supply to the surface waters and causally dampened the production and burial of large and heavily silicified *F. kerguelensis*. Contrastingly, *T. lentiginosa* mean VA were slightly larger during the MIS 6 than during the MIS 2-4 (Figs. 5.5 and 5.6), while *T. lentiginosa* fluxes were similar in all glacial periods of the last 150 ka, which probably reflects the fact that this species can survive in less favourable conditions where nutrient availability is low but sufficient (Armand et al., 2008; Rigual-Hernandez et al., 2015; Shukla et al., 2016). To note that during MIS 2, between 26.5-24.3 ka BP, an abrupt peak in fluxes of both species is recorded in core SK 200/33 (Fig. 5.6), potentially indicating a millennial reinforcement of the SO upwelling and associated nutrient supply. The presence of heavy sea ice may however have prevented both species to grow larger valves (Fig. 5.6). Such millennial events were not evidenced during MIS 6. However, this needs further investigation since these are the first records extending back to the MIS 6.

5.5.3 Interglacials

In core SK 200-33, *F. kerguelensis* and *T. lentiginosa* mean VA and fluxes during the Holocene are the lowest of the last 161 ka (Figs. 5.5 and 5.6). New size records are in agreement with previous results from the Atlantic POOZ (Shukla et al., 2013, 2016), wherein the smaller Holocene diatom size was attributed to low macro- and micro-nutrient stocks in Antarctic surface waters. However, *F. kerguelensis* and *T. lentiginosa* mean VA were larger during the MIS 5 than during the MIS 1. Fluxes of both species were also slightly higher during the MIS 5 (Figs. 5.4-6). It is suggested that the differences observed between the two interglacial periods were nurtured in the previous terminations. The intense SO upwelling may have rapidly exhausted the deep reservoir during Termination I (Martinez-Boti et al., 2015) as indicated by the deglacial pulses in biogenic silica burial recorded in the low latitude of the Atlantic Ocean (Mekler et al., 2013) despite higher productivity in the SO (Anderson et al., 2009). As such, despite a possible reinvigoration of the SO upwelling after 8 ka BP (Studer et al., 2017), the limited deep stock of Si and Fe could not sustain large siliceous productivity during the MIS 1 (Fig. 5.6g), thereby leading to the observed reduction in mean sizes and fluxes of both the species (Fig. 5.6b-f). Conversely, while the deep nutrient and CO_2 stock may have been similarly exhausted during Termination II, its longer pacing as compared to Termination I may have allowed a greater deep regeneration and the strong deepening of the AMOC at the end of

Termination II may have allowed more nutrient to the SO surface waters (Deaney et al., 2017). In addition, the greater size and fluxes of both species recorded during the MIS 5 could be owing to the lower winter sea-ice presence (Crosta et al., 2004; Schneider-Mor et al., 2005), thus resulting in conditions within their ecological range (Fig. 5.6j). Based on the observations covering 161 ka, it is proposed that variations in mean sizes and fluxes of *F. kerguelensis* and *T. lentiginosa* at the core site SK 200/33 resulted from the interplay of sea ice, SST and macro- and micro-nutrients via their role on diatom productivity and initial cell size. However, more studies from different sectors and realms of the SO are necessary to decipher the respective role of each process.

5.6 Conclusions

Fragilariopsis kerguelensis and *Thalassiosira lentiginosa* mean valve area (VA) and sedimentary fluxes were analysed in the Indian POOZ over the last 161 ka. New records do not show clear glacial-interglacial patterns as observed in the PFZ and SAZ realms, but only focusing on the last glacial cycle. Overall, low mean VA and fluxes were here recorded over the last 161 ka, except during the deglaciations. It is suggested that low VA and fluxes during the glacial periods resulted from low SST, high sea-ice cover limiting the ability of these species to make use of the low macro-nutrients stock despite high dust load. Largest mean VA and fluxes during the deglaciations resulted from the intensification of the SO upwelling supplying high amount of macro- and micro-nutrient to the surface waters along with sea-ice retreat and increasing SST allowing diatom to better use the available nutrients. Low mean VA and fluxes during the interglacial periods resulted from low micro- and macro-nutrient stocks as the SO upwelling supplied nutrient-poor deep waters (as compared to the deglaciations) and the dust source was cut-off. Mean VA and fluxes were much higher during Termination I than during Termination II arguing for a much greater supply of nutrients via a more intense, and maybe deeper-sourced, SO upwelling. The greater exhaustion of the SO deep nutrient stock may explain the smaller mean VA and fluxes observed during the Holocene than during the MIS 5.

CHAPTER – 6

PALEO SEA SURFACE TEMPERATURE AND SEA ICE VARIABILITY FROM THE KERGUELEN ISLAND REGION, SOUTHERN OCEAN

6.1 Introduction

The Southern Ocean (SO) is an extreme region with the strongest wind on earth, the largest ice shelf and the widest range of seasonal sea ice (Wunsch 1998; Thomas and Dieckman 2003). The interactions between the atmosphere, oceans and cryosphere have a strong impact on dynamics throughout the formation of the entire climate system. Moreover, SO plays an important role in having global control over water mass formation, carbon sequestration, freshwater distribution, etc. due to its unique geographical condition which allows the exchange of water masses over the major oceanic basins (Rintoul et al. 2001; Tomczak and Godfrey 2003). Although according to the official definition the limit of the SO is to the area south of 60˚S, but a more consistent oceanographic designation includes all waters of Antarctic and Subantarctic water, about 40˚S. By this definition, the SO covers for 20% of the world's oceanic area (Weijer et al., 2012). The large portion of the SO is covered by sea ice, spreading over an area of 18 x 10^6 km^2 in winter. This concentration drastically reduces to 3 x 10^6 km^2 during summer (Parkinson et al., 2004). The extensive sea ice cover has a variety of effects on the regional climate along with the flora and fauna in the vicinity thus studying and understanding the sea ice cover and its fluctuations in these regions has grown to be a crucial component of Earth System Science research (Parkinson et al., 2016).

Changes in the SO sea ice and high latitude temperature drop have previously been shown to have an influence over northward migration of the ACC and the fronts because of expansion of the winter sea ice cover during the glacial stages (Gersonde and Zielinski 2000; Crosta et al., 2004; Ghadi et al., 2020). This has been attributed to wind stress forcings (westerlies) and the feedback changes which are linked to the oceanic and the atmospheric temperature (Gersonde and Zielinski 2000; Crosta et al., 2004; Ferry et al., 2015; Ghadi et al., 2020). The large scale wind fields from SO especially the westerly winds of Southern Hemisphere also affects the Agulhas system. It is a system around southern Africa and forms a crucial element of global ocean circulation. In essence, with the shifting of westerlies towards the south during warming climate, the oceanic gateway between the Africa and STF widens thus increasing the leakage from the Indian Ocean to the Atlantic. On the other hand, northward shift during colder climate narrows the gateway thus reducing the leakage (Beal et al., 2011). It is also observed that the Agulhas leakage and Agulhas Return Current (RC) are anticorrelated (M.Civel-Mazens et al., 2021). RC is thought to have a strong impact on the SO especially in the Indian sector oceanography and also the phytoplankton productivity in the past. Sicre et al., 2005 supports this hypothesis via their study from alkenone-based sea-surface temperature record, showing

high temperatures during MIS 2 and MIS 3 north-east of the Kerguelen Plateau. However, the lack of paleoclimate records from the Southern Ocean prevented it from a comprehensive understanding of the role of this important component of the global climate system. Therefore this component is presented which is an attempt to understand the sea ice variation and sea surface temperature and their relation to the other governing factors. The chapter presents ocean temperature reconstructed based on the diatoms from the Kerguelen region.

6.2 Chronology

Sample No.	Sample reference	Depth	Nature	Age BP	Error age BP
SacA44304	MD12-3401 Cq / 2-3 cm G.bulloides	2	Foraminifera	1640	30
SacA44305	MD12-3401 Cq / 54-55 cm G.bulloides	54		4340	35
SacA44306	MD12-3401 Cq / 86-87 cm G.bulloides	86		7040	30
SacA44308	MD12-3401 Cq / 114-115 cm G.bulloides	114		9420	40
SacA44455	MD12-3401 Cq / 130-131 cm N.pachyderma senestre	130		11335	40
SacA44456	MD12-3401 Cq / 142-143 cm G.bulloides	142		12045	40
SacA44457	MD12-3401 Cq / 146-147 cm N.pachyderma senestre	146		12590	45
SacA44458	MD12-3401 Cq / 154-155 cm G.bulloides	154		13170	45
SacA44461	MD12-3401 Cq / 162-163 cm N.pachyderma senestre	162		13380	50
SacA44442	MD12-3401 Cq / 174-175 cm G.bulloides	174		14235	45
SacA44445	MD12-3401 Cq / 194-195 cm G.bulloides	194		14930	50
SacA44448	MD12-3401 Cq / 210-211 cm N.pachyderma senestre	210		15980	60
SacA44450	MD12-3401 Cq / 250-251 cm N.pachyderma senestre	250		18190	70
		274	Correlation pointers with MD12-3396cq and EDC for the older part of the core	21404	
		459	Correlation pointers with MD12-3396cq and EDC for the older part of the core	33191	

Table 6.1: MD 12 3401 cq core chronology. The age control is provided by radiocarbon dates of monospecific planktic foraminifera samples (*G. bulloides* and *N. pachyderma* s.). Beyond radiocarbon ages, the ages are obtained by tuning MD 12-3396 cq and EDC for the older part of the core.

The age model of sediment core MD 12-3401 cq is based on radiocarbon dates of monospecific planktic foraminifera samples (*G. bulloides* and *N. pachyderma* (s.). Core MD 12-3401 cq is located today within the sub-antarctic zone and GLODAP reconstruction of preindustrial $\Delta^{14}C$ ocean distribution indicates a surface water reservoir age of ~600 years at this core location (Olsen et al., 2016). It is assumed that similar and coeval radiocarbon reservoir age changes occurred at MD 12-3401 cq and MD 12-3396 cq (Gottschalk et al., 2020) sites as both cores

are located today within the sub-antarctic zone and as on marine radiocarbon timescale (uncorrected for reservoir age), the two cores show coeval changes across the last deglaciation, within the error of their ^{14}C age scale. Hence uses the surface ocean reservoir ages changes obtained for MD 12-3396 cq (Gottschalk et al., 2020) to correct the 19 radiocarbon ages of core MD 12-3401 cq. The calendar ages were then calculated considering a deposition model (P_Sequence("MD-3401CQ",0.5,0.25,U(-1,1)) with the *Oxcal* bayesian software (Ramsey 2008, Bronk Ramsey and Lee, 2013).

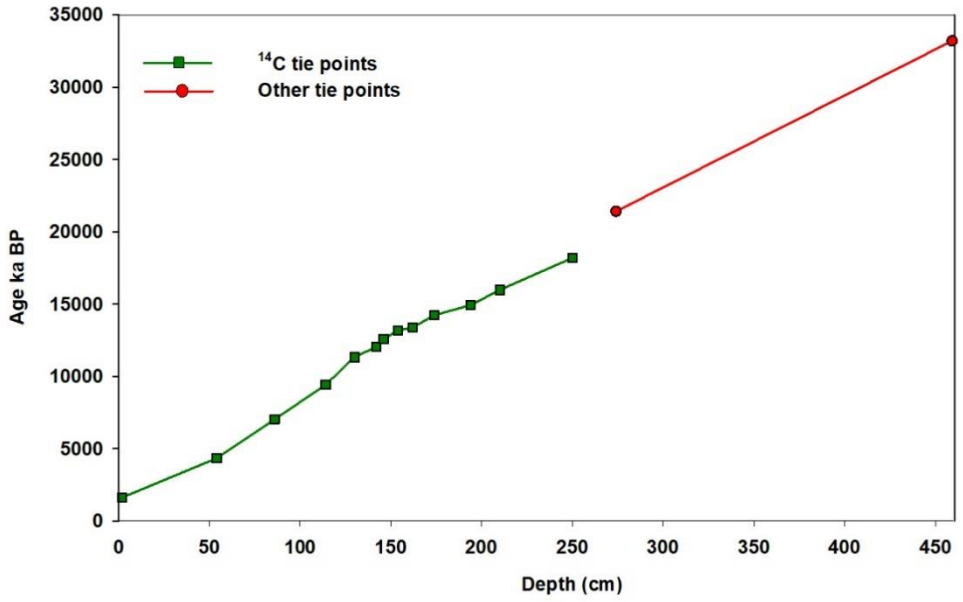

Fig: 6.1: Age model for MD 12 3401 cq. The age control is provided by radiocarbon dates of monospecific planktic foraminifera samples (*G. bulloides* and *N. pachyderma* s.) indicated in green colour. Beyond radiocarbon ages, the ages are obtained by tuning MD 12-3396 cq and EDC for the older part of the core indicated by red colour.

6.3 Results

Down-core variations in diatom assemblages

In this study, the records are presented for the sediment core MD 12 3401 cq for the top 400cm based on fossil diatoms. Their relative abundance has been calculated and plotted against the age (Fig. 6.1). The sea ice diatoms varies between 0 to 6%. The core site shows presence of sea ice diatoms throughout the downcore. During cooler stage the increase in the relative

abundance of this group can be seen, wherein the abundance varies between 2.5-6%. With the change in the cooler to warmer condition, the abundance of sea ice diatom also decreases. At places it is as low as 0 % and highest recorded is 3% (Fig. 6.2d). Similar trend is shown by The 'Water stratification Group' group of diatom (refer Chapter 3) as that of sea ice diatoms. With persisting warmer conditions these group of diatoms abundance records the lowest abundance. Throughout the downcore they vary from 10-50% of the total diatom abundance (Fig. 6.2c). The POOZ group abundance is varying from 55 to 85% over a period of last 29kyr. With the cooler conditions, the POOZ diatoms abundance decreases and opposite is seen during the warmer times. They show 20% notable decrease in the cooler conditions (Fig. 6.2b). The SAZ group abundance varies from 2-15%. Similar trend to that of POOZ diatoms is shown by the SAZ diatoms (Fig. 6.2a). The overall diatom abundance varies between 60-80 x 10^6 valves/g of sediments. Sharp decrease in the total abundance is noted at 19.5 kyr with the lowest abundance of 33 x 106 valves/g of sediments. From then a gradual increase is seen as we move towards the present warmer time (Fig. 6.2e).

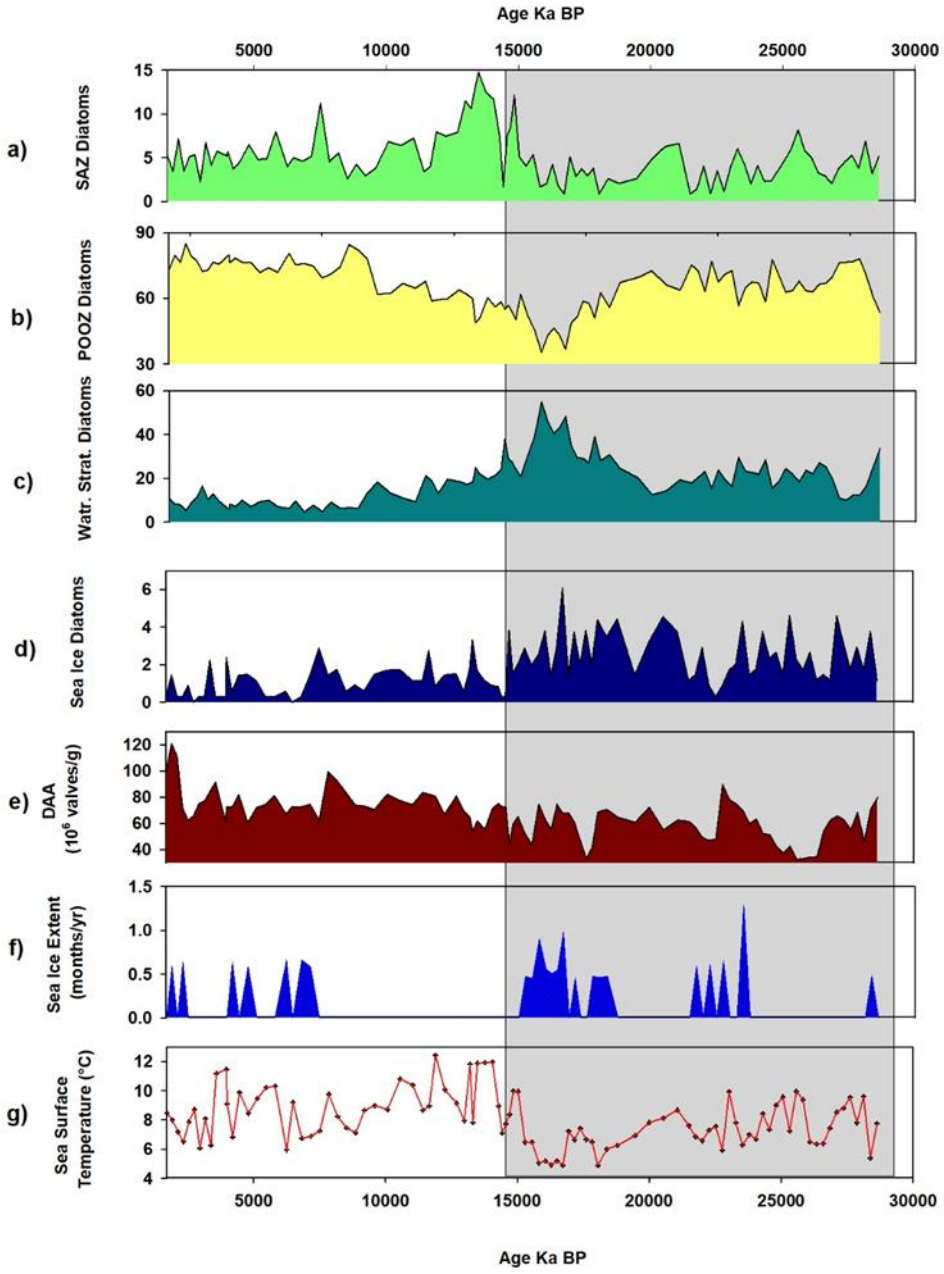

Fig. 6.2: Downcore relative and absolute abundance plotted against age a) Sub Antarctic zone diatom group; b) Permanent open ocean zone (POOZ) diatom group; c) Water stratification diatom group; d) Sea-ice diatom group; e) Diatom absolute abundance; f) Sea ice extent (SIE); g) Sea surface temperature (SST). Grey band indicates glacial period.

The Modern Analog Technique (MAT) applied to the fossil diatom assemblages estimates between 0.5 to 1 month of SIE at different time intervals in the downcore records. In the cooler stage the core site records a presence of sea ice for 0.5 to 1 month/yr. But a sporadic appearance

of the sea ice is also seen during the warmer time periods (Fig. 6.2f). Down core records of SST at the core site reveal a temperature variation from 5˚ to 12˚C. The results suggests the temperatures at the core location during glacial were between 5-9 ˚C. With the transition from glacial to interglacial, between 17 to 13kyr the core recorded the highest temperature, 12 ˚C, at the site. The interglacial was characterised by temperatures varying between 6-11 ˚C (Fig. 6.2g).

6.4 Discussion

Diatom based MD 12 3401 CQ records from the SO shows warming SSTs during the glacial time. The temperature here varies from 5˚C to 12 ˚C (Fig. 6.2g). With the glacial to interglacial transition the core shows elevated temperature marking the highest temperature of 11 to 12 ˚C. Further from 12.5 kyr to 6 kyr, lowered SSTs are marked which follows a similar trend to the EDC δ^{18} O record (Bazin et al., 2013 Fig. 6.4d). The MD 12 3401 cq results are compared with the two sediment cores MD 3396 (M. Civel-Mazens et al., 2021) from 47˚43.880 S - 86˚41.710 E, and MD 94-103 (Sicre et al., 2005) from 45˚35S - 86˚31E Kerguelen Region. Fig 6.3 shows positions of the core MD 94-103 and MD12 3396 with respect to MD 12 3401 cq.

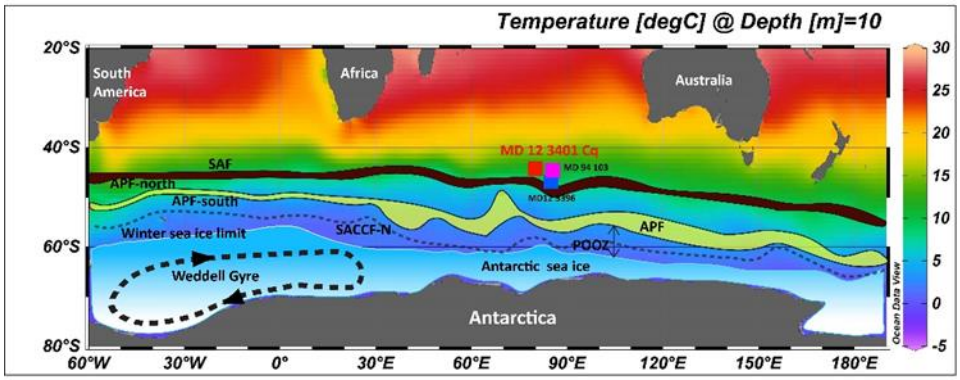

Fig. 6.3: Study area showing core site MD 12 3401 cq location (red square) along with the locations of the published sea-ice records used here; blue square – MD 12 3396, M. Civel-Mazens et al., 2021 and pink square – Sicre et al 2005. The position of the Antarctic Polar Front, both northern and southern branches (APF-north and APF-south), is marked based on Anilkumar et al. (2006), Luis et al. (2009) and Belkin and Gordon (1996) while the position of the Southern Antarctic Circumpolar Current Front (SACCF) ans SAF is marked based on Sokolov and Rintoul. (2009a,b). Modern winter sea-ice limit is marked based on Comiso et al. (2003). The mean summer sea-surface temperature data is taken from the World Ocean Atlas

2013 (Locarnini et al., 2013) and has been gridded with the Ocean Data View software (Schlitzer, 2002).

As seen from the Fig 6.4g it is evident that the SSTs recorded in MD 94-103 glacial is warmer in comparison to the glacials of MD 12 3401 cq and MD 12 3396. Here the temperatures of 5˚C to 12 ˚C are marked in MD 12 3401 cq; in MD 94 103 it is varying between 9.5 to 13˚C whereas MD 12 3396 registers between 4 to 14˚C.

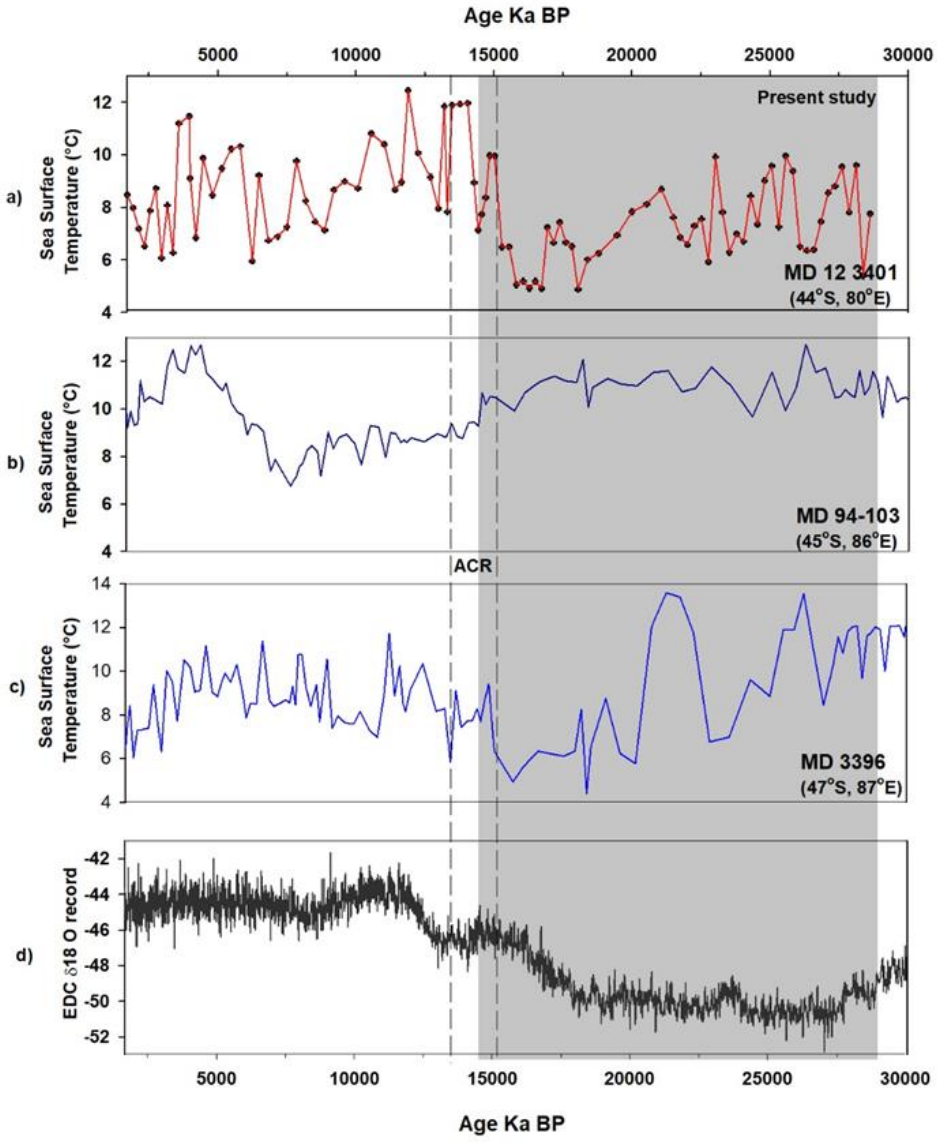

Fig. 6.4: Comparison of the SST from Indian Sector of SO with that of the cores from the latitudinal transect. SST of a. MD 12 3401 Cq (present study), b. MD 94-103 (Sicre et al.,

2005), c. MD 12 3396 (M. Civel-Mazens et al., 2021) and d. EDC delta 18 O records (Bazin et al., 2013). Grey band indicates glacial period.

The core MD 12 3396 shows a warming trend from 28 to 20kyr. The SST records show short scale variability around the plateau during the Antarctic Cold Reversal, which is also noted in MD 3396 (M. Civel-Mazens et al., 2021). The same trend is marked in MD 12 3401Cq (Fig. 6.4a and d). A gradual decrease in the temperatures are seen from Termination 1 towards the Holocene in all the cores (Fig. 6.4). Core MD 12 3401 cq along with the compared cores MD 12 3396 cq, and MD 94 103 records warm interglacial following the general trend of EDC δ^{18} O record (Bazin et al., 2013 Fig. 6.4d). But they also mark warmer glacials (MIS 2). It has been observed that the sediment cores lies in region where Dynamical Subtropical Front (DSTF) merges with SAF thus bringing the warmth from the lower latitudes of the Indian Ocean (M. Civel-Mazens et al., 2021, Graham and De Boer, 2013). The interplay between the Agulhas Return Currents (RC) intensity and the modification in the SO fronts has been suggested as a possible reason in delivering the warm water at the core site MD 12 3396 (M. Civel-Mazens et al., 2021). The SST difference between the surface (diatoms) and subsurface (radiolarians) temperature also points towards surface currents as the controlling factor as a normal glacial interglacial trend with subsists are seen (Civel-Mazens et al., 2021).

The alkenone based record from Sicre et al., 2005 also highlights an overall warming trend in the MIS 2. This was first estimated to be due to different growth season or depth habitat of the calcareous coccolithophorid *Emiliania huxleyi* from which alkenones are extracted. But it was also noted that long distance advection of bottom sediments from the North to the core site (Sicre et al 2005) which is on southern flank of the South Indian Ridge was unlikely (Sicre et al., 2005; Mazaud et al., 2002). Thus advection by strong surface current becomes a more plausible mechanism to explain the observed temperature anomaly (Sicre et al., 2005). Since Agulhas current and its retroflection feeds the warmer water to ACC, it is expected that warmer SSTs reflected in MD 94 103 are due to the strong advection of warm alkenones in the subantarctic zone by surface waters of the Agulhas current (Sicre et al., 2005).

It is observed that the cores located at 46˚S and 47˚S had witnessed warmer temperature than the core at 44˚S. Thus we see a latitudinal variation with respect to temperature is documented during the glacial as well as interglacial period. This latitudinal variation is presumed to be within the warmer SSTs of glacial which can be due to the intensity of the Agulhas current and

its retroflection. The subsurface temperature from both the locations, MD 12 3396 (radiolarians) and MD 94 103 (foraminifera) indicates no anomalies in the temperature thus following a general glacial interglacial trend of cooling and warming respectively.

6.5 Conclusion

The diatom record form the Indian Sector of the Southern Ocean from the Kerguelen region provides a high resolution information about the paleoceonography. Sediment core MD 12 3401 cq retrived from the Kerguelen region emphasis on understanding the paleo SIE, frontal positions and their interaction with the ocean circulation over the last glacial-interglacial cycle on a higher resolution scale. Down core records of SST at the core site reveal an overall temperature variation from 5˚ to 12˚C. The modern temperature registered at the site is 10.8˚C. The core shows the sporadic occurrences of sea ice during MIS 2. The overall diatom abundance varies between 60-80 x 10^6 valves/g of sediments. Strong warming is noted during glacial period (MIS 2). Comparative study of the core with that of the cores from surrounding region indicates the control of surface currents i.e. Agulhas current and its retroflection over the estimated SSTs. Additional data records from the Kerguelen Region are required to explain the phenomenon happening in the vicinity.

It is seen that Oxygen and thermometry measurements are of paramount importance in such fields. The oxygen isotope analysis of foraminifera (d^{18}Oforam) is a widely used palaeoceanographic technique that allows researchers to reconstruct various environmental variables, such as deep water formation, surface and bottom water temperature, salinity, global ice volume, and water column stratification((e.g., Mulitza et al., 1997; Barrera and Johnson, 1999; Niebler et al., 1999; Ravelo and Andreasen, 1999; Zachos et al., 2001; Simstich et al., 2003; Rohling et al., 2004). Furthermore the calcareous phytoplankton provides a good control on the stratigraphy based on the calibrations of the d^{18}O (Flores et al., 1998). A pioneering work to use d18O in carbonates was carried out by Urey 1947 and Emiliani 1955, 1966 to reconstruct the SSTs. Laboratory experiments have established empirical equations linking calcification temperature to oxygen isotope fractionation in carbonates (Erez and Luz, 1983; Bemis et al., 1998; Ziveri et al., 2003; Coplen, 2007; Day and Henderson, 2011). However in the natural environment, the oxygen isotopic composition (d18O) of carbonates cannot be solely considered a direct indicator of sea surface temperatures (SSTs). This is because variations in ice volume, regional hydrographic conditions, and changes in the proportion of 18O/16O in seawater significantly influence the d18O values in carbonates. Consequently, due

to the uncertainty of the proxy, reconstructing SSTs from sediment cores necessitates additional information about past seawater conditions.

The limitation of using Coccolithophores, foraminifera and other carbonates in palaeoceanography also arises because of their scarcity or absence in sediment records in certain regions, particularly in high latitude areas like the North Pacific Ocean and the Southern Ocean. These regions are considered sensitive to and potential drivers of global climatic change.

Fortunately, cores from these regions often contain abundant diatom microfossils, which have been analyzed through various methods to reconstruct changes in SST, sea-ice extent, and palaeoproductivity (Romero et al., 2003; Crosta et al., 2004; Gersonde et al., 2005; Kienast et al., 2006). The measurement of diatom oxygen isotopes (d^{18}Odiatom) has the potential to offer valuable additional paleoceanographic insights, especially in regions where carbonate data is scarce. For example, using a core in the South Atlantic Ocean, Shemesh et al. (1992) employed both d18Odiatom and planktonic d18Oforam (Neogloboquadrina pachyderma, dextral) to reconstruct variations in surface d18Owater and SST during the past 30,000 years (Swann and Leng 2009). However later studies on the Southern Ocean have primarily concentrated on interpreting the raw d18Odiatom data rather than obtaining specific quantitative paleoenvironmental reconstructions, including SST. Studies of three cores from the Southern Ocean's Atlantic and Indian sectors, situated south of the Polar front, have shown periodic d18Odiatom reductions of approximately 2-3% during the last glacial period (Shemesh et al., 1994). However, linking these changes to glacial SST increases contradicts other paleotemperature records from the region, including diatom transfer functions and other paleoceanographic data (Swann and Leng 2009). Thus their lies many uncertainities with respect to d18Odiatom data like Shemesh et al. (1992) proposed that the d18Odiatom temperature calibration might be unreliable in high latitude waters due to the influence of localized upwelling, which significantly affects the diatom-water oxygen isotope equilibrium. The effect of secondary isotope exchange and dissolution on d18Odiatom is also observed (Swann and Leng 2009). There are also challenges associated with purifying and isolating individual taxa, diatom oxygen isotope measurements are typically conducted on mixed species assemblages in bulk (Swann et al., 2007). Thus, considering the challenges associated with the d18Odiatom data set, the transfer function provides a better estimations of the SSTs from different locations.

SUMMARY AND CONCLUSION

The aim of this study was to use fossil diatoms to create a new dataset relevant to sea ice extent (SIE) and sea surface temperature (SST) from the Indian Southern Ocean (SO) sector, which had been largely unstudied in the SO during past interglacial periods. The focus is on a quantitative and process-oriented understanding of past SO changes to improve the understanding of future climate and environment. Two sediment cores from the SO sector of India, namely SK 200/33 and MD12 3401 cq, were utilised and studied. The ages of both sediment cores are obtained by ^{14}C dating of accelerator mass spectrometry (AMS). The SK 200/33 chronology is based on bulk organic carbon and correlates the SK 200/33 SST and winter sea ice duration (WSID) records with the ice core temperature record EPICA Dome C (EDC) to get more data (Jouzel, et al., 2007). Additional tuning to the EDC dust was also provided by SK 200/33 magnetic susceptibility signal, resulting in additional tie points (Lambert et al., 2008). The sediment core MD 12 3401 Cq chronology is based on radiocarbon ages of monospecific planktonic foraminiferal samples (*G. bulloides and N. pachyderma s.).*

Diatoms were extracted from the sediments to prepare permanent slides on which diatom relative abundance, total abundance and morphometric measurements were performed. A transfer function (Crosta et al., 2004) was applied to provide quantitative estimates of SIE and SST. Records from the SK 200/33 (55°S – 45°E) sediment core helped us understand the historical variability of Antarctic sea ice and past productivity over glacial-interglacial timescales of 156,000 years (Chapter 4). The effects of Antarctic sea ice on ocean circulation, biological productivity, and the distribution of carbon dioxide (CO_2) between the ocean and the atmosphere have a major impact on global climate. However, little is known about its past, especially in the South Seas region of southwestern India. In this chapter, the narrow ecological preference of SO diatoms is used to infer paleoceanographic conditions, including SST, winter sea ice concentration (WSIC) and WSID.

The results achieved are also compared here with previous productivity records. In addition, the results are also compared with those from other sectors of SO to understand the evolution of SST, WSIC and WSID in other regions of SO. A combination of new records and regional data indicates that hydrologic structures shifted several degrees north during all glacial periods, with the Southern Antarctic Circumpolar Current Front reaching the core site, the Antarctic Polar Front at 46°S, and the WSI likely extending to 49°S.

However, during the early Holocene and the last interglacial, the hydrofront and WSI edge shifted poleward by few degrees of latitude. Available data indicate that variations in WSI

amplitudes were stronger in the Atlantic sector compared to those in the other sectors compared to the Indo- and Western Pacific sectors during the last glacial–interglacial cycle. This discrepancy is attributed to the presence of the Weddell Gyre, which carries the sea ice far to the north. The data also indicate that the productivity of the glacial period of the POOZ decreased, possibly due to larger WSI and shorter growing seasons.

On the glacial-interglacial timescale, primary productivity is also assessed based on the size variability of *Fragilariopsis kerguelensis* and *Thalassiosira lentiginosa* (Chapter 5). Since SO is dominated by the presence of diatoms, primary productivity is also largely controlled by diatoms. Among the various types of diatoms, the *Fragilariopsis kerguelensis* (O'Meara) Hustedt and *Thalassiosira lentiginosa* (Janisch) Fryxell are important silica carriers in the SO seafloor due to their abundance and high degree of silicification (Shukla et al., 2013, 2016). The results in this chapter imply that larger sea-ice coverage, greater water column stratification, reduced SO upwelling, and a northward shift of the Southern Hemisphere westerly winds contributed to smaller sizes and lower fluxes of *F. kerguelensis* and *T. lentiginosa* at the core site during the glacial phases. Over the glacial stages (MIS 2 and 6) subtle changes in the numbers and fluxes of both species indicate that the two glacial stages had different environmental conditions. *F. kerguelensi*s was smaller in size and flux from *F. kerguelensis* and *T. lentiginosa* in MIS 6 than in MIS 2. Observations show a significant discrepancy in size and flux during Termination I compared to Termination II. This was attributed to the stronger SO lift during Termination I compared to Termination II, which provided POOZ with large amounts of macro- and micronutrients. Overall, this suggests that different factors influence the size and flux of these species on different time scales.

Chapter 6 focuses on understanding paleo-SIE, frontal positions, and interactions with ocean circulation over the past glacial interglacial cycle at a high-resolution scale constructed using the MD 12 3401 Cq sediment core. The sediment core is located at 44°40'S, 80°23'E, east of the Kerguelen Plateau in the Indian Sector of the SO. Down-core sea surface temperature (SST) logs at the core site show an overall temperature range of 5°C to 12°C. The overall abundance of diatoms varies between 60 and 80 x 10^6 valves/g sediment. Strong warming is noted during glacial period (MIS 2). Comparative study of the core with that of the cores from surrounding region indicates the control of surface currents i.e. Agulhas current and its retroflection over the estimated SSTs.

REFERENCES

Abelmann, A., Gersonde, R., Knorr, G., Zhang, X., Chapligin, B., Maier, E., ... & Tiedemann, R. (2015). The seasonal sea-ice zone in the glacial Southern Ocean as a carbon sink. *Nature communications*, *6*(1), 1-13.

Abernathey, R. P., Cerovecki, I., Holland, P. R., Newsom, E., Mazloff, M., & Talley, L. D. (2016). Water-mass transformation by sea ice in the upper branch of the Southern Ocean overturning. *Nature Geoscience*, *9*(8), 596-601.

Ackley, S. F., Gow, A. J., Buck, K. R., & Golden, K. M. (1980). Sea ice studies in the Weddell Sea aboard USCGC Polar Sea. *Antarctic Journal of the United States*, *15*(5), 84-86.

Adkins, J. F. (2013). The role of deep ocean circulation in setting glacial climates. Paleoceanography, 28(3), 539-561.

Adkins, J. F., McIntyre, K., & Schrag, D. P. (2002). The salinity, temperature, and δ18O of the glacial deep ocean. *Science*, *298*(5599), 1769-1773.

Ainley, D., Woehler, E. J., & Lescroël, A. (2017). Birds and Antarctic sea ice.

Akiba, F. (1982). Late Quaternary diatom biostratigraphy of the Bellingshausen Sea, Antarctic Ocean. *Rept. Tech. Res. Center, JNOC*, (16), 31-74.

Alkama, R., Koffi, E. N., Vavrus, S. J., Diehl, T., Francis, J. A., Stroeve, J., Forzieri, G., Vihma, T. and Cescatti, A. (2020). Wind amplifies the polar sea ice retreat. *Environmental Research Letters*, *15*(12), 124022.

Ancel, A., Kooyman, G. L., Ponganis, P. J., Gendner, J. P., Lignon, J., Mestre, X., Huin, N., Thorson, P.H., Robisson, P. & Le Maho, Y. (1992). Foraging behaviour of emperor penguins as a resource detector in winter and summer. *Nature*, *360*(6402), 336-339.

Anderson, R. F., Ali, S., Bradtmiller, L. I., Nielsen, S. H. H., Fleisher, M. Q., Anderson, B. E., & Burckle, L. H. (2009). Wind-driven upwelling in the Southern Ocean and the deglacial rise in atmospheric CO2. *science*, *323*(5920), 1443-1448.

Anderson, R. F., Kumar, N., Mortlock, R. A., Froelich, P. N., Kubik, P., Dittrich-Hannen, B., & Suter, M. (1998). Late-Quaternary changes in productivity of the Southern Ocean. *Journal of Marine Systems*, *17*(1-4), 497-514.

Anilkumar, N., Luis, A. J., Somayajulu, Y. K., Babu, V. R., Dash, M. K., Pednekar, S. M., ... & Pandey, P. C. (2006). Fronts, water masses and heat content variability in the Western Indian sector of the Southern Ocean during austral summer 2004. *Journal of Marine Systems*, *63*(1-2), 20-34.

Ardyna, M., & Arrigo, K. R. (2020). Phytoplankton dynamics in a changing Arctic Ocean. *Nature Climate Change*, *10*(10), 892-903.

Armand, L. (1997). The use of diatom transfer functions in estimating sea-surface temperature and sea-ice in cores from the southeast Indian Ocean.

Armand, L. K. (2000). An ocean of ice-advances in the estimation of past sea ice in the Southern Ocean. *GSA Today*, *10*(3), 1-7.

Armand, L. K., & Leventer, A. (2003). Palaeo Sea Ice Distribution±Reconstruction and Palaeoclimatic Significance. *Sea Ice: Physics, Chemistry and Biology*, 333-372.

Armand, L. K., & Zielinski, U. (2001). Diatom species of the genus Rhizosolenia from Southern Ocean sediments: distribution and taxonomic notes. *Diatom Research*, *16*(2), 259-294.

Armand, L. K., Crosta, X., Romero, O., & Pichon, J. J. (2005). The biogeography of major diatom taxa in Southern Ocean sediments: 1. Sea ice related species. *Palaeogeography, Palaeoclimatology, Palaeoecology*, *223*(1-2), 93-126.

Armand, L. K., Crosta, X., Romero, O., & Pichon, J. J. (2005). The biogeography of major diatom taxa in Southern Ocean sediments: 1. Sea ice related species. *Palaeogeography, Palaeoclimatology, Palaeoecology*, *223*(1-2), 93-126.

Arrigo, K. R., van Dijken, G. L., & Bushinsky, S. (2008). Primary production in the Southern Ocean, 1997–2006. *Journal of Geophysical Research: Oceans*, *113*(C8).

Assmy, P., Henjes, J., Smetacek, V., & Montresor, M. (2006). AUXOSPORE FORMATION BY THE SILICA-SINKING, OCEANIC DIATOM FRAGILARIOPSIS KERGUELENSIS (BACILLARIOPHYCEAE) 1. *Journal of Phycology*, *42*(5), 1002-1006.

Bard, E. (1988). Correction of accelerator mass spectrometry 14C ages measured in planktonic foraminifera: Paleoceanographic implications. *Paleoceanography*, *3*(6), 635-645.

Bard, E., & Rickaby, R. E. (2009). Migration of the subtropical front as a modulator of glacial climate. *Nature*, *460*(7253), 380-383.

Bareille, G., Labracherie, M., Bertrand, P., Labeyrie, L., Lavaux, G., & Dignan, M. (1998). Glacial–interglacial changes in the accumulation rates of major biogenic components in Southern Indian Ocean sediments. *Journal of Marine Systems*, *17*(1-4), 527-539.

Barrera, E., & Savin, S. M. (1999). Evolution of late Campanian-Maastrichtian marine climates and oceans. *Evolution of the Cretaceous ocean-climate system*.

Battarbee, R. W., & Berglund, B. E. (1986). Handbook of Holocene palaeoecology and palaeohydrology. *Diatom analysis. Wiley, New York*, 527-570.

Bazin, L., Landais, A., Lemieux-Dudon, B., Kele, H. T. M., Veres, D., Parrenin, F., ... & Wolff, E. W. (2013). The Antarctic ice core chronology (AICC2012). *PANGAEA [data set]*, *10*.

Beal, L. M., De Ruijter, W. P., Biastoch, A., & Zahn, R. (2011). On the role of the Agulhas system in ocean circulation and climate. *Nature*, *472*(7344), 429-436.

Belkin, I. M., & Gordon, A. L. (1996). Southern Ocean fronts from the Greenwich meridian to Tasmania. *Journal of Geophysical Research: Oceans*, *101*(C2), 3675-3696.

Benz, V., Esper, O., Gersonde, R., Lamy, F., & Tiedemann, R. (2016). Last Glacial Maximum sea surface temperature and sea-ice extent in the Pacific sector of the Southern Ocean. *Quaternary Science Reviews*, *146*, 216-237.

Berkman, P. A., & Forman, S. L. (1996). Pre-bomb radiocarbon and the reservoir correction for calcareous marine species in the Southern Ocean. *Geophysical Research Letters*, *23*(4), 363-366.

Böhm, E., Lippold, J., Gutjahr, M., Frank, M., Blaser, P., Antz, B., ... & Deininger, M. (2015). Strong and deep Atlantic meridional overturning circulation during the last glacial cycle. *Nature*, *517*(7532), 73-76.

Bostock, H. C., Hayward, B. W., Neil, H. L., Sabaa, A. T., & Scott, G. H. (2015). Changes in the position of the Subtropical Front south of New Zealand since the last glacial period. *Paleoceanography*, *30*(7), 824-844.

Bouttes, N., Paillard, D., Roche, D. M., Brovkin, V., & Bopp, L. (2011). Last Glacial Maximum CO2 and δ13C successfully reconciled. *Geophysical Research Letters*, *38*(2).

Boyd, P., Watson, A. J., Law, C. S., Abraham, E. R., Trull, T., Murdoch, R., ... & Zeldis, J. (2000). Mesoscale iron fertilization elevates phytoplankton stocks in the polar Southern Ocean. *Nature*, *407*, 695-702.

Bradley, R. S. (1999). *Paleoclimatology: reconstructing climates of the Quaternary*. Elsevier.

Bradley, R. S. (2013). *Paleoclimatology: Reconstructing climates of the Quaternary*. Academic Press.

Buesseler, K., Ball, L., Andrews, J., Benitez-Nelson, C., Belastock, R., Chai, F., & Chao, Y. (1998). Upper ocean export of particulate organic carbon in the Arabian Sea derived from thorium-234. *Deep Sea Research Part II: Topical Studies in Oceanography*, *45*(10-11), 2461-2487.

Burckle, L. H., & Cirilli, J. (1987). Origin of diatom ooze belt in the Southern Ocean; implications for late Quaterary paleoceanography. *Micropaleontology*, *33*(1), 82-86.

Burckle, L. H., & Mortlock, R. (1998). Sea-ice extent in the Southern Ocean during the Last Glacial Maximum: another approach to the problem. *Annals of Glaciology*, *27*, 302-304.

Cai, W., Yang, K., Wu, L., Huang, G., Santoso, A., Ng, B., Wang, G & Yamagata, T. (2021). Opposite response of strong and moderate positive Indian Ocean Dipole to global warming. *Nature Climate Change*, *11*(1), 27-32.

Caldeira, K., & Duffy, P. B. (2000). The role of the Southern Ocean in uptake and storage of anthropogenic carbon dioxide. *Science*, *287*(5453), 620-622.

Caley, T., Kim, J. H., Malaizé, B., Giraudeau, J., Laepple, T., Caillon, N., Charlier, K., Rebaubier, H., Rossignol, L., Castañeda, I. S., Schouten & Sinninghe Damsté, J. S. (2011). High-latitude obliquity as a dominant forcing in the Agulhas current system. *Climate of the Past*, *7*(4), 1285-1296.

Candelier, Y., Minoletti, F., Probert, I., & Hermoso, M. (2013). Temperature dependence of oxygen isotope fractionation in coccolith calcite: A culture and core top calibration of the genus Calcidiscus. *Geochimica et cosmochimica acta*, *100*, 264-281.

Carter, L. I. O. N. E. L., & Cortese, G. I. U. S. E. P. P. E. (2009). Change in the Southern Ocean: responding to Antarctica. *PAGES news*, *17*, 1-3.

Carter, L., Bostock-Lyman, H., & Bowen, M. (2022). Water masses, circulation and change in the modern Southern Ocean. In *Antarctic Climate Evolution* (pp. 165-197). Elsevier.

Cefarelli, A. O., Ferrario, M. E., Almandoz, G. O., Atencio, A. G., Akselman, R., & Vernet, M. (2010). Diversity of the diatom genus Fragilariopsis in the Argentine Sea and Antarctic waters: morphology, distribution and abundance. *Polar biology*, *33*(11), 1463-1484.

Charrassin, J. B., Hindell, M., Rintoul, S. R., Roquet, F., Sokolov, S., Biuw, M., ... & Guinet, C. (2008). Southern Ocean frontal structure and sea-ice formation rates revealed by elephant seals. *Proceedings of the National Academy of Sciences*, *105*(33), 11634-11639.

Chase, Z., Anderson, R. F., Fleisher, M. Q., & Kubik, P. W. (2003). Accumulation of biogenic and lithogenic material in the Pacific sector of the Southern Ocean during the past 40,000 years. *Deep Sea Research Part II: Topical Studies in Oceanography*, *50*(3-4), 799-832.

Civel-Mazens, M., Crosta, X., Cortese, G., Michel, E., Mazaud, A., Ther, O., ... & Itaki, T. (2021). Antarctic Polar Front migrations in the Kerguelen Plateau region, Southern Ocean, over the past 360 kyrs. *Global and Planetary Change*, *202*, 103526.

Comiso, J. C. (2003). Large-scale characteristics and variability of the global sea ice cover. *Sea ice: an introduction to its physics, chemistry, biology and geology*, 112-142.

Comiso, J. C., Kwok, R., Martin, S., & Gordon, A. L. (2011). Variability and trends in sea ice extent and ice production in the Ross Sea. *Journal of Geophysical Research: Oceans*, *116*(C4).

Constable, A. J., Melbourne-Thomas, J., Corney, S. P., Arrigo, K. R., Barbraud, C., Barnes, D. K., ... & Ziegler, P. (2014). Climate change and Southern Ocean ecosystems I: how changes in physical habitats directly affect marine biota. *Global change biology*, *20*(10), 3004-3025.

Cortese, G., & Gersonde, R. (2007). Morphometric variability in the diatom Fragilariopsis kerguelensis: Implications for Southern Ocean paleoceanography. *Earth and Planetary Science Letters*, *257*(3-4), 526-544.

Cortese, G., Gersonde, R., Maschner, K., & Medley, P. (2012). Glacial-interglacial size variability in the diatom Fragilariopsis kerguelensis: Possible iron/dust controls?. *Paleoceanography*, *27*(1).

Crosta, X. (2009). Holocene size variations in two diatom species off East Antarctica: Productivity vs environmental conditions. *Deep Sea Research Part I: Oceanographic Research Papers*, *56*(11), 1983-1993.

Crosta, X. (2011, May). Marine diatoms in polar and sub-polar environments and their application to Late Pleistocene paleoclimate reconstruction. In *IOP Conference Series: Earth and Environmental Science* (Vol. 14, No. 1, p. 012006). IOP Publishing.

Crosta, X., & Koç, N. (2007). Chapter eight diatoms: From micropaleontology to isotope geochemistry. *Developments in marine geology*, *1*, 327-369.

Crosta, X., Denis, D., & Ther, O. (2008). Sea ice seasonality during the holocene, adelie land, east antarctica. *Marine Micropaleontology*, *66*(3-4), 222-232.

Crosta, X., Kohfeld, K. E., Bostock, H. C., Chadwick, M., Du Vivier, A., Esper, O., Etourneau, J., Jones, J., Leventer, A., Müller, J. and Rhodes, R.H., & Yang, J. (2022). Antarctic sea ice over the past 130 000 years–Part 1: a review of what proxy records tell us. *Climate of the Past*, *18*(8), 1729-1756.

Crosta, X., Pichon, J. J., & Burckle, L. H. (1998a). Application of modern analog technique to marine Antarctic diatoms: Reconstruction of maximum sea-ice extent at the Last Glacial Maximum. *Paleoceanography*, *13*(3), 284-297.

Crosta, X., Romero, O., Armand, L., & Pichon, J. J. (2005a). The biogeography of major diatom taxa in Southern Ocean sediments. 2. Open ocean related species. *Palaeogeography, Palaeoclimatology, Palaeoecology*, 223, 66–92.

Crosta, X., Sturm, A., Armand, L., & Pichon, J. J. (2004). Late Quaternary sea ice history in the Indian sector of the Southern Ocean as recorded by diatom assemblages. *Marine Micropaleontology*, *50*(3-4), 209-223.

Cunningham, W. L., & Leventer, A. (1998b). Diatom assemblages in surface sediments of the Ross Sea: relationship to present oceanographic conditions. *Antarctic Science*, *10*(2), 134-146.

De Deckker, P., Moros, M., Perner, K., & Jansen, E. (2012). Influence of the tropics and southern westerlies on glacial interhemispheric asymmetry. *Nature Geoscience*, *5*(4), 266-269.

de Vernal, A., Gersonde, R., Goosse, H., Seidenkrantz, M. S., & Wolff, E. W. (2013). Sea ice in the paleoclimate system: the challenge of reconstructing sea ice from proxies–an introduction. *Quaternary Science Reviews*, *79*, 1-8.

Deacon, G. E. R. (1937). Note on the dynamics of southern ocean. *Discovery Report*, *15*, 125-152.

Deaney, E. L., Barker, S., & Van de Flierdt, T. (2017). Timing and nature of AMOC recovery across Termination 2 and magnitude of deglacial CO2 change. *Nature Communications*, *8*(1), 1-10.

Defelice, D. R., & Wise Jr, S. W. (1981). Surface lithofacies, biofacies, and diatom diversity patterns as models for delineation of climatic change in the southeast Atlantic Ocean. *Marine micropaleontology*, *6*(1), 29-70.

Delille, B., Vancoppenolle, M., Geilfus, N. X., Tilbrook, B., Lannuzel, D., Schoemann, V., ... & Tison, J. L. (2014). Southern Ocean CO2 sink: The contribution of the sea ice. *Journal of Geophysical Research: Oceans*, *119*(9), 6340-6355.

DeVries, T. (2014). The oceanic anthropogenic CO2 sink: Storage, air-sea fluxes, and transports over the industrial era. *Global Biogeochemical Cycles*, *28*(7), 631-647.

Doddridge, E. W., & Marshall, J. (2017). Modulation of the seasonal cycle of Antarctic sea ice extent related to the Southern Annular Mode. *Geophysical Research Letters*, *44*(19), 9761-9768.

Doddridge, E. W., Marshall, J., Song, H., Campin, J. M., & Kelley, M. (2021). Southern Ocean heat storage, reemergence, and winter sea ice decline induced by summertime winds. *Journal of Climate*, *34*(4), 1403-1415.

Dutta, K. (2008). Marine 14C reservoir age and Suess effect in the Indian Ocean. *Earth Science India*, *1*.

E. Michel personal communication (2022).

Eayrs, C., Li, X., Raphael, M. N., & Holland, D. M. (2021). Rapid decline in Antarctic sea ice in recent years hints at future change. *Nature Geoscience*, *14*(7), 460-464.

Eicken, H. (1992). The role of sea ice in structuring Antarctic ecosystems. In *Weddell Sea Ecology* (pp. 3-13). Springer, Berlin, Heidelberg.

Emiliani, C. (1955). Pleistocene temperatures. *The Journal of geology*, *63*(6), 538-578.

Esper, O., & Gersonde, R. (2014). New tools for the reconstruction of Pleistocene Antarctic sea ice. *Palaeogeography, Palaeoclimatology, Palaeoecology*, *399*, 260-283.

Esper, O., & Gersonde, R. (2014). Quaternary surface water temperature estimations: New diatom transfer functions for the Southern Ocean. *Palaeogeography, Palaeoclimatology, Palaeoecology*, *414*, 1-19.

Fan, T., Deser, C., & Schneider, D. P. (2014). Recent Antarctic sea ice trends in the context of Southern Ocean surface climate variations since 1950. *Geophysical Research Letters*, *41*(7), 2419-2426.

Fenner, J., Schrader, H. J., & Wienigk, H. (1976). Diatom phytoplankton studies in the southern Pacific Ocean, composition and correlation to the Antarctic Convergence and its paleoecological significance. *Initial Reports of the Deep Sea Drilling Project*, *35*, 757-813.

Ferrari, R., Jansen, M. F., Adkins, J. F., Burke, A., Stewart, A. L., & Thompson, A. F. (2014). Antarctic sea ice control on ocean circulation in present and glacial climates. *Proceedings of the National Academy of Sciences*, *111*(24), 8753-8758.

Ferry, A. J., Crosta, X., Quilty, P. G., Fink, D., Howard, W., & Armand, L. K. (2015). First records of winter sea ice concentration in the southwest Pacific sector of the Southern Ocean. *Paleoceanography*, *30*(11), 1525-1539.

Finkel, Z. V., Vaillancourt, C. J., Irwin, A. J., Reavie, E. D., & Smol, J. P. (2009). Environmental control of diatom community size structure varies across aquatic ecosystems. *Proceedings of the Royal Society B: Biological Sciences*, *276*(1662), 1627-1634.

Flores, J. A., Gersonde, R., & Sierro, F. J. (1999). Pleistocene fluctuations in the Agulhas Current Retroflection based on the calcareous plankton record. *Marine Micropaleontology*, *37*(1), 1-22.

Foldvik, A., & Gammelsrød, T. (1988). Notes on Southern Ocean hydrography, sea-ice and bottom water formation. *Palaeogeography, Palaeoclimatology, Palaeoecology*, *67*(1-2), 3-17.

Francois, R., Altabet, M. A., Yu, E. F., Sigman, D. M., Bacon, M. P., Frank, M., ... & Labeyrie, L. D. (1997). Contribution of Southern Ocean surface-water stratification to low atmospheric CO2 concentrations during the last glacial period. *Nature*, *389*(6654), 929-935.

Frank, M., Gersonde, R., van der Loeff, M. R., Bohrmann, G., Nürnberg, C. C., Kubik, P. W., ... & Mangini, A. (2000). Similar glacial and interglacial export bioproductivity in the Atlantic sector of the Southern Ocean: Multiproxy evidence and implications for glacial atmospheric CO2. *Paleoceanography*, *15*(6), 642-658.

Fraser, W. R., Trivelpiece, W. Z., Ainley, D. G., & Trivelpiece, S. G. (1992). Increases in Antarctic penguin populations: reduced competition with whales or a loss of sea ice due to environmental warming?. *Polar biology*, *11*(8), 525-531.

Fryxell, G. A., & Hasle, G. R. (1979). The genus Thalassiosira: species with internal extensions of the strutted processes. *Phycologia*, *18*(4), 378-393.

Fryxell, G. A., Sims, P. A., & Watkins, T. P. (1986). Azpeitia (Bacillariophyceae): related genera and promorphology. *Systematic botany monographs*, 1-74.

Galbraith, E., & de Lavergne, C. (2019). Response of a comprehensive climate model to a broad range of external forcings: relevance for deep ocean ventilation and the development of late Cenozoic ice ages. *Climate Dynamics*, *52*(1), 653-679.

Garabato, A. C. N., Polzin, K. L., Ferrari, R., Zika, J. D., & Forryan, A. (2016). A microscale view of mixing and overturning across the Antarctic Circumpolar Current. *Journal of Physical Oceanography*, *46*(1), 233-254.

Gersonde, R., & Zielinski, U. (2000). The reconstruction of late Quaternary Antarctic sea-ice distribution—the use of diatoms as a proxy for sea-ice. *Palaeogeography, Palaeoclimatology, Palaeoecology*, *162*(3-4), 263-286.

Gersonde, R., Abelmann, A., Brathauer, U., Becquey, S., Bianchi, C., Cortese, G., ... & Fütterer, D. K. (2003). Last glacial sea surface temperatures and sea-ice extent in the Southern Ocean (Atlantic-Indian sector): A multiproxy approach. *Paleoceanography*, *18*(3).

Gersonde, R., Crosta, X., Abelmann, A., & Armand, L. (2005). Sea-surface temperature and sea ice distribution of the Southern Ocean at the EPILOG Last Glacial Maximum—a circum-Antarctic view based on siliceous microfossil records. *Quaternary science reviews*, *24*(7-9), 869-896.

Ghadi, P., Nair, A., Crosta, X., Mohan, R., Manoj, M. C., & Meloth, T. (2020). Antarctic sea-ice and palaeoproductivity variation over the last 156,000 years in the Indian sector of Southern Ocean. *Marine Micropaleontology*, *160*, 101894.

Gille, S. T. (1994). Mean sea surface height of the Antarctic Circumpolar Current from Geosat data: Method and application. *Journal of Geophysical Research: Oceans*, *99*(C9), 18255-18273.

Gordon, A. L. (1991). Two stable modes of Southern Ocean winter stratification. In *Elsevier Oceanography Series* (Vol. 57, pp. 17-35). Elsevier.

Gottschalk, J., Michel, E., Thöle, L. M., Studer, A. S., Hasenfratz, A. P., Schmid, N., ... & Jaccard, S. L. (2020). Glacial heterogeneity in Southern Ocean carbon storage abated by fast South Indian deglacial carbon release. *Nature communications*, *11*(1), 1-14.

Govin, A., E. Michel, L. Labeyrie, C. Waelbroeck, F. Dewilde, and E. Jansen (2009), Evidence for northward expansion of Antarctic Bottom Water mass in the Southern Ocean during the last glacial inception, Paleoceanography, 24, PA1202, doi:10.1029/2008PA001603.

Graham, R. M. (2014). *The role of Southern Ocean fronts in the global climate system* (Doctoral dissertation, Department of Geological Sciences, Stockholm University).

Graham, R. M., De Boer, A. M., Heywood, K. J., Chapman, M. R., & Stevens, D. P. (2012). Southern Ocean fronts: Controlled by wind or topography?. *Journal of Geophysical Research: Oceans*, *117*(C8).

Hasle, G. R. (1965). Nitzschia and Fragilariopsis species studied in the light and electron microscopes. II. The group Pseudonitzschia. *Skr. Norske Vidensk-Akad. I. Mat.-Nat. Kl. Ny Serie*, *18*, 1-45.

Hasle, G. R. (1976, April). The biogeography of some marine planktonic diatoms. In Deep Sea Research and Oceanographic Abstracts (Vol. 23, No. 4, pp. 319-IN6). Elsevier.

Hasle, G. R., & Heimdal, B. R. (1968). Morphology and distribution of the marine centric diatom Thalassiosira antarctica Comber. *Journal of the Royal Microscopical Society*, *88*(3), 357-369.

Hasle, G. R., & Semina, H. J. (1987). The marine planktonic diatoms Thalassiothrix longissima and Thalassiothrix antarctica with comments on Thalassionema spp. and Synedra reinboldii. Diatom Research, 2(2), 175-192.

Hasle, G.R., Syvertsen, E.E. (1996). Marine Diatoms. In: Tomas, C.R. (Ed), Identifying Marine Phytoplankton, Academic Press, London, pp. 5–385.

Henley, S. F., Cavan, E. L., Fawcett, S. E., Kerr, R., Monteiro, T., Sherrell, R. M., Bowie, A.R., Boyd, P.W., Barnes, D.K., Schloss, I.R. and Marshall, T. (2020). Changing biogeochemistry of the Southern Ocean and its ecosystem implications. *Frontiers in marine science*, *7*, 581.

Hertzberg, M., & Schreuder, H. (2016). Role of atmospheric carbon dioxide in climate change. Energy & Environment, 27(6-7), 785-797.

Hertzberg, M., & Schreuder, H. (2016). Role of atmospheric carbon dioxide in climate change. *Energy & Environment*, *27*(6-7), 785-797.

Hobbs, W. R., & Raphael, M. N. (2010). The Pacific zonal asymmetry and its influence on Southern Hemisphere sea ice variability. *Antarctic Science*, *22*(5), 559-571.

Hobbs, W. R., Massom, R., Stammerjohn, S., Reid, P., Williams, G., & Meier, W. (2016). A review of recent changes in Southern Ocean sea ice, their drivers and forcings. *Global and Planetary Change*, *143*, 228-250.

Holland, P. R. (2014). The seasonality of Antarctic sea ice trends. *Geophysical Research Letters*, *41*(12), 4230-4237.

Holland, P. R., & Kwok, R. (2012). Wind-driven trends in Antarctic sea-ice drift. *Nature Geoscience*, *5*(12), 872-875.

Hustedt, F. (1930). Die Kieselalgen Deutschlands, O¨ sterreichs und der Schweiz. In: Rabenhorst, L. (Ed.), Kryptogamen-Flora Deutschlands. O¨ sterreichs und der Schweiz, pp. 1–920.

Hustedt, F. (1958). Diatomeen aus der Antarktis und dem Sqdatlantik. Reprinted from bDeutsche Antarktishe Expedition 1938/1939Q Band II, Geographisch-kartographische Anstalt bMundusQ. Hamburg. 191 pp. pl. 3–13.

Iida, T., & Odate, T. (2014). Seasonal variability of phytoplankton biomass and composition in the major water masses of the Indian Ocean sector of the Southern Ocean. *Polar science*, *8*(3), 283-297.

Iudicone, D., Madec, G., Blanke, B., & Speich, S. (2008). The role of Southern Ocean surface forcings and mixing in the global conveyor. *Journal of Physical Oceanography*, *38*(7), 1377-1400.

Jaccard, S. L., Hayes, C. T., Martinez-Garcia, A., Hodell, D. A., Anderson, R. F., Sigman, D. M., & Haug, G. H. (2013). Two modes of change in Southern Ocean productivity over the past million years. *Science*, *339*(6126), 1419-1423.

Jansen, E., Overpeck, J., Briffa, K. R., Duplessy, J. C., Joos, F., Masson-Delmotte, V., ... & Zhang, D. (2007). Palaeoclimate. Chapter 6. In *Climate Change 2007. The Physical Science Basis*.

Jena, B., Kumar, A., Ravichandran, M., & Kern, S. (2018). Mechanism of sea-ice expansion in the Indian Ocean sector of Antarctica: Insights from satellite observation and model reanalysis. *Plos one*, *13*(10), e0203222.

Johansen, J. R., & Fryxell, G. A. (1985). The genus Thalassiosira (Bacillariophyceae): studies on species occurring south of the Antarctic Convergence Zone. *Phycologia*, *24*(2), 155-179.

Jones, J. M., Gille, S. T., Goosse, H., Abram, N. J., Canziani, P. O., Charman, D. J., ... & Vance, T. R. (2016). Assessing recent trends in high-latitude Southern Hemisphere surface climate. *Nature Climate Change*, *6*(10), 917-926.

Jouzel, J., Masson-Delmotte, V., Cattani, O., Dreyfus, G., Falourd, S., Hoffmann, G., ... & Wolff, E. W. (2007). Orbital and millennial Antarctic climate variability over the past 800,000 years. *science*, *317*(5839), 793-796.

Kahru, M., Lee, Z., & Mitchell, B. G. (2017). Contemporaneous disequilibrium of bio-optical properties in the Southern Ocean. *Geophysical Research Letters*, *44*(6), 2835-2842.

Karl, T. R., & Trenberth, K. E. (2003). Modern global climate change. science, 302(5651), 1719-1723.

Kemp, A. E., Pike, J., Pearce, R. B., & Lange, C. B. (2000). The "Fall dump"—a new perspective on the role of a "shade flora" in the annual cycle of diatom production and export flux. *Deep Sea Research Part II: Topical Studies in Oceanography*, *47*(9-11), 2129-2154.

Kennett, J. P. (1977). Cenozoic evolution of Antarctic glaciation, the circum-Antarctic Ocean, and their impact on global paleoceanography. *Journal of geophysical research*, *82*(27), 3843-3860.

Kloster, M., Rigual-Hernández, A. S., Armand, L. K., Kauer, G., Trull, T. W., & Beszteri, B. (2019). Temporal changes in size distributions of the Southern Ocean diatom Fragilariopsis kerguelensis through high-throughput microscopy of sediment trap samples. *Diatom Research*, *34*(3), 133-147.

Knox, G. A. (1980). Plate tectonics and the evolution of intertidal and shallow-water benthic biotic distribution patterns of the southwest Pacific. *Palaeogeography, Palaeoclimatology, Palaeoecology*, *31*, 267-297.

Knox, G. A. (2006). *Biology of the southern ocean*. CRC press.

Koc Karpuz, N., & Schrader, H. (1990). Surface sediment diatom distribution and Holocene paleotemperature variations in the Greenland, Iceland and Norwegian Sea. *Paleoceanography*, *5*(4), 557-580.

Kohfeld, K. E., & Chase, Z. (2017). Temporal evolution of mechanisms controlling ocean carbon uptake during the last glacial cycle. Earth and Planetary Science Letters, 472, 206-215.

Kohfeld, K. E., Graham, R. M., De Boer, A. M., Sime, L. C., Wolff, E. W., Le Quéré, C., & Bopp, L. (2013). Southern Hemisphere westerly wind changes during the Last Glacial Maximum: paleo-data synthesis. *Quaternary Science Reviews*, *68*, 76-95.

KOOISTRA, W. H., Gersonde, R., Medlin, L. K., & Mann, D. G. (2007). The origin and evolution of the diatoms: their adaptation to a planktonic existence. *Evolution of primary producers in the sea*, 207-249.

Kumar, N., Anderson, R. F., Mortlock, R. A., Froelich, P. N., Kubik, P., Dittrich-Hannen, B., & Suter, M. (1995). Increased biological productivity and export production in the glacial Southern Ocean. *Nature*, *378*(6558), 675-680.

Kunz-Pirrung, M., Gersonde, R., & Hodell, D. A. (2002). Mid-Brunhes century-scale diatom sea surface temperature and sea ice records from the Atlantic sector of the Southern Ocean (ODP Leg 177, sites 1093, 1094 and core PS2089-2). *Palaeogeography, Palaeoclimatology, Palaeoecology*, *182*(3-4), 305-328.

Labeyrie, L., Labracherie, M., Gorfti, N., Pichon, J. J., Vautravers, M., Arnold, M., Duplessy, J.C., Paterne, M., Michel, E., Duprat, J. and Caralp, M. (1996). Hydrographic changes of the Southern Ocean (southeast Indian sector) over the last 230 kyr. *Paleoceanography*, *11*(1), 57-76.

Labrousse, S., Sallée, J. B., Fraser, A. D., Massom, R. A., Reid, P., Hobbs, W., ... & Charrassin, J. B. (2017). Variability in sea ice cover and climate elicit sex specific responses in an Antarctic predator. *Scientific Reports*, *7*(1), 1-13.

Labrousse, S., Williams, G., Tamura, T., Bestley, S., Sallée, J. B., Fraser, A. D., Sumner, M., Roquet, F., Heerah, K., Picard, B. & Guinet, C. (2018). Coastal polynyas: Winter oases for subadult southern elephant seals in East Antarctica. *Scientific Reports*, *8*(1), 1-15.

Lambert, F., Delmonte, B., Petit, J. R., Bigler, M., Kaufmann, P. R., Hutterli, M. A., ... & Maggi, V. (2008). Dust-climate couplings over the past 800,000 years from the EPICA Dome C ice core. *Nature*, *452*(7187), 616-619.

Lamy, F., Gersonde, R., Winckler, G., Esper, O., Jaeschke, A., Kuhn, G., ... & Kilian, R. (2014). Increased dust deposition in the Pacific Southern Ocean during glacial periods. *Science*, *343*(6169), 403-4

Lannuzel, D., Tedesco, L., Van Leeuwe, M., Campbell, K., Flores, H., Delille, B., Miller, L., Stefels, J., Assmy, P., Bowman, J. and Brown, K. (2020). The future of Arctic sea-ice biogeochemistry and ice-associated ecosystems. *Nature Climate Change*, *10*(11), 983-992.

Laws, R. A. (1983). Preparing strewn slides for quantitative microscopical analysis: a test using calibrated microspheres. *Micropaleontology*, 60-65.

Lefèvre, N., & Watson, A. J. (1999). Modeling the geochemical cycle of iron in the oceans and its impact on atmospheric CO2 concentrations. *Global Biogeochemical Cycles*, *13*(3), 727-736.

Li, J., Hao, X., Liao, H., Hu, J., & Chen, H. (2021). Meteorological impact on winter PM2. 5 pollution in Delhi: present and future projection under a warming climate. *Geophysical Research Letters*, *48*(13), e2021GL093722.

Lisiecki, L. E., & Raymo, M. E. (2005). A Pliocene-Pleistocene stack of 57 globally distributed benthic δ18O records. *Paleoceanography*, *20*(1).

Liu, J., Curry, J. A., & Martinson, D. G. (2004). Interpretation of recent Antarctic sea ice variability. *Geophysical Research Letters*, *31*(2).

Locarnini, R. A., Mishonov, A. V., Antonov, J. I., Boyer, T. P., Garcia, H. E., Baranova, O. K., ... & Seidov, D. (2013). World Ocean Atlas 2013, Volume 1: Temperature, edited by: Levitus, S. *A. Mishonov Technical Ed., NOAA Atlas NESDIS*, *73*, 40.

Loeb, V. J., & Santora, J. A. (2015). Climate variability and spatiotemporal dynamics of five Southern Ocean krill species. *Progress in Oceanography*, *134*, 93-122.

Lourey, M. J., & Trull, T. W. (2001). Seasonal nutrient depletion and carbon export in the Subantarctic and Polar Frontal Zones of the Southern Ocean south of Australia. *Journal of Geophysical Research: Oceans*, *106*(C12), 31463-31487.

Luis, A. J., & Sudhakar, M. (2009). Upper-ocean hydrodynamics along meridional sections in the southwest Indian sector of the Southern Ocean during austral summer 2007. *Polar Science*, *3*(1), 13-30.

Lumpkin, R., & Speer, K. (2007). Global ocean meridional overturning. *Journal of Physical Oceanography*, *37*(10), 2550-2562.

Lüthi, D., Le Floch, M., Bereiter, B., Blunier, T., Barnola, J. M., Siegenthaler, U., ... & Stocker, T. F. (2008). High-resolution carbon dioxide concentration record 650,000–800,000 years before present. *nature*, *453*(7193), 379-382.

Lutjeharms, J. E., & Valentine, H. R. (1984). Southern Ocean thermal fronts south of Africa. *Deep Sea Research Part A. Oceanographic Research Papers*, *31*(12), 1461-1475.

Manoj, M. C., & Thamban, M. (2015). Shifting frontal regimes and its influence on bioproductivity variations during the Late Quaternary in the Indian sector of Southern Ocean. *Deep Sea Research Part II: Topical Studies in Oceanography*, *118*, 261-274.

Marchetti, A., & Cassar, N. (2009). Diatom elemental and morphological changes in response to iron limitation: a brief review with potential paleoceanographic applications. *Geobiology*, *7*(4), 419-431.

Margalef, R. (1969). Size of centric diatoms as an ecological indicator: With 4 figures and 1 table in the text. Internationale Vereinigung für Theoretische und Angewandte Limnologie: Mitteilungen, 17(1), 202-210.

Marino, G., Rohling, E. J., Rodríguez-Sanz, L., Grant, K. M., Heslop, D., Roberts, A. P., ... & Yu, J. (2015). Bipolar seesaw control on last interglacial sea level. *Nature*, *522*(7555), 197-201.

Marshall, J., Speer, K. (2012). Closure of the meridional overturning circulation through Southern Ocean upwelling. Nat. Geosci. 5(3), 171– 180. Doi:10.1038/ngeo1391.

Martínez-Botí, M. A., Marino, G., Foster, G. L., Ziveri, P., Henehan, M. J., Rae, J. W., ... & Vance, D. (2015). Boron isotope evidence for oceanic carbon dioxide leakage during the last deglaciation. *Nature*, *518*(7538), 219-222.

Martínez-Garcia, A., Rosell-Melé, A., Jaccard, S. L., Geibert, W., Sigman, D. M., & Haug, G. H. (2011). Southern Ocean dust–climate coupling over the past four million years. *Nature*, *476*(7360), 312-315.

Martinson, D. G. (2012). Antarctic circumpolar current's role in the Antarctic ice system: An overview. *Palaeogeography, Palaeoclimatology, Palaeoecology*, *335*, 71-74.

Martinson, D. G., Pisias, N. G., Hays, J. D., Imbrie, J., Moore, T. C., & Shackleton, N. J. (1987). Age Dating and the Orbital Theory of the Ice Ages: Development of a High-Resolution 0 to 300,000-Year Chronostratigraphy1. *Quaternary research*, *27*(1), 1-29.

Mazaud, A., Sicre, M. A., Ezat, U., Pichon, J. J., Duprat, J., Laj, C., ... & Turon, J. L. (2002). Geomagnetic-assisted stratigraphy and sea surface temperature changes in core MD94-103 (Southern Indian Ocean): possible implications for North–South climatic relationships around H4. *Earth and Planetary Science Letters*, *201*(1), 159-170.

Meckler, A. N., Sigman, D. M., Gibson, K. A., François, R., Martinez-Garcia, A., Jaccard, S. L., ... & Haug, G. H. (2013). Deglacial pulses of deep-ocean silicate into the subtropical North Atlantic Ocean. *Nature*, *495*(7442), 495-498.

Medlin, L. K. (2016). Evolution of the diatoms: major steps in their evolution and a review of the supporting molecular and morphological evidence. *Phycologia*, *55*(1), 79-103.

Meir, W.N., et al. (2011). Sea ice (Chapter 9). In: Snow, Water, Ice and Permafrost in the Arctic: Climate Change and the Cryosphere. Arctic Monitoring and Assessment Program (AMAP), Oslo, Norway, pp. 1-82.

Mikaloff Fletcher, S. E., Gruber, N., Jacobson, A. R., Doney, S. C., Dutkiewicz, S., Gerber, M., ... & Mouchet, A. Mu uller, SA, and Sarmiento, JL. (2006). Inverse estimates of anthropogenic CO2 uptake, transport, and storage by the ocean. *Glob. Biogeochem. Cy*, *20*.

Moore, J. K., & Abbott, M. R. (2000). Phytoplankton chlorophyll distributions and primary production in the Southern Ocean. *Journal of Geophysical Research: Oceans*, *105*(C12), 28709-28722.

Mulitza, S., Dürkoop, A., Hale, W., Wefer, G., & Stefan Niebler, H. (1997). Planktonic foraminifera as recorders of past surface-water stratification. *Geology*, *25*(4), 335-338.

Nair, A., Mohan, R., Crosta, X., Manoj, M. C., Thamban, M., & Marieu, V. (2019). Southern Ocean sea ice and frontal changes during the Late Quaternary and their linkages to Asian summer monsoon. *Quaternary Science Reviews*, *213*, 93-104.

Nair, A., Mohan, R., Manoj, M. C., & Thamban, M. (2015). Glacial-interglacial variability in diatom abundance and valve size: Implications for Southern Ocean paleoceanography. *Paleoceanography*, *30*(10), 1245-1260.

Neil, H.L., Carter, L., Morris, M.Y. (2004). Thermal isolation of Campbell plateau, New Zealand, by the Antarctic circumpolar current over the past 130 kyr. *Paleoceanography* 19, PA4008.

Nicholls, K. W., Østerhus, S., Makinson, K., Gammelsrød, T., & Fahrbach, E. (2009). Ice-ocean processes over the continental shelf of the southern Weddell Sea, Antarctica: A review. *Reviews of Geophysics*, *47*(3).

Nicolas, J. P., Vogelmann, A. M., Scott, R. C., Wilson, A. B., Cadeddu, M. P., Bromwich, D. H., ... & Wille, J. D. (2017). January 2016 extensive summer melt in West Antarctica favoured by strong El Niño. *Nature communications*, *8*(1), 1-10.

Niebler, H. S., Hubberten, H. W., & Gersonde, R. (1999). Oxygen isotope values of planktic foraminifera: a tool for the reconstruction of surface water stratification. *Use of Proxies in Paleoceanography: examples from the South Atlantic*, 165-189.

Norkko, A., Thrush, S. F., Cummings, V. J., Gibbs, M. M., Andrew, N. L., Norkko, J., & Schwarz, A. M. (2007). Trophic structure of coastal Antarctic food webs associated with changes in sea ice and food supply. *Ecology*, *88*(11), 2810-2820.

Olsen, A. (2017). Autonomous observing platform CO2 data shed new light on the Southern Ocean carbon cycle. *Global Biogeochemical Cycles*, *31*(6), 1032-1035.

Olsen, A., Key, R. M., Van Heuven, S., Lauvset, S. K., Velo, A., Lin, X., ... & Suzuki, T. (2016). The Global Ocean Data Analysis Project version 2 (GLODAPv2)–an internally consistent data product for the world ocean. *Earth System Science Data*, *8*(2), 297-323.

Orr, J. C., Maier-Reimer, E., Mikolajewicz, U., Monfray, P., Sarmiento, J. L., Toggweiler, J. R., ... & Boutin, J. (2001). Global oceanic uptake of anthropogenic carbon dioxide as predicted by four 3-D ocean models. *Global Biogeochem. Cycles*, *15*(1), 43-60.

Orsi, A. H., Whitworth III, T., & Nowlin Jr, W. D. (1995). On the meridional extent and fronts of the Antarctic Circumpolar Current. *Deep Sea Research Part I: Oceanographic Research Papers*, *42*(5), 641-673.

Panassa, E., Völker, C., Wolf-Gladrow, D., & Hauck, J. (2018). Drivers of interannual variability of summer mixed layer depth in the Southern Ocean between 2002 and 2011. *Journal of Geophysical Research: Oceans*, *123*(8), 5077-5090.

Parkinson, C. L. (2002). Trends in the length of the Southern Ocean sea-ice season, 1979–99. *Annals of Glaciology*, *34*, 435-440.

Parkinson, C. L. (2004). Southern Ocean sea ice and its wider linkages: insights revealed from models and observations. *Antarctic Science*, *16*(4), 387-400.

Parkinson, C. L. (2019). A 40-y record reveals gradual Antarctic sea ice increases followed by decreases at rates far exceeding the rates seen in the Arctic. *Proceedings of the National Academy of Sciences*, *116*(29), 14414-14423.

Parkinson, C. L., & Cavalieri, D. J. (2012). Antarctic sea ice variability and trends, 1979–2010. *The Cryosphere*, *6*(4), 871-880.

Parkinson, C. L., & DiGirolamo, N. E. (2016). New visualizations highlight new information on the contrasting Arctic and Antarctic sea-ice trends since the late 1970s. *Remote Sensing of Environment*, *183*, 198-204.

Pfitzer, E. (1871). *Untersuchungen über bau und entwicklung der bacillariaceen (diatomaceen)* (Vol. 2). A. Marcus.

Pichon, J. J., Labeyrie, L. D., Bareille, G., Labracherie, M., Duprat, J., & Jouzel, J. (1992). Surface water temperature changes in the high latitudes of the Southern Hemisphere over the last glacial-interglacial cycle. *Paleoceanography*, *7*(3), 289-318.

Pichon, J. J., Labracherie, M., Labeyrie, L. D., & Duprat, J. (1987). Transfer functions between diatom assemblages and surface hydrology in the Southern Ocean. *Palaeogeography, Palaeoclimatology, Palaeoecology*, *61*, 79-95.

Pinkerton, M. H., Boyd, P. W., Deppeler, S., Hayward, A., Höfer, J., & Moreau, S. (2021). Evidence for the impact of climate change on primary producers in the Southern Ocean. *Frontiers in Ecology and Evolution*, *9*, 592027.

Pollard, R. T., & Read, J. F. (2001). Circulation pathways and transports of the Southern Ocean in the vicinity of the Southwest Indian Ridge. *Journal of Geophysical Research: Oceans*, *106*(C2), 2881-2898.

Pollard, R. T., Lucas, M. I., & Read, J. F. (2002). Physical controls on biogeochemical zonation in the Southern Ocean. *Deep Sea Research Part II: Topical Studies in Oceanography*, *49*(16), 3289-3305.

Pörtner, H. O., Roberts, D. C., Adams, H., Adler, C., Aldunce, P., Ali, E., ... & Stevens, N. (2022). Climate Change 2022: Impacts, Adaptation, and Vulnerability. Contribution of Working Group II to the Sixth Assessment Report of the Intergovernmental Panel on Climate Change.

Rae, J. W., Burke, A., Robinson, L. F., Adkins, J. F., Chen, T., Cole, C., ... & Taylor, B. J. (2018). CO2 storage and release in the deep Southern Ocean on millennial to centennial timescales. *Nature*, *562*(7728), 569-573.

Ragueneau, O., Tréguer, P., Leynaert, A., Anderson, R. F., Brzezinski, M. A., DeMaster, D. J., ... & Quéguiner, B. (2000). A review of the Si cycle in the modern ocean: recent progress and missing gaps in the application of biogenic opal as a paleoproductivity proxy. *Global and Planetary Change*, *26*(4), 317-365.

Ramsey, C. B. (2008). Deposition models for chronological records. *Quaternary Science Reviews*, *27*(1-2), 42-60.

Ramsey, C. B., & Lee, S. (2013). Recent and planned developments of the program OxCal. *Radiocarbon*, *55*(2), 720-730.

Randelhoff, A., & Guthrie, J. D. (2016). Regional patterns in current and future export production in the central Arctic Ocean quantified from nitrate fluxes. *Geophysical Research Letters*, *43*(16), 8600-8608.

Rathburn, A. E., Pichon, J. J., Ayress, M. A., & De Deckker, P. (1997). Microfossil and stable-isotope evidence for changes in Late Holocene palaeoproductivity and palaeoceanographic conditions in the Prydz Bay region of Antarctica. *Palaeogeography, Palaeoclimatology, Palaeoecology*, *131*(3-4), 485-510.

Ravelo, A. C., & Andreasen, D. H. (1999). Using planktonic foraminifera as monitors of the tropical surface ocean. In *Reconstructing Ocean History: A Window Into the Future* (pp. 217-243). Boston, MA: Springer US.

Reimi, M. A., Marcantonio, F., Lynch-Stieglitz, J., Jacobel, A. W., McManus, J. F., & Winckler, G. (2019). The penultimate glacial termination and variability of the Pacific intertropical convergence zone. *Geophysical Research Letters*, *46*(9), 4826-4835.

Rigual-Hernández, A. S., Trull, T. W., Bray, S. G., Closset, I., & Armand, L. K. (2015). Seasonal dynamics in diatom and particulate export fluxes to the deep sea in the Australian sector of the southern Antarctic Zone. *Journal of Marine Systems*, *142*, 62-74.

Rigual-Hernández, A. S., Trull, T. W., Bray, S. G., Cortina, A., & Armand, L. K. (2015). Latitudinal and temporal distributions of diatom populations in the pelagic waters of the Subantarctic and Polar Frontal zones of the Southern Ocean and their role in the biological pump. *Biogeosciences*, *12*(18), 5309-5337.

Rintoul, S. R., Hughes, C. W., & Olbers, D. (2001). The Antarctic circumpolar current system. In *International Geophysics* (Vol. 77, pp. 271-XXXVI). Academic Press.

Robinson, R. S., Sigman, D. M., DiFiore, P. J., Rohde, M. M., Mashiotta, T. A., & Lea, D. W. (2005). Diatom-bound 15N/14N: New support for enhanced nutrient consumption in the ice age subantarctic. *Paleoceanography*, *20*(3).

Rohling, E. J., Sprovieri, M., Cane, T., Casford, J. S., Cooke, S., Bouloubassi, I., ... & Kroon, D. (2004). Reconstructing past planktic foraminiferal habitats using stable isotope data: a case history for Mediterranean sapropel S5. *Marine Micropaleontology*, *50*(1-2), 89-123.

Romero, O. E., Armand, L. K., Crosta, X., & Pichon, J. J. (2005). The biogeography of major diatom taxa in Southern Ocean surface sediments: 3. Tropical/Subtropical species. *Palaeogeography, Palaeoclimatology, Palaeoecology*, *223*(1-2), 49-65.

Rossi, L., Sporta Caputi, S., Calizza, E., Careddu, G., Oliverio, M., Schiaparelli, S., & Costantini, M. L. (2019). Antarctic food web architecture under varying dynamics of sea ice cover. *Scientific reports*, *9*(1), 1-13.

Round, F. E., Crawford, R. M., & Mann, D. G. (1990). *Diatoms: biology and morphology of the genera*. Cambridge university press.

Round, F.E., Crawford, R.M., Mann, D.G. (Eds.)., 1990. The Diatoms: Biology and Morphology of the Genera. Cambridge University Press, Cambridge, p. 747.

Rysgaard, S., Bendtsen, J., Delille, B., Dieckmann, G. S., Glud, R. N., Kennedy, H., … Tison, J. (2011). Sea ice contribution to the air–sea CO₂ exchange in the Arctic and southern oceans. *Tellus B: Chemical and Physical Meteorology*, *63*(5), 823. doi:10.1111/j.1600-0889.2011.00571.x

Sabu, P., Subeesh, M. P., Sivakrishnan, K. K., & Anilkumar, N. (2021). Causes and impacts of anomalous warming in the Prydz Bay, East Antarctica during austral summer 2016-17. *Polar Science*, *30*, 100660.

Sallée, J. B., Pellichero, V., Akhoudas, C., Pauthenet, E., Vignes, L., Schmidtko, S., Garabato, A.N., Sutherland, P. and Kuusela, M. (2021). Summertime increases in upper-ocean stratification and mixed-layer depth. *Nature*, *591*(7851), 592-598.

Schlitzer, R. (2002). Carbon export fluxes in the Southern Ocean: results from inverse modeling and comparison with satellite-based estimates. *Deep Sea Research Part II: Topical Studies in Oceanography*, *49*(9-10), 1623-1644.

Schneider-Mor, A., Yam, R., Bianchi, C., Kunz-Pirrung, M., Gersonde, R., & Shemesh, A. (2005). Diatom stable isotopes, sea ice presence and sea surface temperature records of the past 640 ka in the Atlantic sector of the Southern Ocean. *Geophysical Research Letters*, *32*(10).

Schrader, H. J. (1978). Diatoms and silicofragellates. Micropaleontological counting methods and techniques-an exercise on an eight meters section of the lower Pliocene of Capo Rosselle, Sicily. *Utrecht Micropaleont. Bull.*, *17*, 129-176.

Schweitzer, P. N. (1995). Monthly averaged polar sea-ice concentration: US Geological Survey Digital Data Series. *Reston, VA.*

Scott, F. J., & Marchant, H. J. (Eds.). (2005). *Antarctic marine protists* (p. 572). Canberra: Australian Biological Resources Study.

Semina, H. J. (2003). SEM-studied diatoms of different regions of the World Ocean. *Iconogr. Diatomol.*, *10*, 1-363.

Shemesh, A., Burckle, L. H., & Froelich, P. N. (1989). Dissolution and preservation of Antarctic diatoms and the effect on sediment thanatocoenoses. *Quaternary Research*, *31*(2), 288-308.

Shemesh, A., Burckle, L. H., & Hays, J. D. (1994). Meltwater input to the Southern Ocean during the last glacial maximum. *Science*, *266*(5190), 1542-1544.

Shemesh, A., Charles, C. D., & Fairbanks, R. G. (1992). Oxygen isotopes in biogenic silica: global changes in ocean temperature and isotopic composition. *Science*, *256*(5062), 1434-1436.

Shetye, S. S., Mohan, R., & Nair, A. (2014). Latitudinal shifts in the Polar Front in Indian sector of the Southern Ocean: evidences from silicoflagellate assemblage. *Geosciences Journal*, *18*(2), 241-246.

Shukla, S. K., & Crosta, X. (2017). Fragilariopsis kerguelensis size variability from the Indian subtropical Southern Ocean over the last 42 000 years. *Antarctic science*, *29*(2), 139-146.

Shukla, S. K., Crespin, J., & Crosta, X. (2016). Thalassiosira lentiginosa size variation and associated biogenic silica burial in the Southern Ocean over the last 42 kyrs. *Marine Micropaleontology*, *127*, 74-85.

Shukla, S. K., Crosta, X., Cortese, G., & Nayak, G. N. (2013). Climate mediated size variability of diatom Fragilariopsis kerguelensis in the Southern Ocean. *Quaternary Science Reviews*, *69*, 49-58.

Sicre, M. A., Labeyrie, L., Ezat, U., Duprat, J., Turon, J. L., Schmidt, S., ... & Mazaud, A. (2005). Mid-latitude southern indian ocean response to northern hemisphere heinrich events. *Earth and Planetary Science Letters*, *240*(3-4), 724-731.

Sigman, D. M., & Boyle, E. A. (2000). Glacial/interglacial variations in atmospheric carbon dioxide. *Nature*, *407*(6806), 859-869.

Sigman, D. M., Hain, M. P., & Haug, G. H. (2010). The polar ocean and glacial cycles in atmospheric CO2 concentration. *Nature*, *466*(7302), 47-55.

Simmonds, I. (2015). Comparing and contrasting the behaviour of Arctic and Antarctic sea ice over the 35 year period 1979-2013. *Annals of Glaciology*, *56*(69), 18-28.

Simonsen, R. (1974). The diatom plankton of the Indian Ocean Expedition of R/V" Meteor" 1964-1965. *Meteor Forschungsergebnisse: Reihe D, Biologie*, *19*, 1-107.

Simonsen, R. (1979). The diatom system: ideas on phylogeny. *Bacillaria*, *2*, 9-71.

Sims, P. A., Mann, D. G., & Medlin, L. K. (2006). Evolution of the diatoms: insights from fossil, biological and molecular data. *Phycologia*, *45*(4), 361-402.

Simstich, J., Sarnthein, M., & Erlenkeuser, H. (2003). Paired δ18O signals of Neogloboquadrina pachyderma (s) and Turborotalita quinqueloba show thermal stratification structure in Nordic Seas. *Marine Micropaleontology*, *48*(1-2), 107-125.

Sloyan, B. M., & Rintoul, S. R. (2001). The Southern Ocean limb of the global deep overturning circulation. *Journal of Physical Oceanography*, *31*(1), 143-173.

Smetacek, V. (1999). Diatoms and the ocean carbon cycle. *Protist*, *150*(1), 25-32.

Sokolov, S., & Rintoul, S. R. (2002). Structure of Southern Ocean fronts at 140 E. *Journal of Marine Systems*, *37*(1-3), 151-184.

Sokolov, S., & Rintoul, S. R. (2009a). Circumpolar structure and distribution of the Antarctic Circumpolar Current fronts: 1. Mean circumpolar paths. *Journal of Geophysical Research: Oceans*, *114*(C11).

Sokolov, S., & Rintoul, S. R. (2009b). Circumpolar structure and distribution of the Antarctic Circumpolar Current fronts: 2. Variability and relationship to sea surface height. *Journal of Geophysical Research: Oceans*, *114*(C11).

Stephens, B. B., & Keeling, R. F. (2000). The influence of Antarctic sea ice on glacial–interglacial CO2 variations. *Nature*, *404*(6774), 171-174.

Studer, A. S., Sigman, D. M., Martínez-García, A., Thöle, L. M., Michel, E., Jaccard, S. L., ... & Haug, G. H. (2018). Increased nutrient supply to the Southern Ocean during the Holocene and its implications for the pre-industrial atmospheric CO2 rise. *Nature geoscience*, *11*(10), 756-760.

Stuecker, M. F., Bitz, C. M., & Armour, K. C. (2017). Conditions leading to the unprecedented low Antarctic sea ice extent during the 2016 austral spring season. *Geophysical Research Letters*, *44*(17), 9008-9019.

Stuiver, M., Reimer, P.J., Reimer, R.W., 2005. CALIB 6.0 [Program and documentation]. [Available at http://www.calib.qub.ac.uk/.]

Swann, G. E., & Leng, M. J. (2009). A review of diatom δ18O in palaeoceanography. *Quaternary Science Reviews*, *28*(5-6), 384-398.

Swann, G. E., Leng, M. J., Sloane, H. J., Maslin, M. A., & Onodera, J. (2007). Diatom oxygen isotopes: evidence of a species effect in the sediment record. *Geochemistry, Geophysics, Geosystems*, *8*(6).

Swann, G. E., Leng, M. J., Sloane, H. J., Maslin, M. A., & Onodera, J. (2007). Diatom oxygen isotopes: evidence of a species effect in the sediment record. *Geochemistry, Geophysics, Geosystems*, *8*(6).

Talley, L. D. (2011). *Descriptive physical oceanography: an introduction*. Academic press.

Tanimura, Y. (1992). Distribution of diatom species in the surface sediments of Lqtzow-Holm Bay, Antarctica. In: Ishizaki, K., Saito, T. (Eds.), Centenary of Japanese Micropaleontology. Terra Scientific Publishing Company, Tokyo, pp. 399–411.

Thamban, M., Naik, S. S., Mohan, R., Rajakumar, A., Basavaiah, N., D'Souza, W., ... & Pandey, P. C. (2005). Changes in the source and transport mechanism of terrigenous input to the Indian sector of Southern Ocean during the late Quaternary and its palaeoceanographic implications. *Journal of earth system science*, *114*(5), 443-452.

Thomas, D. N., & Dieckmann, G. S. (Eds.). (2008). Sea ice: an introduction to its physics, chemistry, biology and geology.

Timmermann, A., Menviel, L., Okumura, Y., Schilla, A., Merkel, U., Timm, O., ... & Schulz, M. (2010). Towards a quantitative understanding of millennial-scale Antarctic warming events. *Quaternary Science Reviews*, *29*(1-2), 74-85.

Toggweiler, J. R. (2006). The Mid-Latitude Westerlies, Atmospheric CO2, and Climate Change during the Ice Ages. In *AGU Spring Meeting Abstracts* (Vol. 2005, pp. OS13A-03).

Toggweiler, J. R., & Lea, D. W. (2010). Temperature differences between the hemispheres and ice age climate variability. *Paleoceanography*, *25*(2).

Tomczak, M., & Godfrey, J. S. (2003). *Regional oceanography: an introduction*. Daya books.

Toulza, E., Tagliabue, A., Blain, S., & Piganeau, G. (2012). Analysis of the global ocean sampling (GOS) project for trends in iron uptake by surface ocean microbes. *Plos one*, *7*(2), e30931.

Tréguer, P., & Jacques, G. (1992). Review Dynamics of nutrients and phytoplankton, and fluxes of carbon, nitrogen and silicon in the Antarctic Ocean. In *Weddell Sea Ecology* (pp. 149-162). Springer, Berlin, Heidelberg.

Treguer, P., Nelson, D. M., Van Bennekom, A. J., DeMaster, D. J., Leynaert, A., & Quéguiner, B. (1995). The silica balance in the world ocean: a reestimate. *Science*, *268*(5209), 375-379.

Turner, J., Guarino, M. V., Arnatt, J., Jena, B., Marshall, G. J., Phillips, T., Bajish, C.C., Clem, K., Wang, Z., Andersson, T. and Murphy, E.J. (2020). Recent decrease of summer sea ice in the Weddell Sea, Antarctica. *Geophysical Research Letters*, *47*(11), e2020GL087127.

Vancoppenolle, M., Meiners, K. M., Michel, C., Bopp, L., Brabant, F., Carnat, G., Delille, B., Lannuzel, D., Madec, G., Moreau, S. and Tison, J.L., & Van Der Merwe, P. (2013). Role of sea ice in global biogeochemical cycles: emerging views and challenges. *Quaternary science reviews*, *79*, 207-230.

Vernet, M., Geibert, W., Hoppema, M., Brown, P. J., Haas, C., Hellmer, H. H., ... & Verdy, A. (2019). The Weddell Gyre, Southern Ocean: present knowledge and future challenges. *Reviews of Geophysics*, *57*(3), 623-708.

Villareal, T. A., & Fryxell, G. A. (1983). THE GENUS ACTINOCYCLUS (BACILLARIOPHYCEAE): FRUSTULE MORPHOLOGY OF A. SAGITTULUS SP. NOV. AND TWO RELATED SPECIES 1. *Journal of phycology*, *19*(4), 452-466.

Wang, S., & Moore, J. K. (2012). Variability of primary production and air-sea CO2 flux in the Southern Ocean. *Global Biogeochemical Cycles*, *26*(1).

Wang, Y., Zhao, C., McFarquhar, G. M., Wu, W., Reeves, M., & Li, J. (2021). Dispersion of droplet size distributions in supercooled non-precipitating stratocumulus from aircraft observations obtained during the southern ocean cloud radiation aerosol transport experimental study. *Journal of Geophysical Research: Atmospheres*, *126*(6), e2020JD033720.

Weijer, W., Sloyan, B. M., Maltrud, M. E., Jeffery, N., Hecht, M. W., Hartin, C. A., ... & Landrum, L. (2012). The Southern Ocean and its climate in CCSM4. *Journal of Climate*, *25*(8), 2652-2675.

Whitworth III, T., & Nowlin Jr, W. D. (1987). Water masses and currents of the Southern Ocean at the Greenwich Meridian. *Journal of Geophysical Research: Oceans*, *92*(C6), 6462-6476.

Whitworth, T. (1983). Monitoring the transport of the Antarctic circumpolar current at Drake Passage. *Journal of Physical Oceanography*, *13*(11), 2045-2057.

Wolff, E. W., Fischer, H., Fundel, F., Ruth, U., Twarloh, B., Littot, G. C., Mulvaney, R., Röthlisberger, R., de Angelis, M., Boutron, C.F. and Hansson, M., ... & Gaspari, V. (2006). Southern Ocean sea-ice extent, productivity and iron flux over the past eight glacial cycles. *Nature*, *440*(7083), 491-496.

Wright, S. W., Jeffrey, S. W., & Mantoura, R. F. C. (Eds.). (2005). *Phytoplankton pigments in oceanography: guidelines to modern methods*. Paris, France: Unesco Pub.

Wunsch, C. (1998). The work done by the wind on the oceanic general circulation. *Journal of Physical Oceanography*, *28*(11), 2332-2340.

Wüst, G. (1935). The stratosphere of the Atlantic Ocean. Scientific results of the German Atlantic expedition of the research vessel 'Meteor'1925–1927, volume 6. Amerind, 180 pp. *English translation*.

Xiao, W., Esper, O., & Gersonde, R. (2016). Last Glacial-Holocene climate variability in the Atlantic sector of the Southern Ocean. *Quaternary Science Reviews*, *135*, 115-137.

Young, A. L. F. (2010). Using Diatoms (Class Bacillariophyceae) as a biological proxy for environmental changes in the Canterbury high country, Lake Hawdon, New Zealand.

Yuan, N., Ding, M., Ludescher, J., & Bunde, A. (2017). Increase of the Antarctic Sea Ice Extent is highly significant only in the Ross Sea. *Scientific Reports*, *7*(1), 1-8.

Zachos, J., Pagani, M., Sloan, L., Thomas, E., & Billups, K. (2001). Trends, rhythms, and aberrations in global climate 65 Ma to present. *science*, *292*(5517), 686-693.

Zielinski, U. (1993). Quantitative estimation of palaeoenvironmental parameters of the Antarctic Surface Water in the Late Quaternary using transfer functions with diatoms. Ph.D. thesis, Alfred Wegener Institute for Polar and Marine Research, Bremerhaven, Germany, p. 171.

Zielinski, U., & Gersonde, R. (1997). Diatom distribution in Southern Ocean surface sediments (Atlantic sector): Implications for paleoenvironmental reconstructions. *Palaeogeography, Palaeoclimatology, Palaeoecology*, *129*(3-4), 213-250.

Zielinski, U., Gersonde, R., Sieger, R., & Fütterer, D. (1998). Quaternary surface water temperature estimations: Calibration of a diatom transfer function for the Southern Ocean. Paleoceanography and Paleoclimatology, 13(4), 365-383.

Zwally, H. J., Comiso, J. C., Parkinson, C. L., Cavalieri, D. J., & Gloersen, P. (2002). Variability of Antarctic sea ice 1979–1998. *Journal of Geophysical Research: Oceans*, *107*(C5), 9-1.